NASA CONTRACTOR REPORT

NASA CR-2694

SKIN FRICTION REDUCTION BY SLOT INJECTION AT MACH 0.8

Victor Zakkay and Chi R. Wang

Prepared by
NEW YORK UNIVERSITY
Westbury, N.Y. 11590
for Langley Research Center

NATIONAL AERONAUTICS AND SPACE ADMINISTRATION • WASHINGTON, D. C. • JULY 1976

I. INTRODUCTION

Recent experimental results, Refs. 1 and 2, have indicated that a substantial decrease in skin friction may be obtained by slot injection on the surface of a body. These results have been obtained for tests at hypersonic speeds. The amount of reliable experimental data available at subsonic or supersonic speed is meager and gives information mainly on heat transfer rather than on skin friction. The results of both references (1,2) indicated a substantial difference in slot film cooling effectiveness obtained for the supersonic case over that of the subsonic case. In addition to those experimental work, Ref. 3, has provided a numerical analysis which could predict the properties of the flow downstream of the slot injection. The analysis assumed a mixing coefficient which contains an arbitrary constant which could depend on the fluctuating properties of the flow in the immediate downstream region of the slot.

Some experimental results are available in the subsonic range; however, most of these results have been obtained for low speed and therefore could be treated as incompressible. The present research was undertaken in order to bridge the gap between the incompressible and hypersonic range. As a first step the present research effort was concentrated on measuring the skin friction and turbulent intensity due to tangential downstream slot injection.

The measurements were obtained on the inside wall of an axially symmetric test section with axially symmetric slot configurations. This arrangement was chosen to insure two-dimensional flow downstream of the slot. Surface skin friction measurements, boundary layer profiles (static pressure, pitot pressure, and velocity) and turbulent intensity were

obtained. The experiments were performed at $M_\infty = 0.8$, a Re/m of 1.42×10^7 and for adiabatic wall conditions. A floating element skin friction balance, a boundary layer pressure probe and a hot film probe with anemometer were used to perform the measurements. Two wind tunnel configurations were constructed; one for single slot injection (S = 0.636 cm), and the second with two injection slots ($S_1 = S_2 = 0.318$ cm). The skin friction was measured also with a flush mounted hot film probe. The flush mounted hot film probe calibration and a comparison of its measurement with the floating-element skin friction balance are also presented.

II. TEST APPARATUS

The wind tunnel was constructed with a large contraction ratio between the settling chamber and the cylindrical test section. To investigate the effect of slot dimension and multiple slot injection, two different wind tunnel configurations were designed for the present experiments (Figs. 1 and 2). For single slot injection, a slot height of 0.636 cm was used. The slot lip was approximately 0.1 cm thick. The injection slot was placed 115 cm downstream of the settling chamber and was followed by a cylindrical test section 150 cm in length. A venturi tube was used to measure the injection mass flow rate passing through the annular injection chamber. Details of the test section are shown in Fig. 3. Circular ports in the test section instrumentation plate were provided for mounting the floating-element surface skin friction balance. Pressure taps were located along the test section to measure the surface pressure distributions. Additional ports were placed upstream of the injection slot to provide reference measurements. For the double slot injection experiments, an additional injection slot was located upstream of the test section and both slots were modified to have a slot height of 0.318 cm. The two slots were placed at a distance of 45 cm apart ($x/S = 140$). Separate venturi tubes were used to measure the injection mass flow rate through each chamber. Details of the double slot arrangement are shown in Fig. 4.

A Kistler floating-element skin friction balance with 0.94 cm diameter sensing element was used to measure the surface shear force in the test section. This instrument was provided by and calibrated at NASA Langley.

Descriptions of this skin friction balance are presented in Appendix I. A calibration range of 1 gm/cm^2 was found appropriate for the values of the skin friction measured in the present tests.

The boundary layer velocity and turbulent intensity profiles were measured with a hot film probe operated at constant temperature. This hot film probe was connected to a Thermal-System 1050 constant temperature anemometer and was able to measure a mean velocity up to 330 m/sec. Calibration of the hot film probe is described in Appendix II. For single slot injection, boundary layer pressure probes and pressure transducers were also used to measure the profiles of static and total pressures. These probes were mounted on an automatic traversing mechanism which was moved longitudinally to take measurements at different locations downstream of the injection slot.

III. TEST PROCEDURES AND MEASUREMENTS

For the present blowdown type wind tunnel, the free stream Mach number was adjusted by varying the upstream and downstream pressure. For all the tests of this investigation, a free stream Mach number of approximately 0.8 was found with downstream static pressure of 6.096×10^4 Newton/m^2 and a stagnation pressure of 1.035×10^5 Newton/m^2. The wind tunnel total temperature was 290°K and the wall temperature was constant and equal to this tunnel stagnation temperature.

The injection mass flow rate was controlled by adjusting the upstream pressure of the venturi tube. Room temperature air was used as the injectant. Three different injection mass flow rates (λ = 0.11, 0.21, and 0.31) were used for the tests. To obtain a steady flow of the injectant, air was supplied through the injection slot for two seconds prior to starting the tunnel and a steady main flow was established within one second thereafter. Skin friction data and velocity profiles were measured in different test runs to minimize interference.

Pressure transducers, calibrated in a range of 0 - 1.38×10^5 Newton/m^2 within 1% accuracy, were used to measure the surface pressure and the pitot pressure. The operating resistance of the hot film probe was 8.35 ohms with 1.5 overheat ratio. The D.C. voltage and the RMS output of the anemometer were calibrated before each test. The mean velocity and turbulent intensity were determined from these anemometer outputs (see Appendix II). The null-type skin friction balance was also calibrated with a self-testing mechanism before each test. All the output through the pressure transducer, anemometer, and the surface skin friction balance were recorded on a multi-channel Honeywell visicorder.

IV. EXPERIMENTAL RESULTS AND DISCUSSION

1. Single Slot Injection

a) Boundary Layer Profiles

Boundary layer velocity profiles measured with the hot film probe for locations near and downstream of the injection slot are shown in Figs. 5-9. The boundary layer thickness at the location of the injection slot is approximately twice the slot height. The figures show (Fig. 5) that for small λ there is little effect of injection on the initial boundary layer profile; however, there is some interference for $\lambda = 0.339$. The velocity profiles approach the one-seventh power law at locations far downstream from the slot ($x/S \approx 40$), Fig. 9.

Profiles of the turbulent intensity are given in Figs. 10-14. A free stream turbulent intensity of $u'/u_e = 0.035$ is shown in the region of the slot injection. Turbulent intensity in the region near the injection slot decreases significantly as the injection mass flow rate increases. The distance from the wall over which the turbulent intensity is a function of the injection mass flow increases with downstream distance. Isocontours of turbulent intensity are also shown in Fig. 15-17. For $\lambda = 0.118$, the maximum turbulent intensity, $u'/u = 0.21$, was found in a region very near the injection slot; a large region of relatively high turbulent intensity ($u'/u = 0.10 \sim 0.14$) occurred downstream of this region. As the injection mass flow rate increases, the turbulent intensity decreases and the region of maximum turbulent intensity moves downstream. The domain of relatively high turbulent intensity region ($u'/u = 0.10 \approx 0.14$) also decreases as

λ increases.

Boundary layer profiles of the static and total pressures at three downstream locations are shown in Figs. 18-23. Mach number profiles calculated from the measured pressure profiles are shown in Figs. 24-26. Large normal pressure gradients exist near the slot without injection and with small injection (λ = .118). Increasing slot injection decreases the normal pressure gradient and in addition results in a constant static pressure which approaches the free stream static pressure for $\lambda \leq 0.206$. Large Mach number gradients due to flow expansion around the slot lip is found for small injection ratios. Mach number profiles at x/S = 0.08 also indicate that uniform Mach number flow of the injectant exists for $\lambda \leq 0.206$ and boundary layer tyoe Mach number profiles of injectant occurs for λ = 0.339. Slot injection increases the free stream Mach number slightly (from 0.8 to 0.86) downstream of the slot. Some previous theoretical analyses of tangential slot injection have been made with the assumption of zero normal pressure gradient. Present profiles of the static pressure, Fig. 18, indicate that normal pressure gradient do exist near the injection slot for small injection rates ($\lambda \leq 0.118$). This normal pressure gradient in the region close to the injection slot ($x/S \leq 10$) should not be neglected in the determination of the external flow conditions for the case of small injection mass flow rate. Analytical and experimental results of base pressure coefficient of a rearward facing step at supersonic speed can be found in Refs. 4 and 5. Present transonic profile measurements with λ = 0.0 gave an approximate base pressure coefficient of -1.08 and is close to the estimate of Ref. 4. For a rearward facing step a two-dimensional base pressure coefficient of approximately -0.50 at M_∞ = 1.0 was found, Ref. 5. However, the validity

of comparing the base pressure downstream of a backward-facing slot with results for a rearward facing step is not clear and the similarity between the two flow fields needs to be established.

b) Surface Pressure Distributions

For zero slot injection (Fig. 27), a significant longitudinal pressure gradient has been measured in a region of $x/S \leq 10$. Comparisons of the surface pressure, in terms of the free stream static pressure p_e (Figs. 18, 19, and 20), due to different slot injection are given in Fig. 28. Slot injection significantly increases the surface pressure over a distance of $x/S = 10$; the matched pressure condition exists for $x/S \geq 10$.

c) Skin Friction

Local surface skin friction coefficients, $C_f = \tau_w/(\frac{1}{2} \rho_e u_e^2)$ determined from the skin friction balance measurements are shown in Fig. 29, where C_{fo} is the value of the local skin friction coefficient without the existence of injection slot. The value of C_{fo} was linearly interpolated from the values measured at locations upstream ($x/S = -50$) and far downstream ($x/S = 190$) of the slot. For $x/S < 5$, the local skin friction increases as injection mass flow rate increases. Increasing the injection mass flow rate decreases the local skin friction for $x/S > 5$. Except for the case of $\lambda = 0.118$, the present results indicate that the slot injection generally reduces the overall level of skin friction over downstream distance to $x/S < 100$.

For the case of $\lambda = 0.118$ the results seem to be inconsistent with other injection rates (Fig. 29). The results for this case suggest that the separation region formed by the slot (recirculation region) has not yet been driven downstream and therefore forms a reattachment region at about x/S of 10 where the local skin friction is very high. Increasing λ

above 0.118 drives the recirculation region and therefore the reattachment point downstream. The two-dimensional results, Ref. 2, for S = 0.475 cm and λ = 0.064 with $T_{oj}/T_{o\infty}$ = 0.63 in a hypersonic Mach 6 main flow are compared with the results of present transonic experiment in Fig. 29. The total drag reduction over a distance of 100 slot heights in the present single slot injection (S = 0.636 and u_j/u_∞ = 0.33) is approximately 20%. This value may be compared to the results of Ref. 2 for M_∞ = 6 and u_j/u_∞ = 0.3, the value from the total drag reductions in this case is of the order of 28%. It is gratifying to notice the small difference between the values obtained in the transonic range over that obtained in the hypersonic range.

2. Two Slot Injection, S = 0.318 cm

a) Boundary Layer Profiles

Boundary layer profiles measured with hot film probe for various combinations of slot injections at x/S = 0.16 are shown in Figs. 30-32. In all these results for the double slot injection, x is designated as the distance measured from the second slot. Without first slot injection, Fig. 30, flat velocity profiles at the second slot exit were found for $\lambda_2 \leq 0.218$, and large velocity, similar to a boundary layer type profile, occurs near the second slot for λ_2 = 0.310. The effect of the slot injection on the velocity profiles external to the injection slot is very slight. With constant second slot injection (λ_2 = 0.109) and varying the first slot injection, the velocity profiles near the second slot, Fig. 32, still only change slightly. However, there is a little increase in the local boundary layer thickness external to the second slot due to first slot injection (especially for λ_2 = 0.319).

Turbulent intensity profiles due to different combinations of slot injection are also given in Figs. 33-35. Similar to the previous results,

slot injection decreases the turbulent intensity near the second slot exit, Fig. 33. The present results for two-slot injection did not show any effect on the first slot injection on the turbulent intensity downstream of the second slot, Figs. 34-35. This may have been due to the large distance between the first slot and the second slot of the present tunnel setup.

b) Surface Pressure Distributions

Surface pressure downstream of the second slot without slot injection is shown in Fig. 36. A longitudinal adverse pressure gradient exists within a distance of x/S = 10. Results of surface pressure measurements due to different combinations of slot injection are given in Figs. 37-39. Slot injection increases the surface pressure in the region near the second slot and multiple slot injection tends to slightly decrease the surface pressure downstream of the second slot, Fig. 39.

c) Skin Friction

Surface skin friction coefficients, $C_f = \tau_w/(\frac{1}{2}\rho_e u_e^2)$ have also been determined from the measured shear force for different slot injection combinations. Results of injection from only the second slot, Fig. 40, indicate the general effect of skin friction reduction due to tangential slot injection. However, the largest reduction in the skin friction occurs with $\lambda_2 = 0.218$. Results of the surface skin friction with constant injection from the second slot and different first slot injection are shown in Fig. 41. The effect of injection from the first slot on the surface skin friction downstream of the second slot is insignificant except in the region very near the second slot; the largest skin friction reduction occurs with higher injection rates from the first slot.

3. Effects of Slot Height and Multiple Slot Injection

The present experimental results for single slot injection with $S = 0.318$ cm and $S = 0.636$ cm and with approximately the same injection mass flow rate were compared in Fig. 40. Larger reduction in surface skin friction in $x/S \leq 5$ was found for large injection slot height. The local surface skin friction, C'_{fo} without slot injection and with a slot height $S = 0.318$ cm was also measured and shown in this figure. The skin friction approximately equals the value without the existence of the injection slot for $x/S \approx 10$. Slot injection reduces the surface skin friction within a region of $x/S \leq 40$ and the surface skin friction approaches as asymptotic value defined by the injection slot for $x/S \geq 40$.

From the present two slot arrangement, results of the experiment did not show any significant reduction in skin friction due to the first slot injection. It is believed that the distance between the two slots should be reduced. Based on the single slot injection results, Fig. 29, the second slot should be located at $x/S \approx 30$ to further reduce the skin friction downstream of the second injection slot.

V. CONCLUSION

An experimental investigation of the surface skin friction reduction downstream of tangential slot injection from one and two slots has been performed. Boundary layer profiles (velocity, static pressure, total pressure), turbulence intensity and surface skin friction with various slot injection mass flow rates, were measured with a hot film probe, a boundary layer pressure probe, and a floating-element surface skin friction balance, respectively. The following conclusions have been derived from the present experimental results.

1. Tangential slot injection in a transonic main stream ($M_\infty \approx 0.8$) generally reduces the surface skin friction downstream of the injection slot. The effective region for $C_f/C_{fo} < 1$ was independent of the slot dimension for the present tests and equals ≈ 40 slot heights. It is concluded that the total drag reduction obtained due to slot injection at transonic flow is of the same order as that obtained in the hypersonic regime.

2. Slot injection does not continuously decrease the surface skin friction as the injection mass flow rate increases. A significant difference in the effect of injection mass flow rate on skin friction in a region of $x/S < 5$ and in a region of $x/S > 5$ has been found. Increasing the slot mass flow seems to increase the skin friction in the region of $x/S < 5$. The present tests indicated a maximum reduction of skin friction for $\lambda \approx 0.2$.

3. Large turbulence intensity was found near the slot with small injection mass flow rate. Increasing the injection mass flow rate decreases the turbulent intensity near the slot exit and moves the region of higher turbulent intensity downstream of the slot. This higher turbulence region (recirculation region) disappears with a large injection mass flow rate ($\lambda \geq 0.3$).

4. Large normal pressure gradients were found in the region near the slot for low λ. The surface pressure distributions seem to be sensitive to injection flow rates in the transonic region. Due to large normal pressure gradient, surface pressure measurement downstream of the slot is not sufficient for determining the flow field with injection mass flow rate less than 0.2.

5. The effect of slot height on the surface skin friction reduction with injection is insignificant except for a region very near the slot. From the results of two slot injection experiment, it is believed the distance between the two slots should be less than 30 slot heights in order to further reduce the surface skin friction downstream of the second slot.

APPENDIX I: SKIN FRICTION GAUGE

1. Floating Element Skin Friction Balance

The floating element skin friction balance is a 322 M 105 model made by Kistler Instrument Corporation. It is a servo-mechanism system which measures aerodynamic drag produced by the airflow along the wall of a wind tunnel. It consists of two units: a sensor which mounts in the wall of the wind tunnel, and an amplifier and signal conditioning unit. The two units are connected with a multiple conductor cable. The overall unit has been loaned to New York University for this investigation. The complete calibration has been performed at NASA.

The sensor includes a circular end cap which matches the curvature of the interior wall of the test section of the wind tunnel (Dia = 30.48 cm) and is mounted flush with that surface. In its center, a circular portion separation from the end cap by a small annular clearance is mounted with a single degree of freedom in the direction of airflow. Friction of the airflow on the moving portion displaced it downstream, producing a signal which is amplified and returned to the servo-mechanism to restore the moving portion to its null position. The magnitude of the restoring signal is a precise measure of the drag exerted on the moving portion. The amplifier and signal conditioning unit supplies operating power to the system, provides three ranges of amplification with the necessary zero and gain controls, and enables the application of the test and calibration signals to the sensor. The basic gauge is internally ranged to produce an output of 1 volt with a

measure of 10.0 g/cm^2, at an impedence level of 1000 ohms. This output is supplied to the amplifier. A series resistor in the amplifier operates in the current input mode. The range selector switch inserts one of three values of current feedback resistor for gains of 10, 1, or 0.1 to provide full scale output of 100 mv on each range. Two independent, isolated, voltage regulated power supplies are contained in the amplifier case, one for the range amplifier and the other for the self testing circuitry. The self test portion consists of a voltage divider network, a selector switch, and an amplifier. Self test voltages are stabilized by a zener diode. Selected voltages from the divider network are applied to the amplifier and converted to constant current output which energizes a test coil in the gauge, simulating application of the measurement to the sensor.

a. Calibration

The skin friction balance has been calibrated by the NASA Langley Research Center before it was delivered to the NYU Aerospace and Energetics Laboratory for the present transonic wind tunnel experiment. Calibration levels are 100%, 75%, 50%, and 25% of full scale on each of three ranges, 10 gm/cm^2, $1gm/cm^2$, and 0.1 gm/cm^2. The moment arm at point of applied calibration load is 0.815 cm. The moment arm at surface is 0.794 cm. The area of the sensing element is 0.694 cm^2. Results of the calibration are shown in Figs. I2-I4. The linearity deviation is only $\pm$ 0.5% of calibrated range. The repeatability is within $\pm$ 0.1% full scale for each local range.

For the present experiment, calibrations within the range of 1.0 gm/cm^2 is sufficient to cover the range of surface skin friction. The amplifier output of 50% self test load is adjusted over 25.4 cm (10 in.)

span on a Honeywell multichannel visicorder. This gives a linear scale of 0.0504 gm/cm^2/in. in output.

2. Hot Film Skin Friction Gauge

Recent research in turbulence has shown that a flush mounted hot film sensor is a powerful device in measuring both the mean and fluctuating components of the wall shearing stress. However, accurate calibration is required for the measurement of mean shearing stress. Previous studies, Ref. 6, have performed the calibration of a flush mounted hot film sensor using a 40 foot 4 inch diameter stainless steel pipe. The relation between the wall shearing stress and the pressure drop of a fully developed pipe flow was used. Experimental correlation between wall shearing stress and the anemometer D.C. voltage output, similar to the results of Ref. 7, was obtained for small mean flow velocity less than 3 m/sec.

For the present research effort, a more elaborate calibration system was used. The present testing apparatus is an excellent set up to further investigate the use of a flush mounted hot film probe for surface skin friction measurements. The floating-element skin friction balance was used as standard for the calibration of the hot film gauge. A flush mounted flat surface hot film sensor (Thermal-System Model 1237) was calibrated in the present experiment. Results are described in the following discussion.

a. Calibration

The hot film gauge was flush mounted in the center of an annual steel piece similar to the floating balance. Fig. 15, in order to match the curvature of the interior wall of the wind tunnel. The surface strip of the film sensor is 0.012 cm wide by 0.1 cm long and was perpendicular to

the mean flow direction. The gauge was connected to the Thermal-System 1050 anemometer. The wind tunnel setups are similar to that of the slot injection experiments.

The gauge and the floating-element skin friction balance were placed close to each other at the location of $x/S \simeq 100$ ($S = 0.318$ cm). The tunnel was operated at various constant stagnation pressures so that different surface shearing stress corresponding to different free stream velocity (and Reynolds number) could be obtained. Calibration results are given in Fig. I6.

b. Discussion and Application

From the calibration data, correlation between the wall shearing stress and the D.C. anemometer voltage outputs are shown in Fig. I7. Linear correlation similar to that of low speed flow, Ref. 6, could not be found from the present results. However, the present data could be approximated by $E_b^2 = 23.6\ \tau_w^{1/3} + 157$. Previous analysis, Ref. 6, assumed that the thermal layer is much thinner than the viscous sublayer. To assure this situation, a quantitative criterion required specifically

$$(u_* \ell/\nu) < 64(Pr)$$

in order to satisfy the linear correlation given in Ref. 7 . For the present calibration, the Reynolds number, $(u_*\ell/\nu)$, is approximately 300 (Pr).

The use of the hot film gauge has several advantages over the floating skin friction gauge. The response is much faster (order of millisecond), and in addition it provides data on fluctuating shear stress as will be shown in the next section.

Theories of the buildup and decay of sublayer can be found in Refs. 8 and 9, The unsteady Navier-Stokes equation for flow of a thin layer along a flat plate was used to describe the theoretical model of the sublayer development. The velocity gradient in the sublayer has been given as:

$$\frac{du}{dy} = \frac{u_o}{\sqrt{\pi \nu t}} \text{ Exp. } (-y^2/4\nu t)$$

at the surface, y = 0

$$\frac{du}{dy}\Big|_{y=0} = u_o/(\sqrt{\pi \nu t}) \tag{1}$$

and the size of the sublayer thickness at anytime, t, is given by

$$y_s = (2\sqrt{\nu t})/\pi \tag{2}$$

In the calibration of the present flush mounted hot film gauge, the RMS voltage output has also been measured. It is intended to find an experimental correlation between the surface velocity gradient and the RMS output from the present measurements. The following assumptions were made: a) the theoretical model in Ref. 8, is valid for the present study, b) the sublayer thickness can be estimated by $(y_s u_*/\nu) = 10$, and c) the flow velocity u_o at the edge of the sublayer is given by $u_o/u_* = 5.5 + 2.5 \times \ell n\ (y_s u_*/\nu) = 11.25$.

The friction velocity, $u_* = \sqrt{\tau_w/\rho}$, was computed from the measured shearing force and values of y_s and u_o were obtained with the assumptions b) and c). Substituting these values into equations (1) and (2), the velocity gradient at the surface was found. These results are shown in Fig. I8 and a linear correlation between the velocity gradient and RMS output, $(du/dy)_{y=0} = 1.1 \times 10^7 \sqrt{\overline{e^2}}$, has been obtained.

The hot film gauge was also used to measure the surface skin friction due to slot injection. Tests with $\lambda_1 = 0.218$ were repeated to verify the accuracy of probe calibration. Results of skin friction factors are compared with floating skin friction balance outputs in Fig. I9. Similarly, the surface velocity gradients at different x/S obtained from the theory and the present experimental linear correlation are given in Fig. I-10.

It is concluded that the flush mounted hot film gauge can be used to measure the skin friction and the surface velocity gradient with a repeatability within 10%. However, the present calibration of the hot film probe has been limited to a free stream velocity between 200 and 300 meter per second and depended heavily on the calibration with the floating-element balance. The coefficient in the linear correlation of the velocity gradient depends on the assumption of the velocity at the edge of the sublayer. More experimental data over a large variation in free stream conditions are required for further studies.

APPENDIX II: HOT FILM PROBE

Hot wire probes, hot film probes, and anemometers have been used in detailed analysis of fluid flow. The most common hot wires are made of tungsten, platinum, and platinum-iridium alloy. A hot film probe uses a conducting film on a ceramic substance or a quartz rod with a platinum film on the surface. Gold plating on the ends of the rod isolates the sensitive area and provides a heavy metal contact for fastening the sensor to the support. The hot film probe sensor is shorter that the hot wire sensor and with a larger diameter and is particularly helpful in reducing the breakage of the sensor due to impact of the flow.

For the present experiment, special hot film probes and a Thermal-System 1050 constant temperature anemometer were used to measure the mean velocity and turbulence intensity. This hot film probe, Fig. II-1, had a cylindrical alumina coated film sensor 1.78 cm in front of the stainless steel body. The sensor had a diameter of 0.005 cm and was 0.025 cm long. The distance between supports was 0.076 cm. The probe resistance at room temperature was 5.57 ohms and was operated with 1.5 over-heat ratio.

a. Calibration

The usual relationship between the electrical power to the sensor and the velocity past the sensor is given by:

$$E^2 \sim [A + B(\rho u)^{1/n}] (T_s - T_e) \qquad (3)$$

The original work done by King, Ref. 10, indicated that n = 2, giving the typical power relationship between velocity and the voltage on the anemometers bridge. Constants A and B are function of density.

For a single wire normal to a flow, the relation between the local turbulence intensity and the anemometer bridge output can be written as:

$$\sqrt{\overline{u'^2}}/u = (1/n)\ [2E\sqrt{\overline{e^2}}/\ (E_b^2 - E_{bo}^2)] \qquad (4)$$

In order to correct the effect of the density, the calibration of the present hot film probe was performed with DISA type 55D41/42 calibration wind tunnel for a range of velocity between 0 and 100 m/sec. For flow velocity over 100 m/sec ($M \approx 0.3$), the hot film probe was calibrated by a wind tunnel especially built to operate in a range of M = 0.3 to 0.8. The characteristic of the DISA calibration wind tunnel for the velocity and dynamic pressure, Δp, is shown in Fig. II-2. Together with the anemometer bridge voltage output, the nonlinear calibration between the flow velocity and D.C. voltage output of the probe was found, Fig. II-4. Result of the linear calibration is also shown in this figure.

For turbulence intensity, Eq. (4) has been used to calculate the intensity based on the anemometer outputs of D.C. voltage and the RMS values of each test. In order to have accurate nonlinear anemometer outputs to determine the turbulence intensity, the stability effect has been optimized by a built-in square wave.

REFERENCES

1. Parthasarathy, K. and Zakkay, V., "An Experimental Investigation of Turbulent Slot Injection at Mach 6," AIAA Journal, Vol. 8, No. 7, July 1970, pp. 1302-1307.

2. Cary, A.M., Jr., and Hefner, J.N., "Film-Cooling Effectiveness and Skin Friction in Hypersonic Turbulent Flow," AIAA Journal, Vol. 10, No. 9, December 1972, pp. 1188-1192.

3. Beckwith, I.E. and Bushnell, D.M., "Calculation by a Finite Difference Method of Supersonic Turbulent Boundary Layers with Tangential Slot Injection," NASA TN D-6221, 1971.

4. Love, E.S., "Base Pressure at Supersonic Speeds on Two-Dimensional Airfoils and on Bodies of Revolution with and without Fins Having Turbulent Boundary Layer," NACA TN 3819, January 1957.

5. Chapman, D.R., "An Analysis of Base Pressure at Supersonic Velocities and Comparison with Experiment," NACA Rep. 1051, 1951.

6. Geremia, J.O., "An Experimental Investigation of Turbulence Effects at the Solid Boundary Using Flush Mounted Hot Film Sensors," Ph.D. Dissertation and also Engineering Department Report 70-2, United States Naval Academy, January 1970.

7. Liepmann, H. and Skinner, G., "Shearing Stress Measurements by Use of a Heater Element," NACA TM-3268, 1954.

8. Einstein, H.A. and Li, H., "The Viscous Sublayer Along a Smooth Boundary," A.S.C.E. Transactions, Vol. 123, 1958.

9. Black, T.J., "A New Model of the Shear Stress Mechanism in Wall Turbulence," AIAA Paper No. 68-42, Jan. 1968.

10. King, L.V., "On the Convection of Heat from Small Cylinders in a Stream of Fluid," Proc. Roy. Soc. (London), Vol. 214A, No. 14, 1914, p. 373.

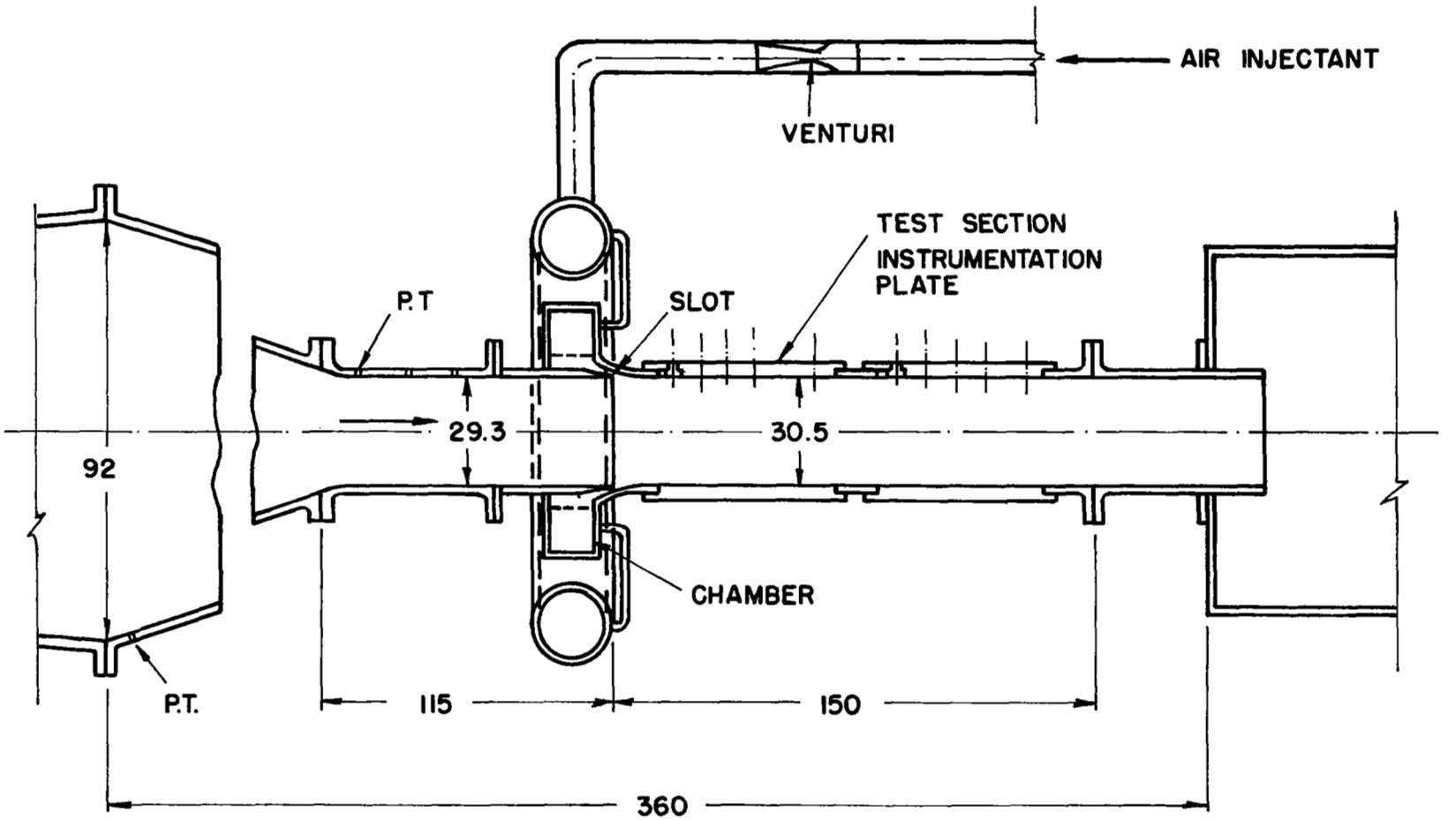

DIMENSIONS IN CM.

Fig. 1 Wind tunnel setup for single slot injection, s = 0.636 cm

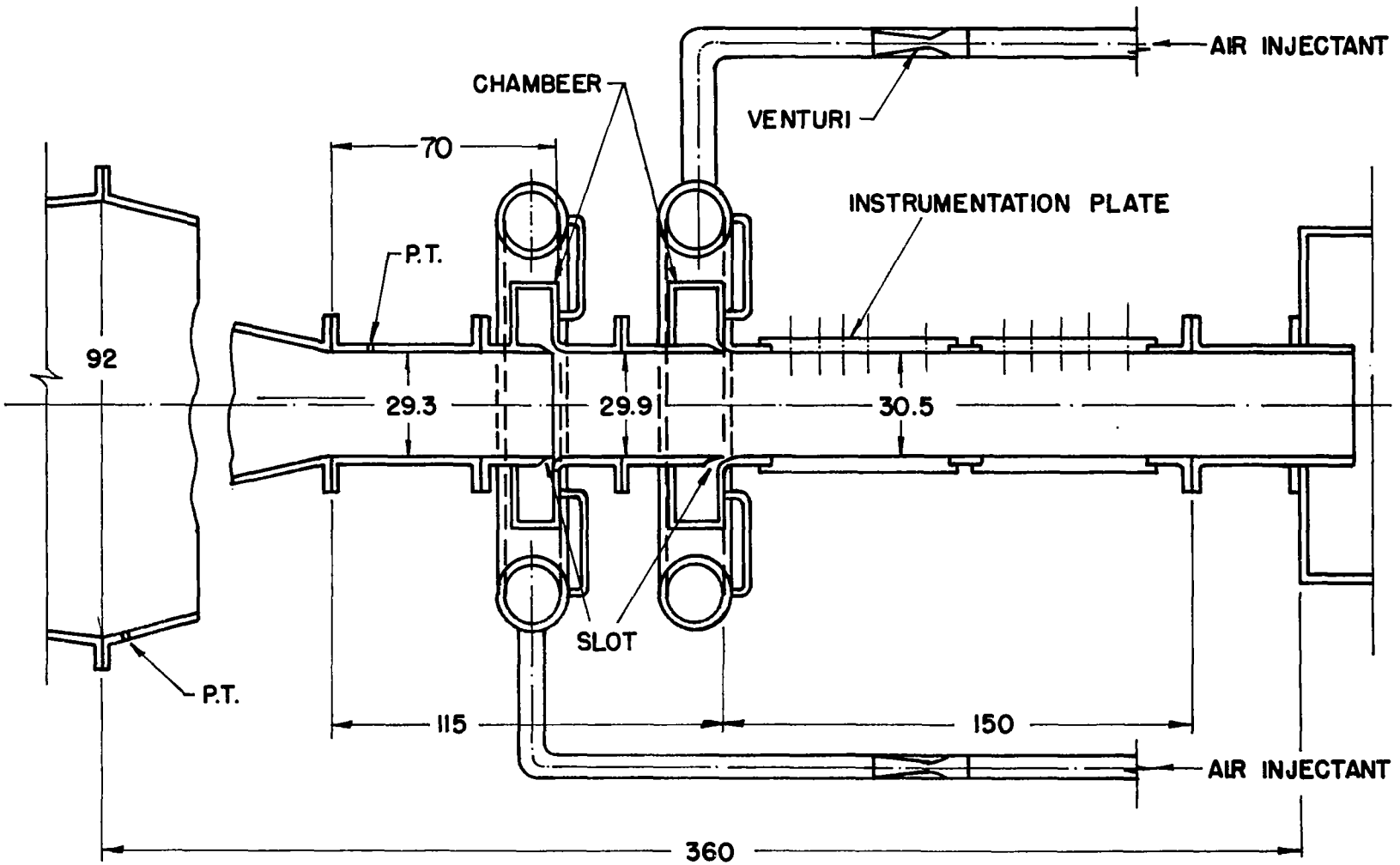

DIMENSIONS IN cm.

Fig. 2 Wind tunnel setup for two slot injection, s = 0.318 cm

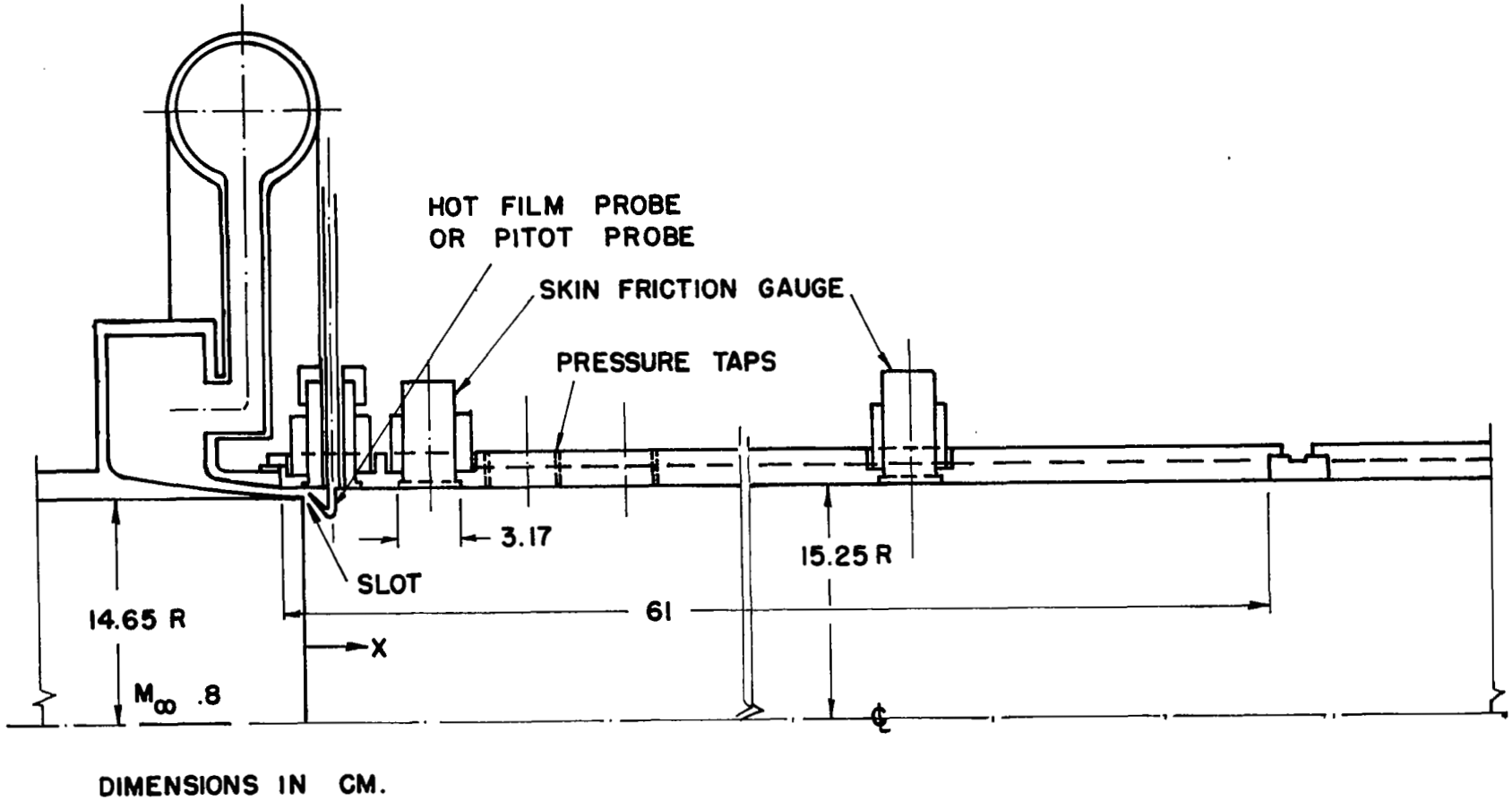

Fig. 3 Detail of the injection slot and the test section, s = 0.636 cm

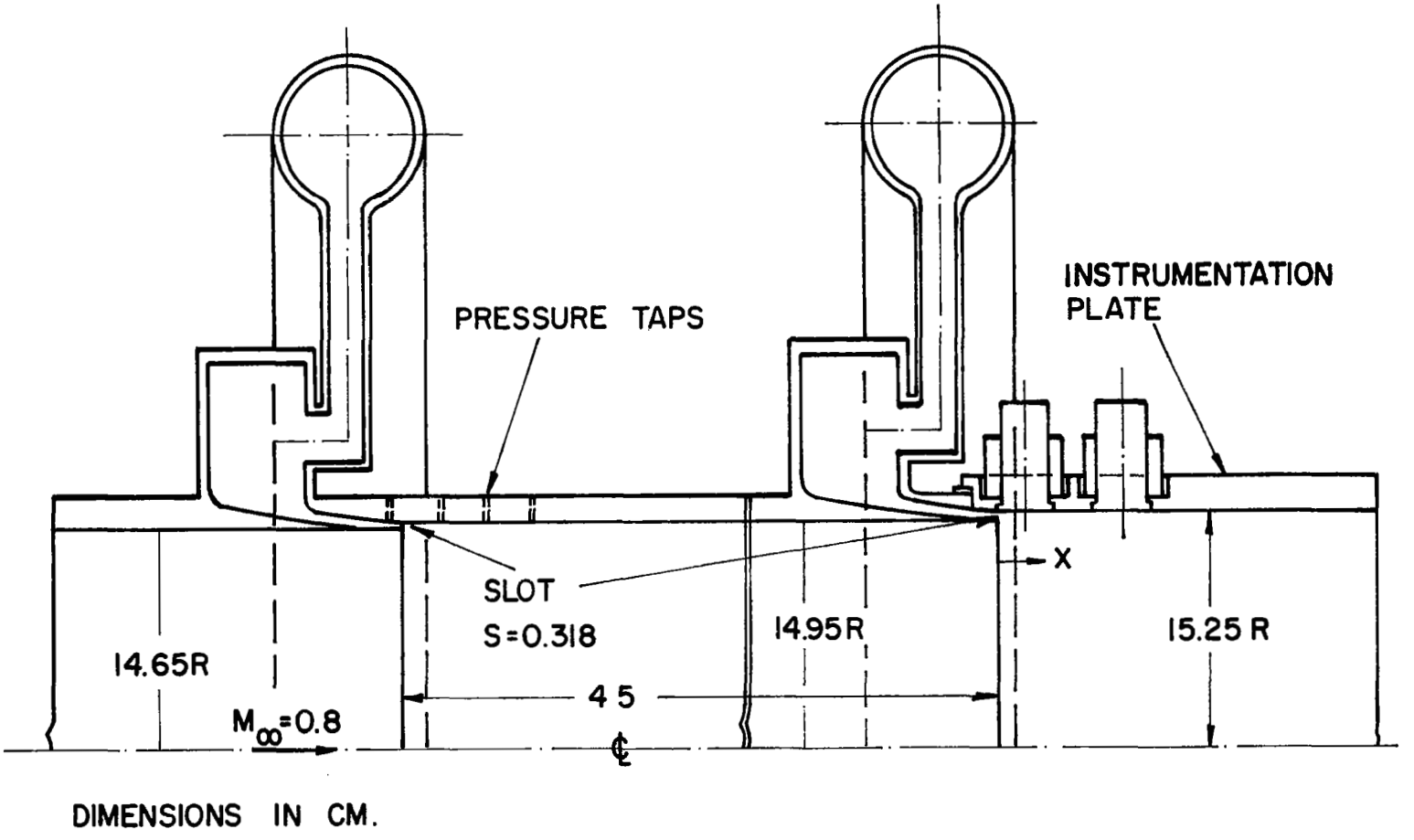

Fig. 4 Detail of the injection slots and the test section, s = 0.318 cm

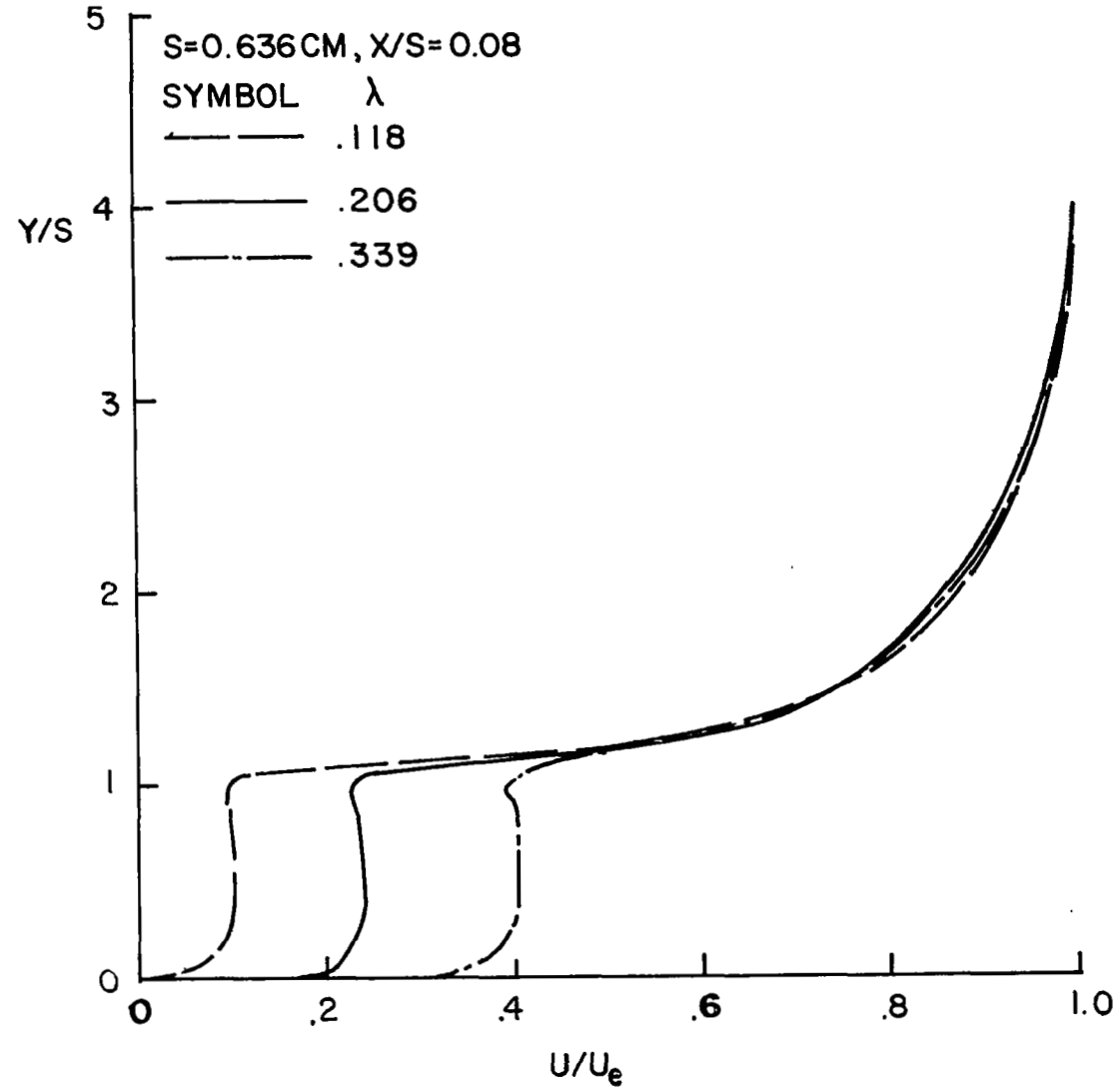

Fig. 5 Boundary layer velocity profiles due to single slot injection

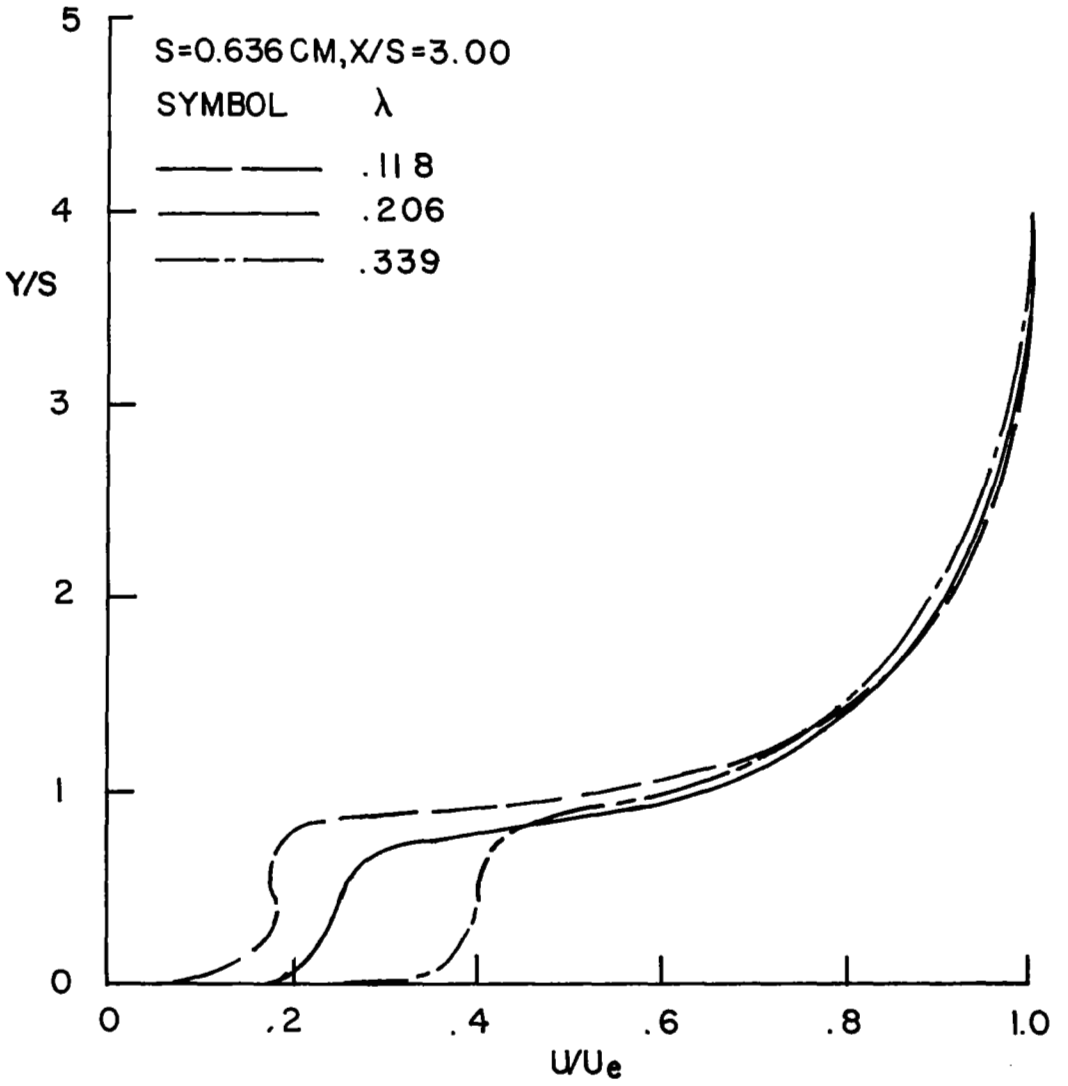

Fig. 6 Boundary layer velocity profiles due to single slot injection

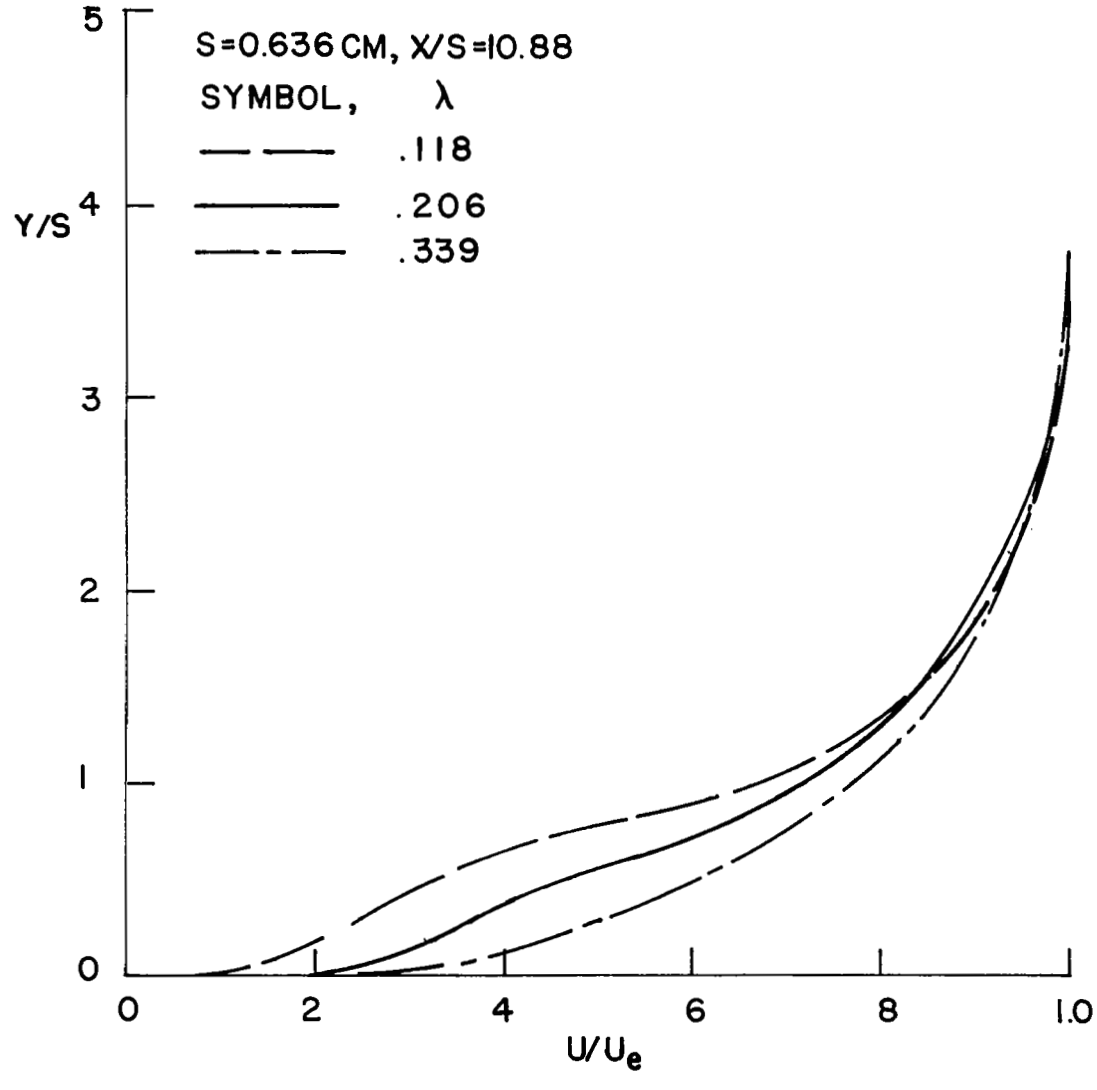

Fig. 7 Boundary layer velocity profiles due to single slot injection

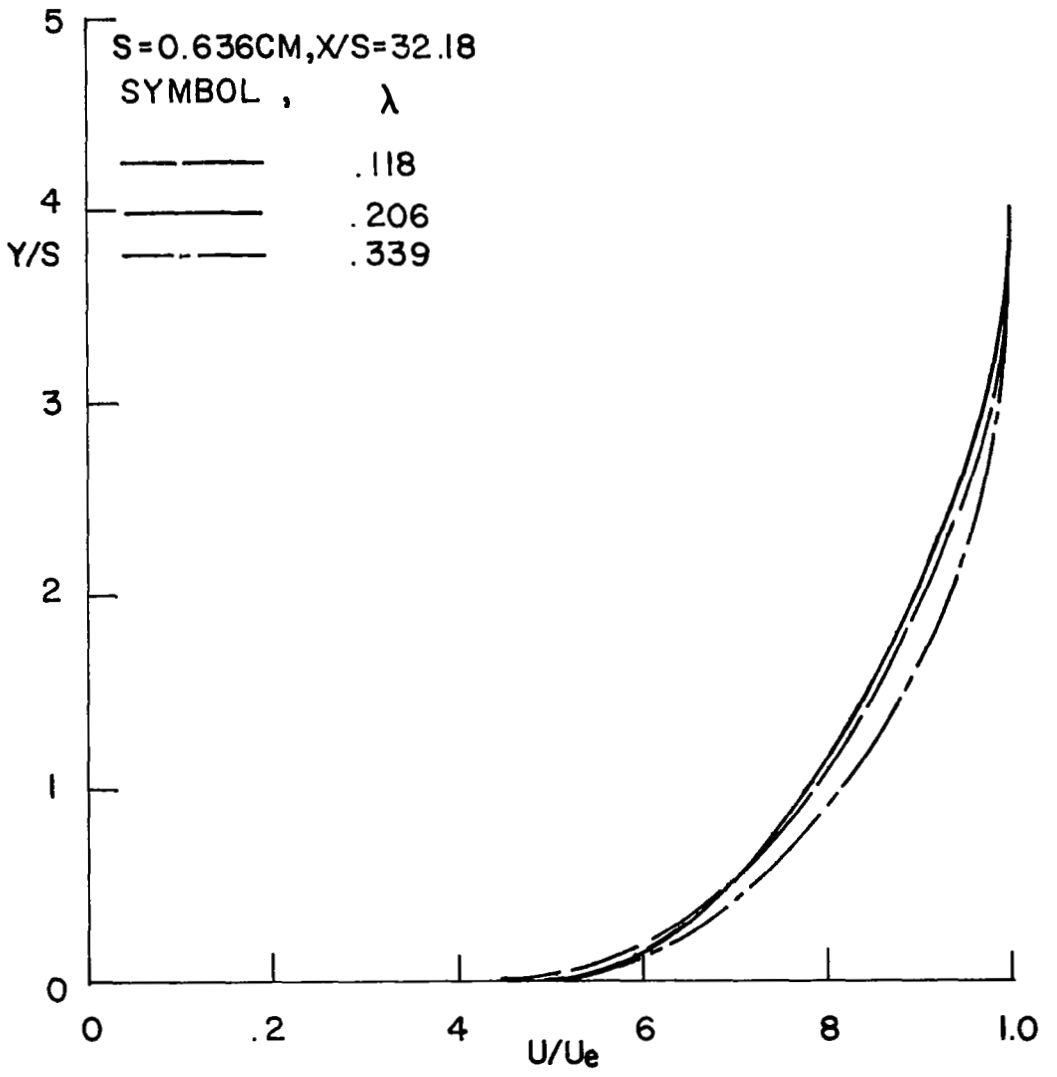

Fig. 8 Boundary layer velocity profiles due to single slot injection

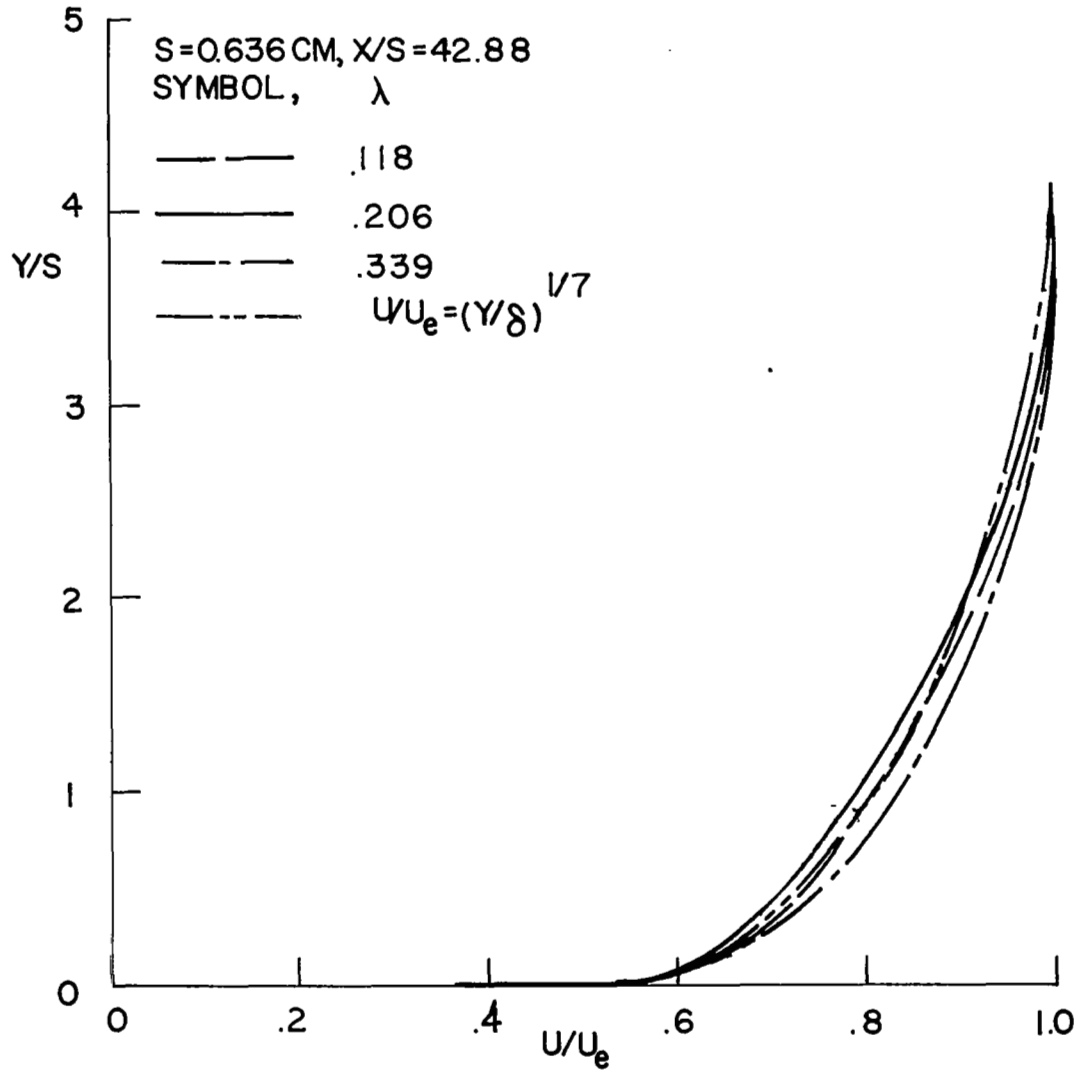

Fig. 9 Boundary layer velocity profiles due to single slot injection

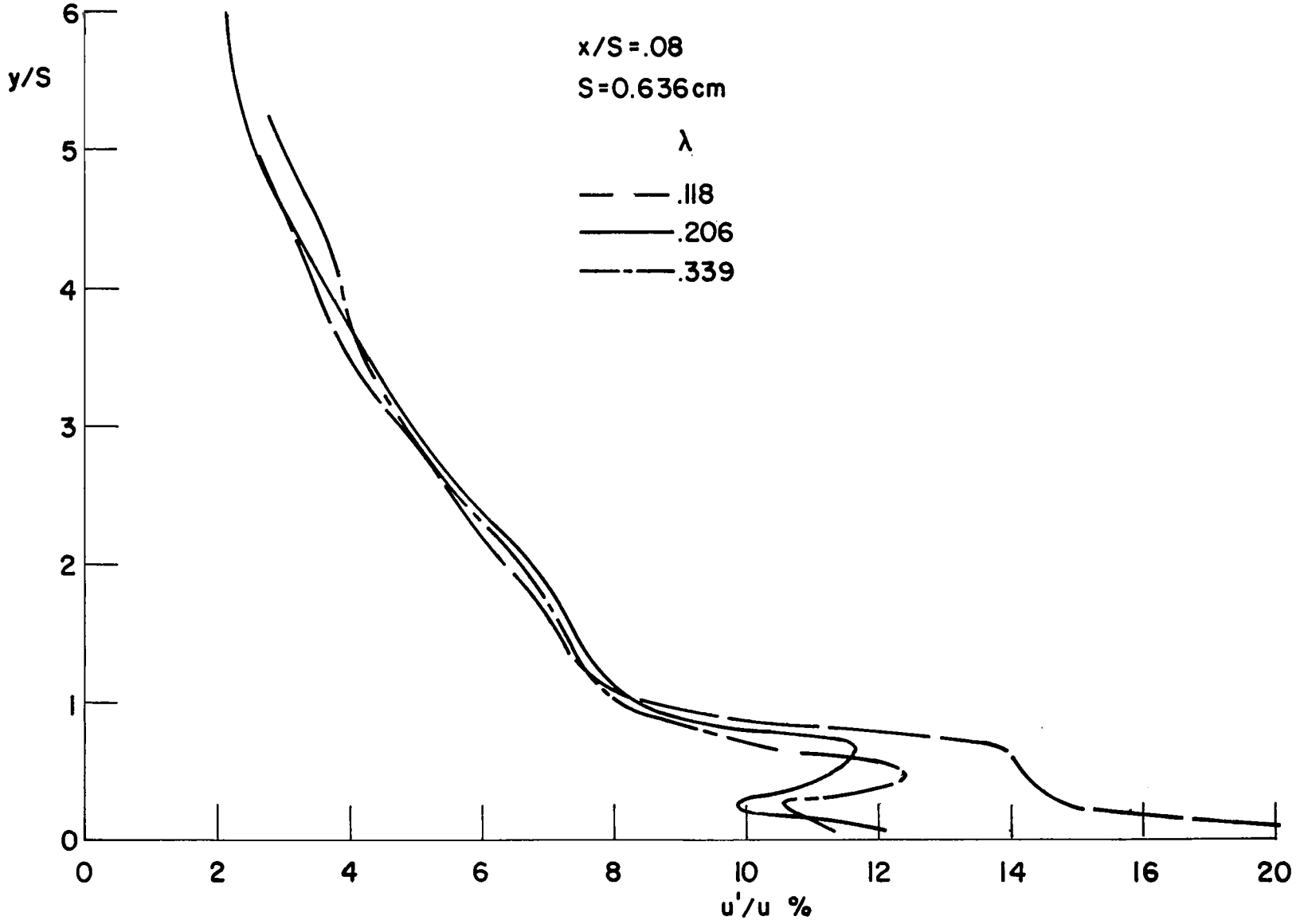

Fig. 10 Boundary layer turbulence intensity profiles due to single slot injection

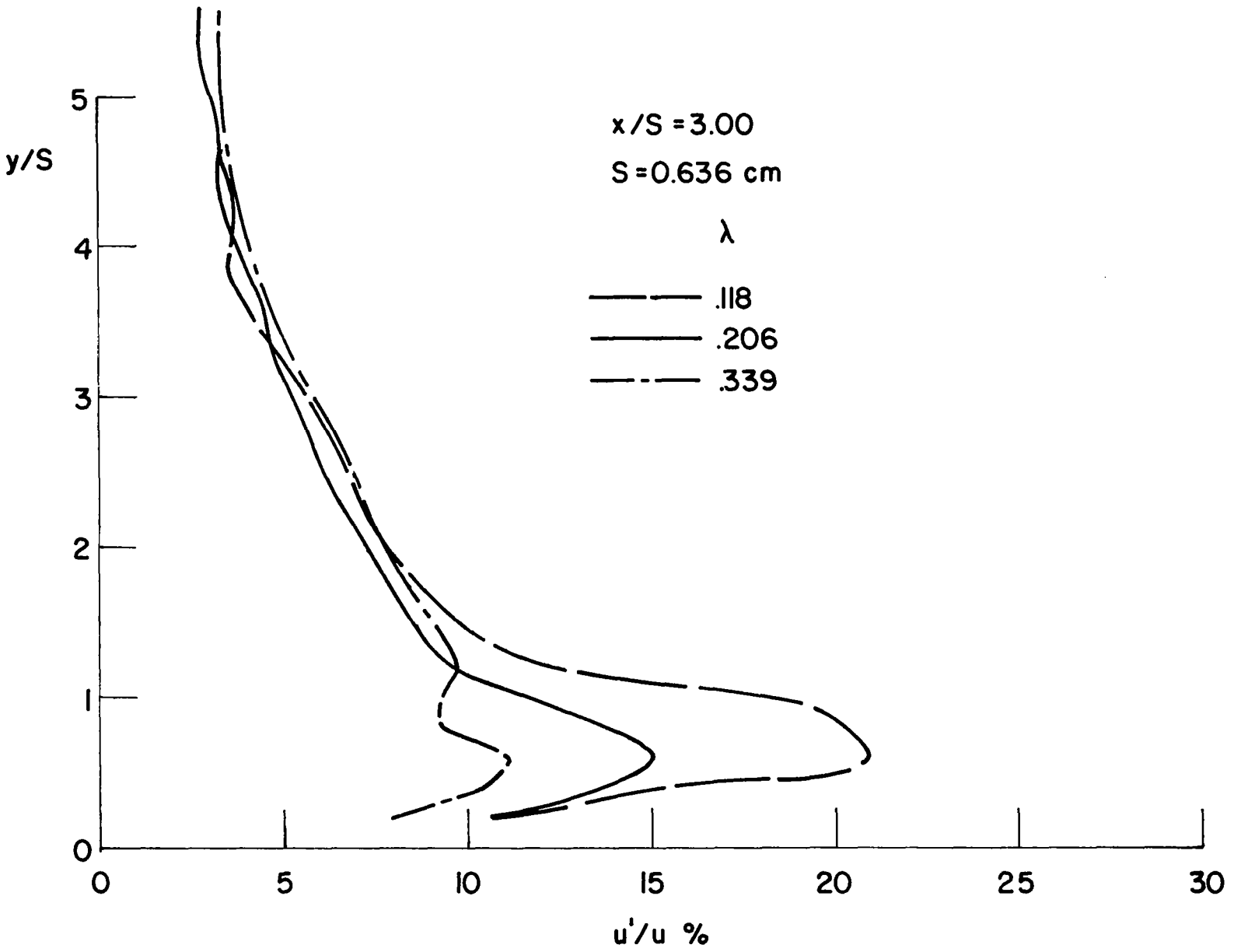

Fig. 11 Boundary layer turbulence intensity profiles due to single slot injection

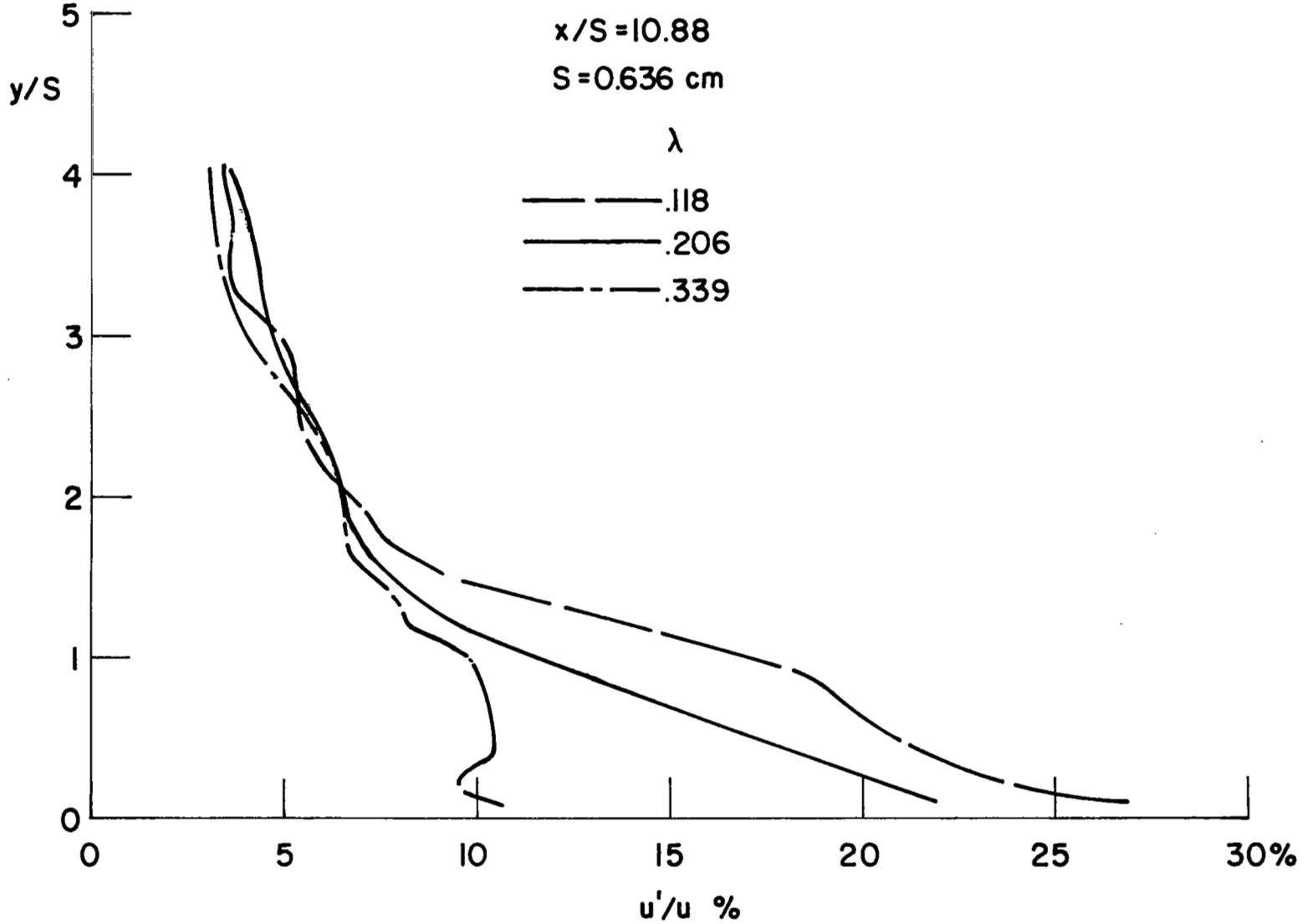

Fig. 12 Boundary layer turbulence intensity profiles due to single slot injection

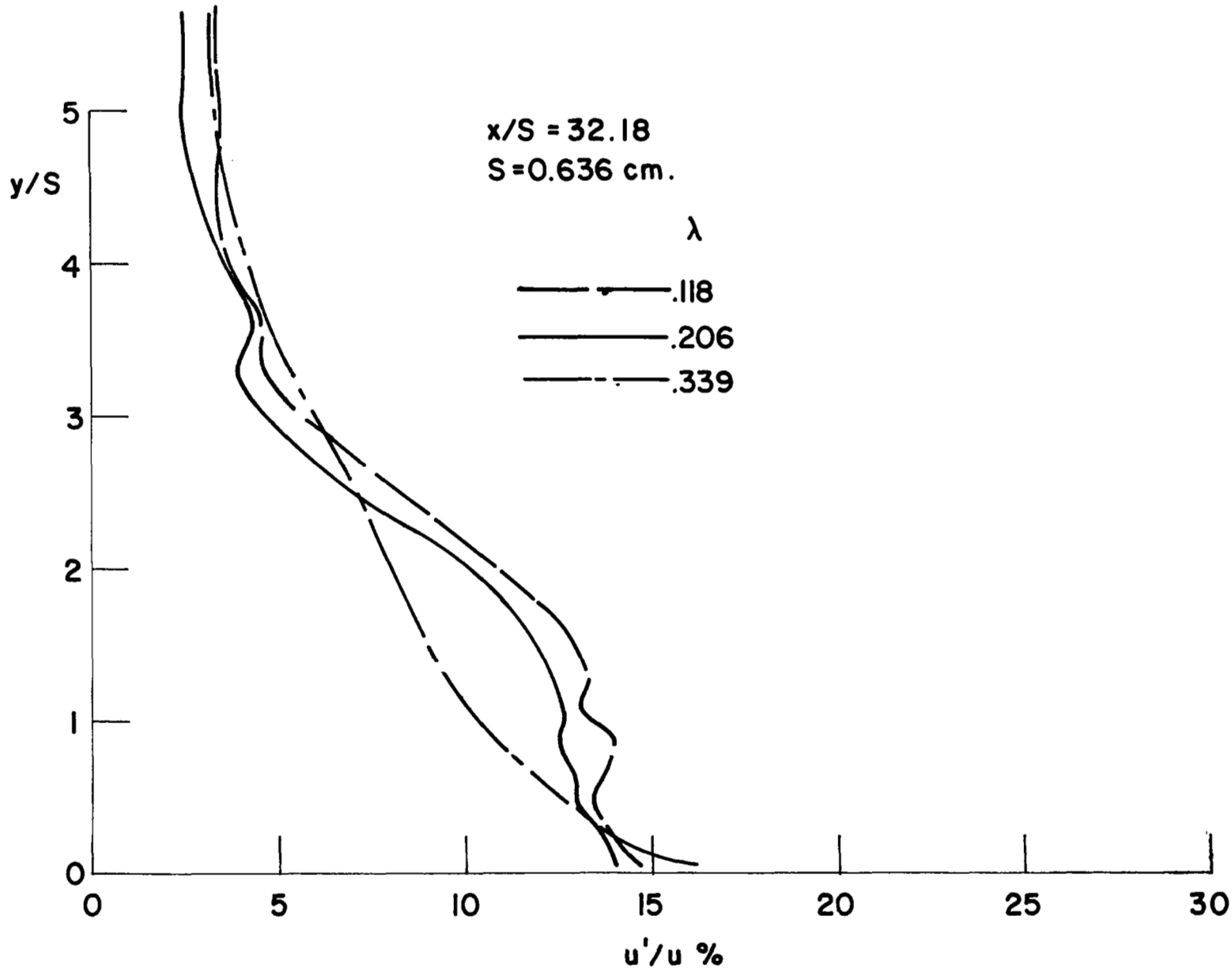

Fig. 13 Boundary layer turbulence intensity profiles due to single slot injection

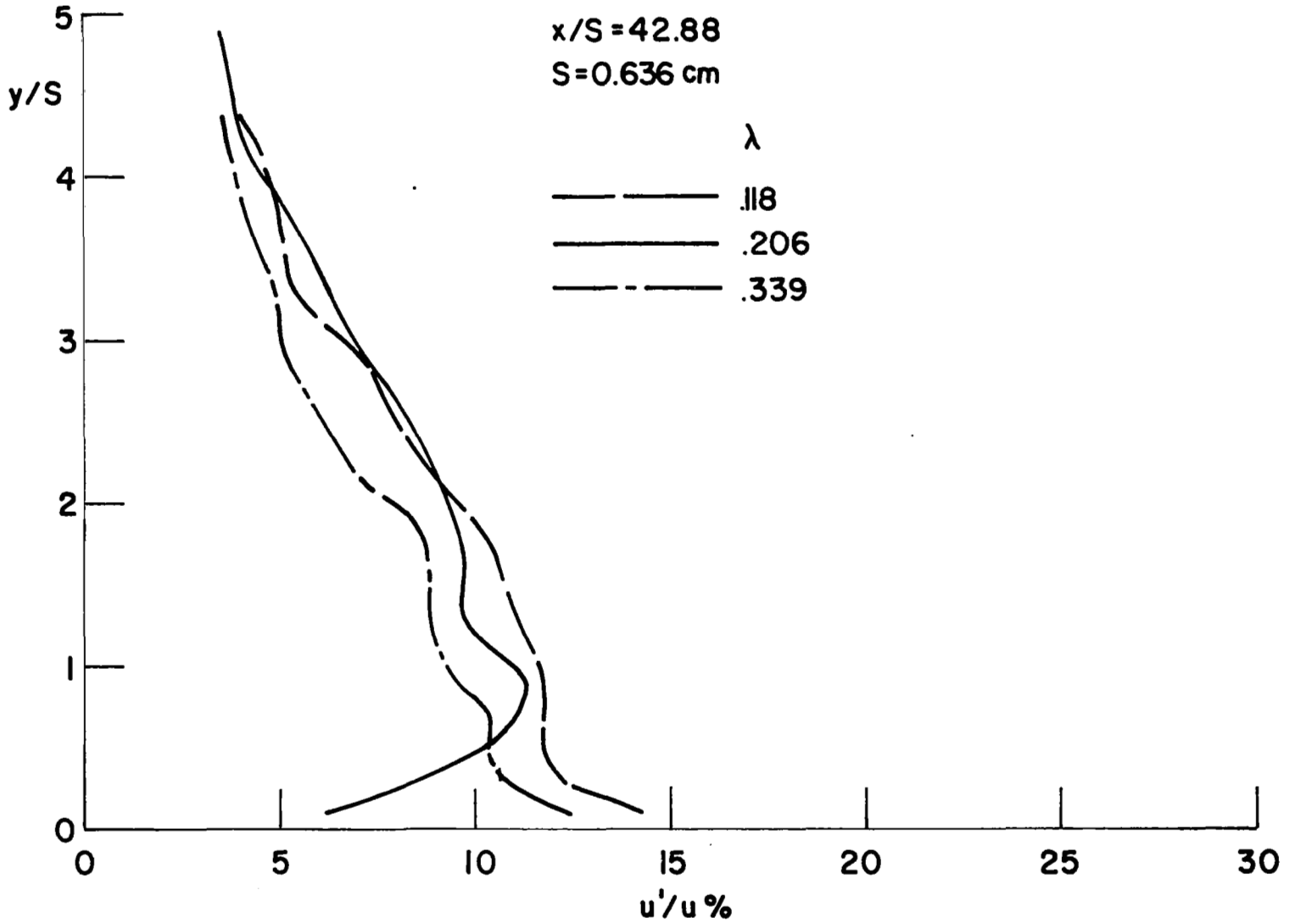

Fig. 14 Boundary layer turbulence intensity profiles due to single slot injection

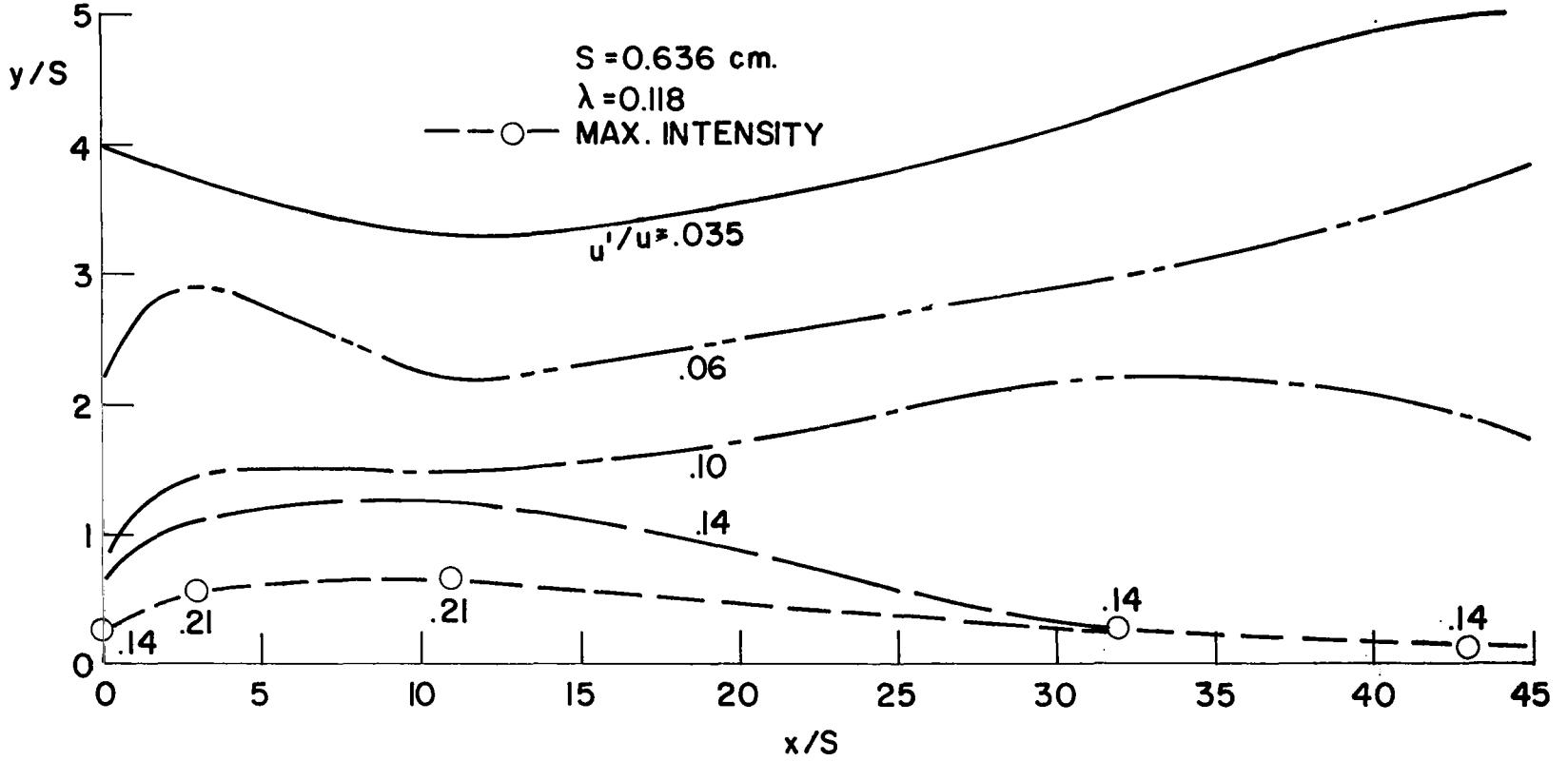

Fig. 15 Isocoutour of turbulence intensity due to single slot injection

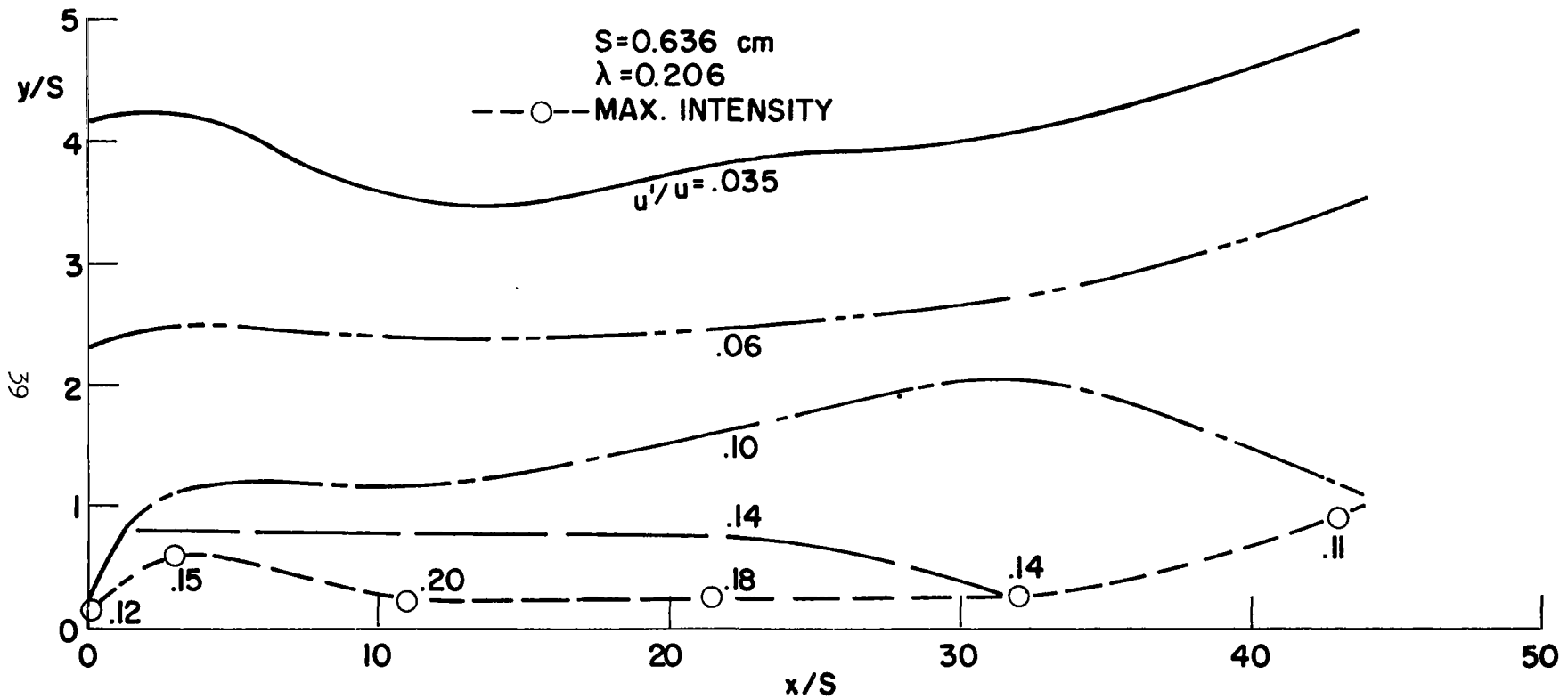

Fig. 16 Isocoutour of turbulence intensity due to single slot injection

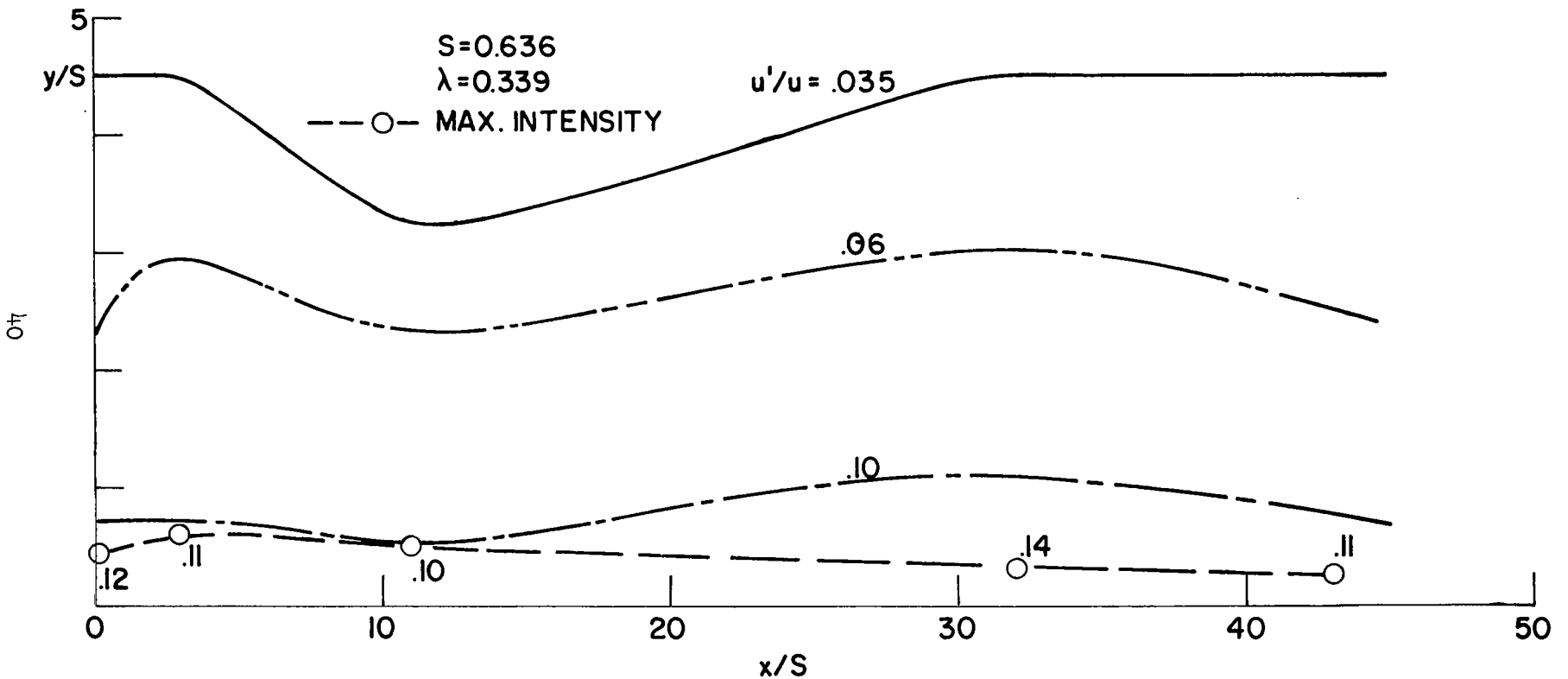

Fig. 17 Isocoutour of turbulence intensity due to single slot injection

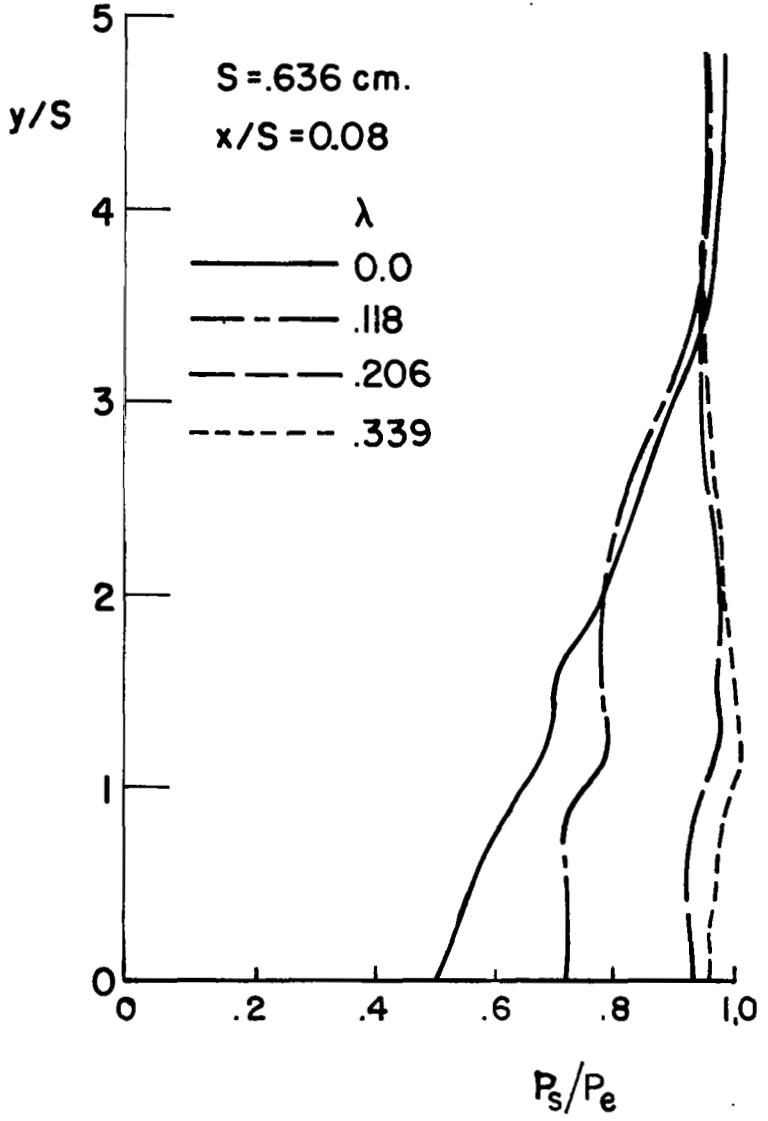

Fig. 18 Boundary layer profiles of static pressure due to single slot injection

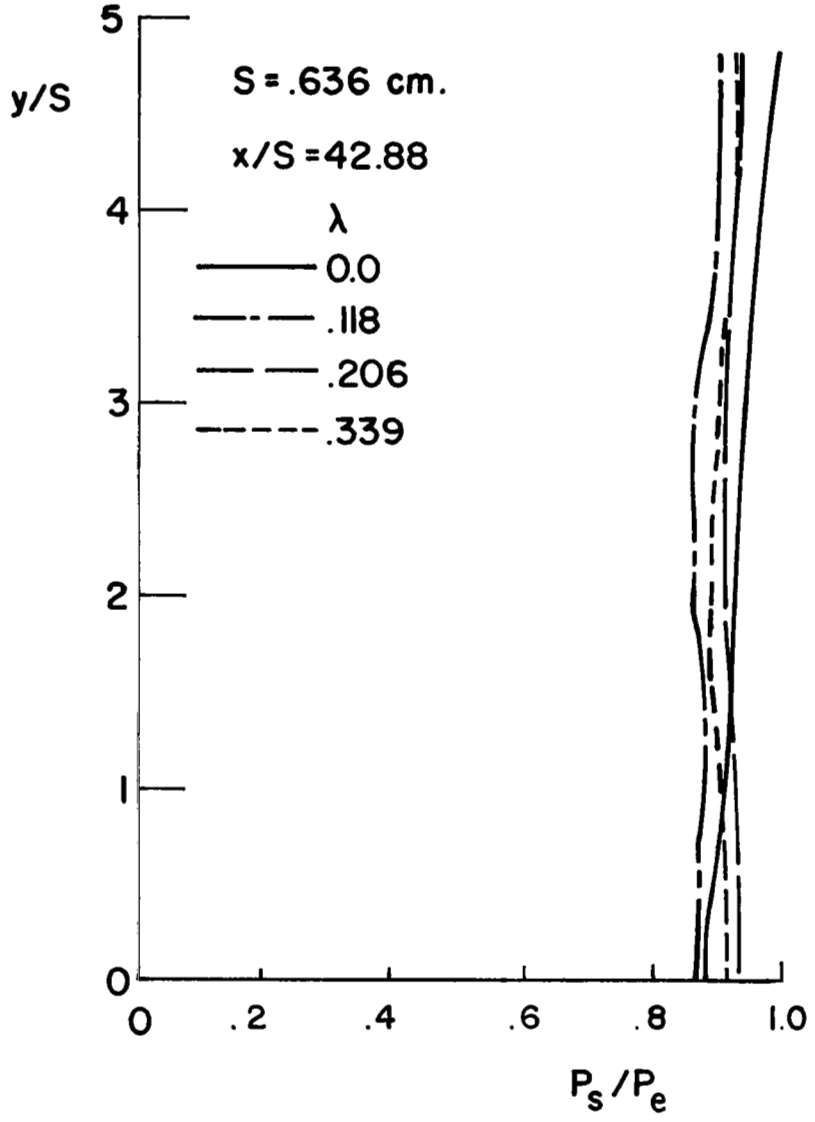

Fig. 19 Boundary layer profiles of static pressure due to single slot injection

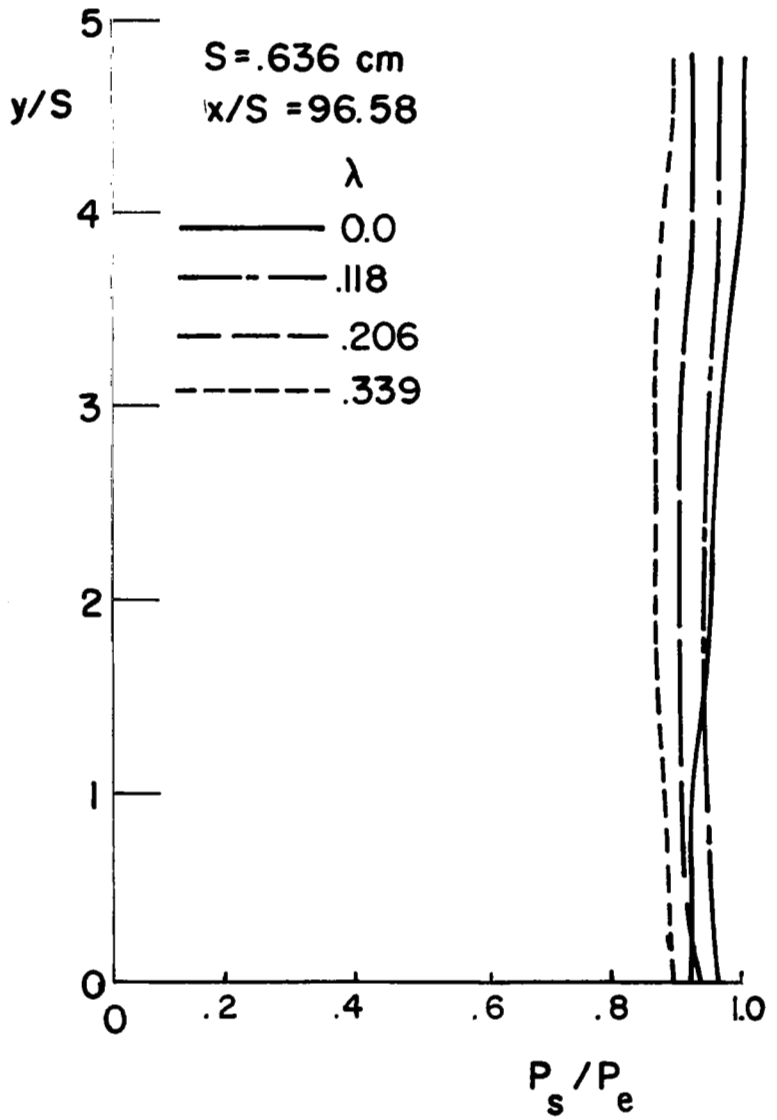

Fig. 20 Boundary layer profiles of static pressure due to single slot injection

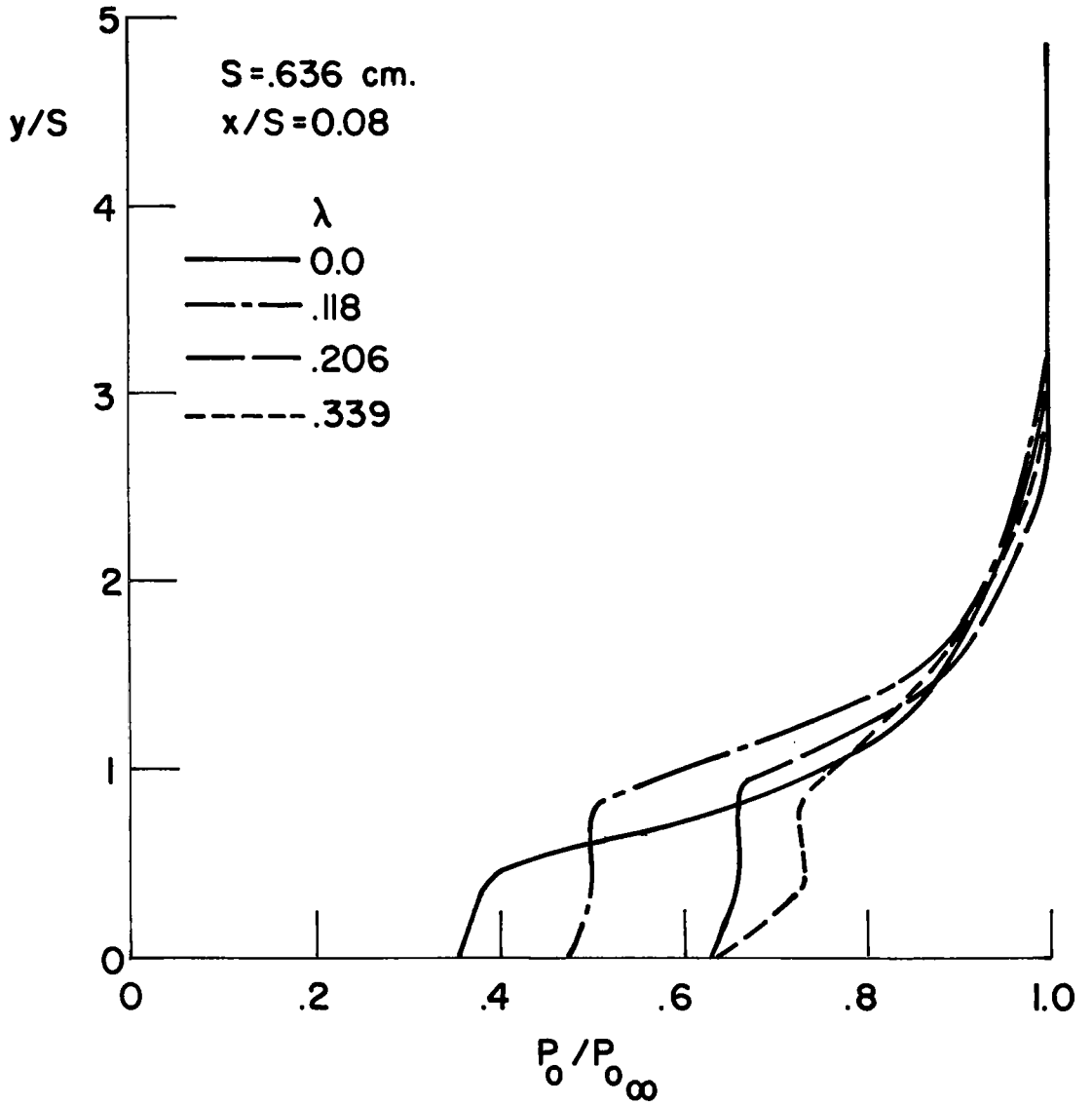

Fig. 21 Boundary layer profiles of total pressure due to single slot injection

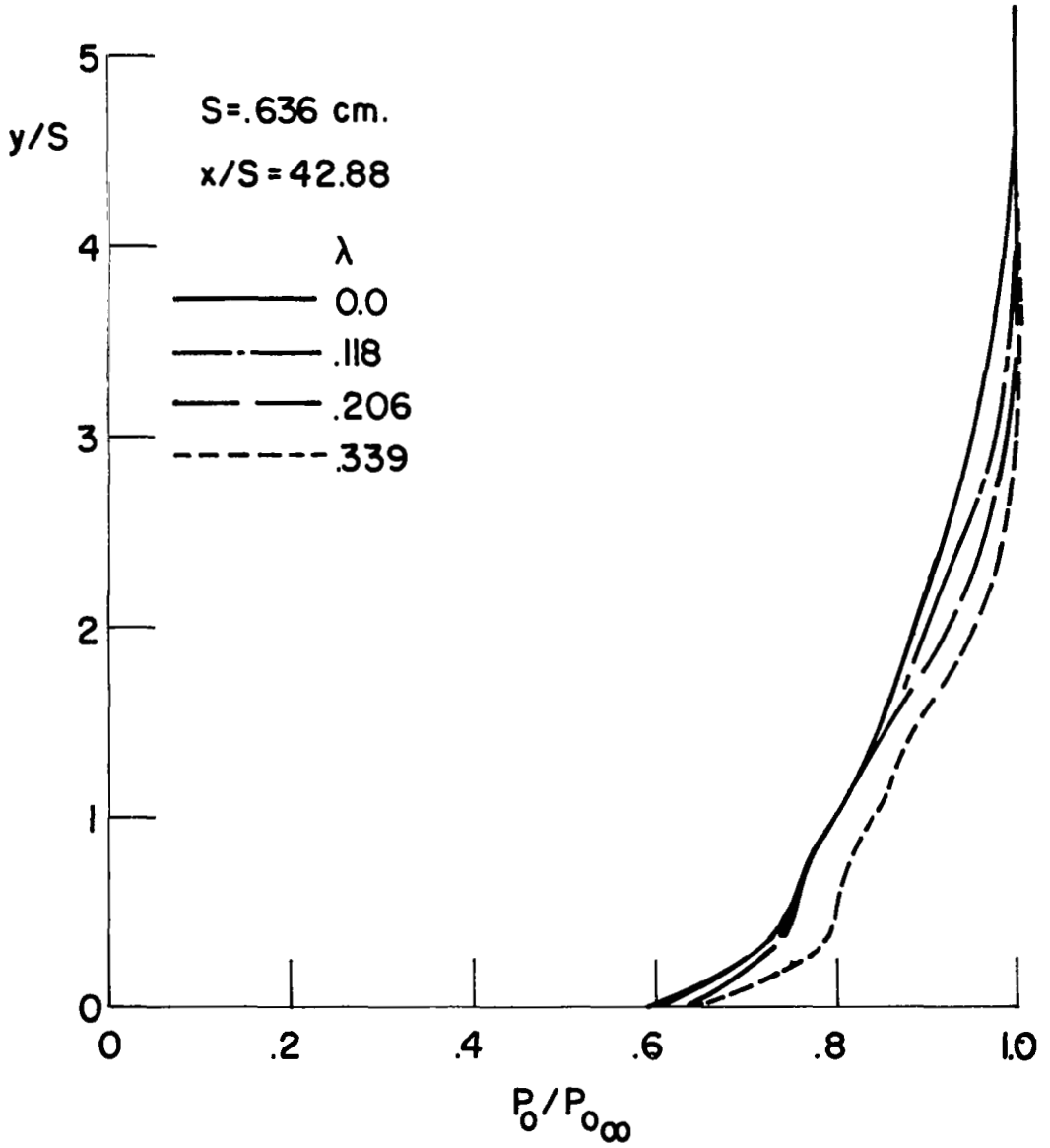

Fig. 22 Boundary layer profiles of total pressure due to single slot injection

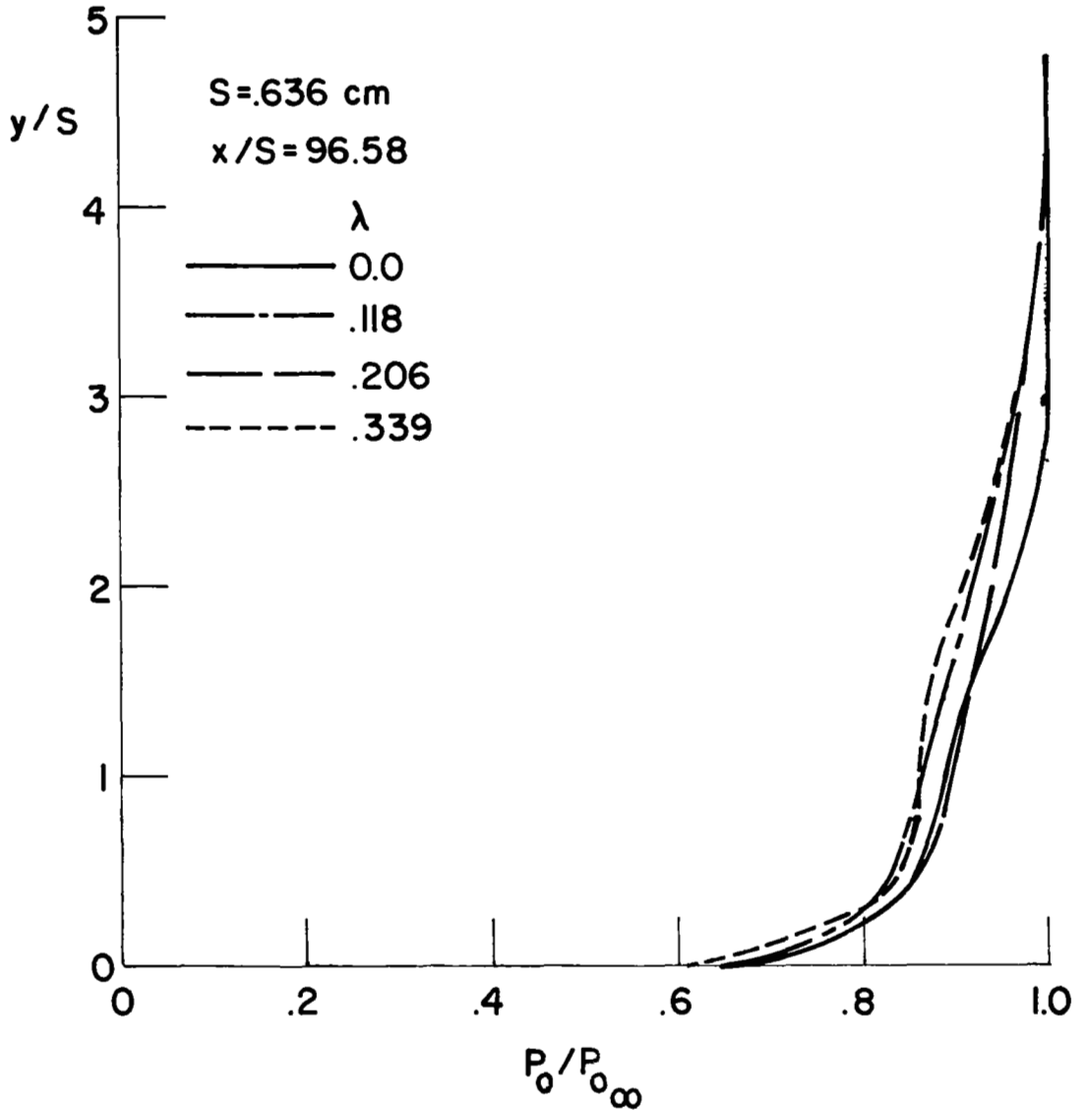

Fig. 23 Boundary layer profiles of total pressure due to single slot injection

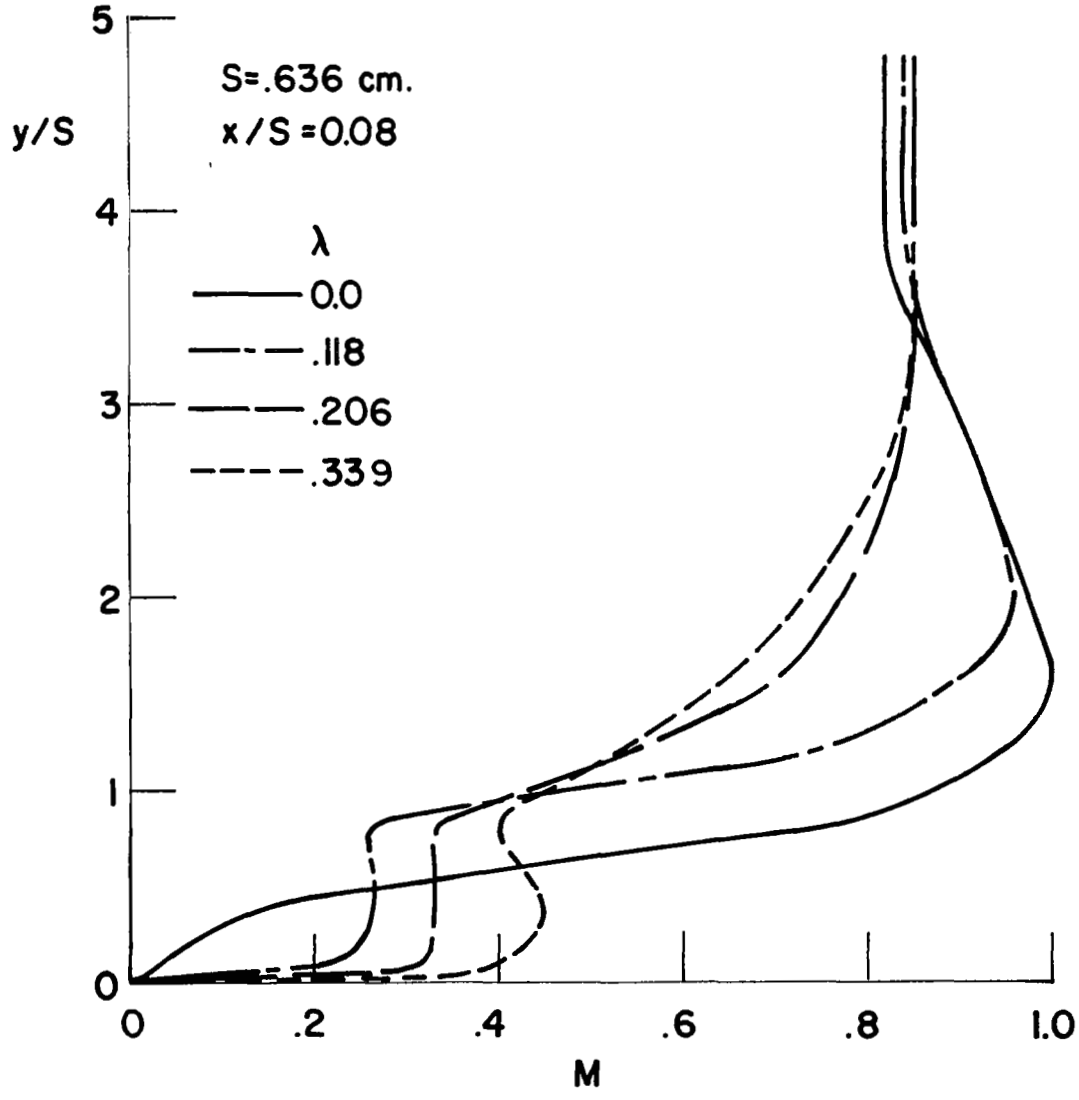

Fig. 24 Boundary layer profiles of Mach number due to single slot injection

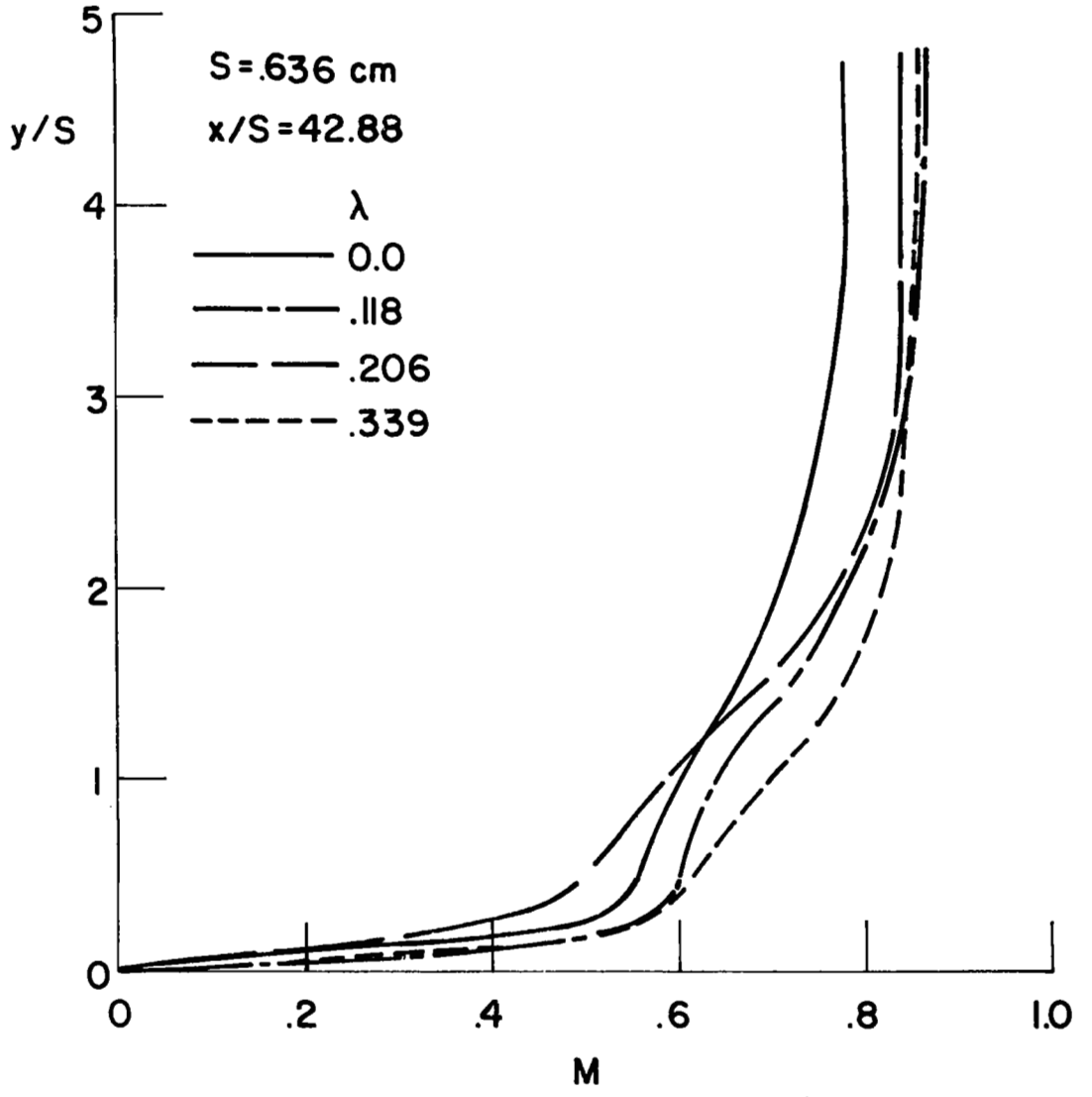

Fig. 25 Boundary layer profiles of Mach number due to single slot injection

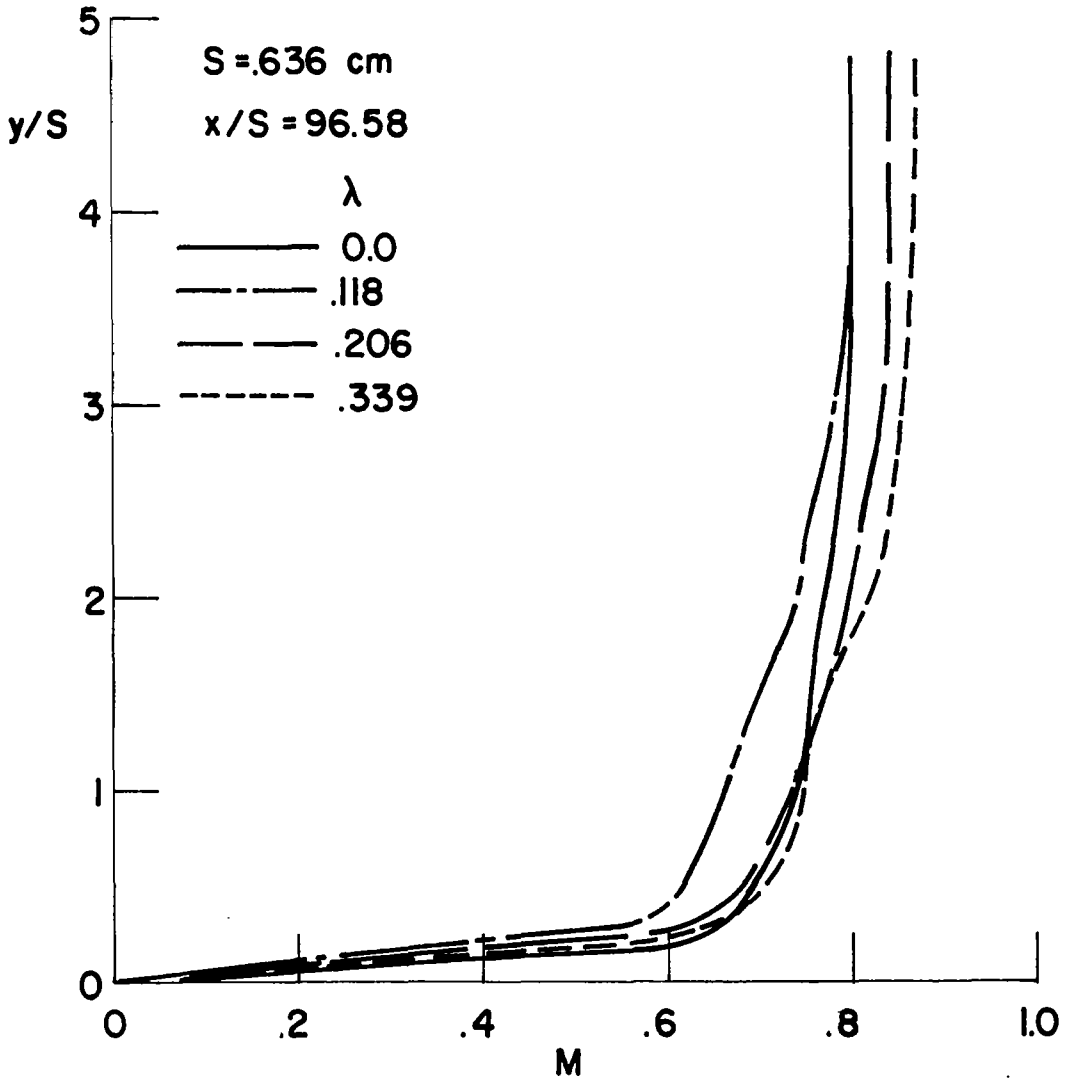

Fig. 26 Boundary layer profiles of Mach number due to single slot injection

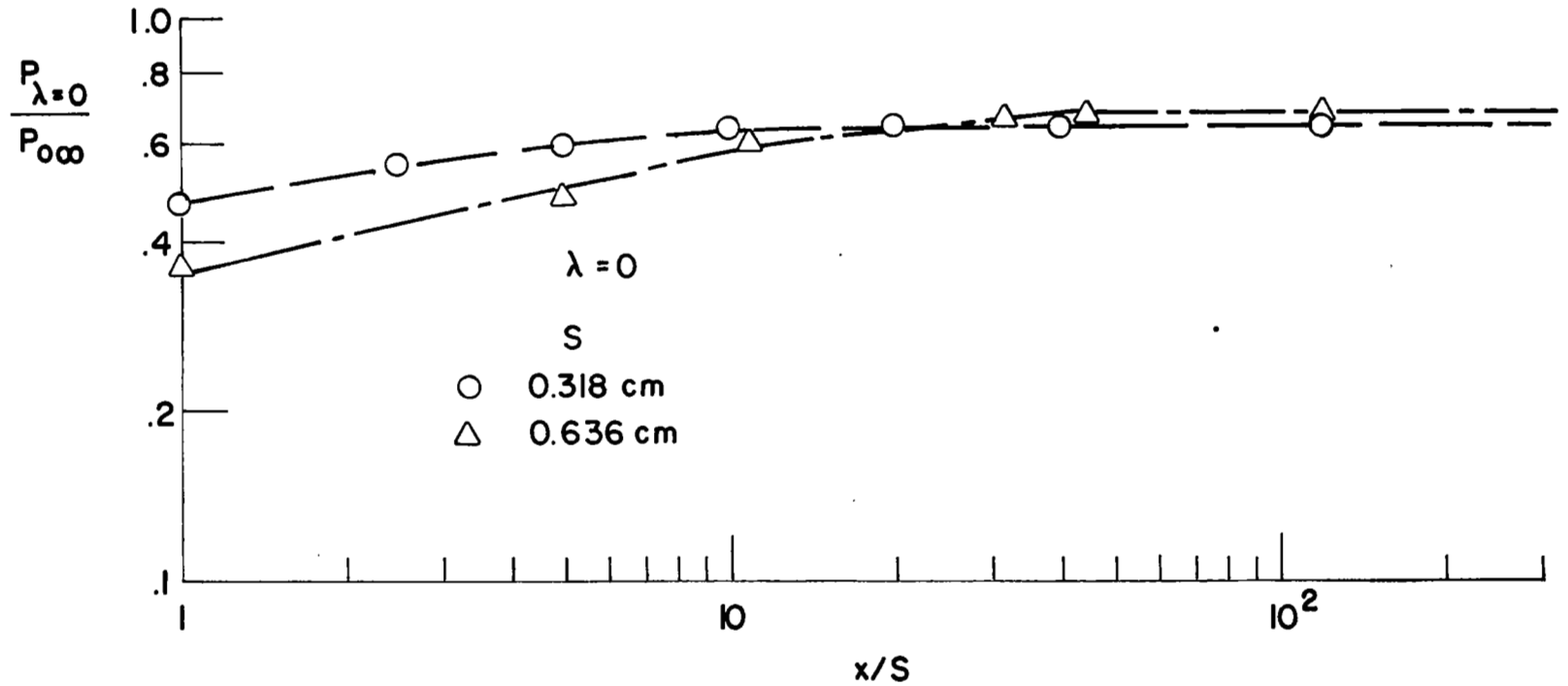

Fig. 27 Surface pressure distribution, s = 0.636 cm, λ = 0

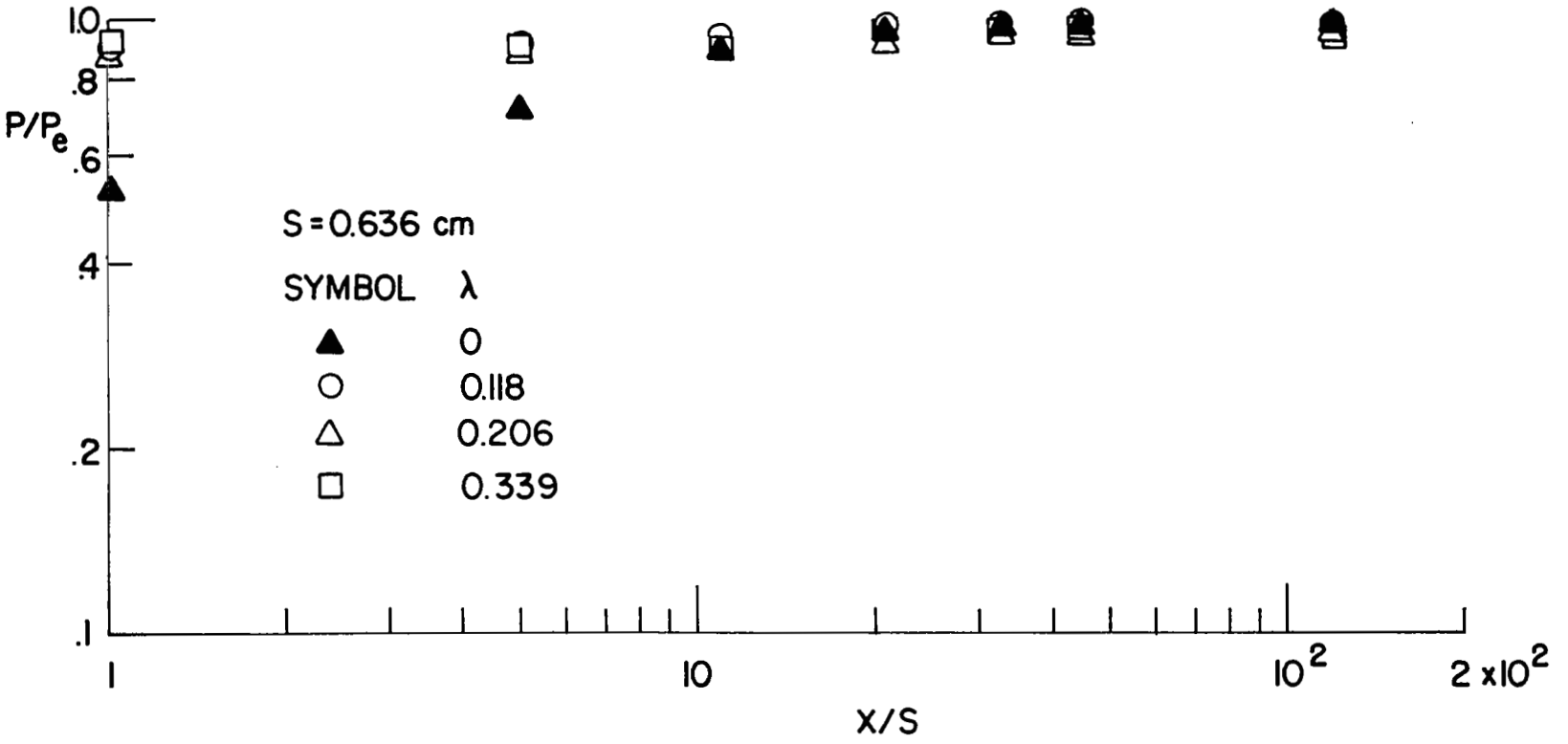

Fig. 28 Surface pressure distribution, s = 0.636 cm, $\lambda \geq 0$

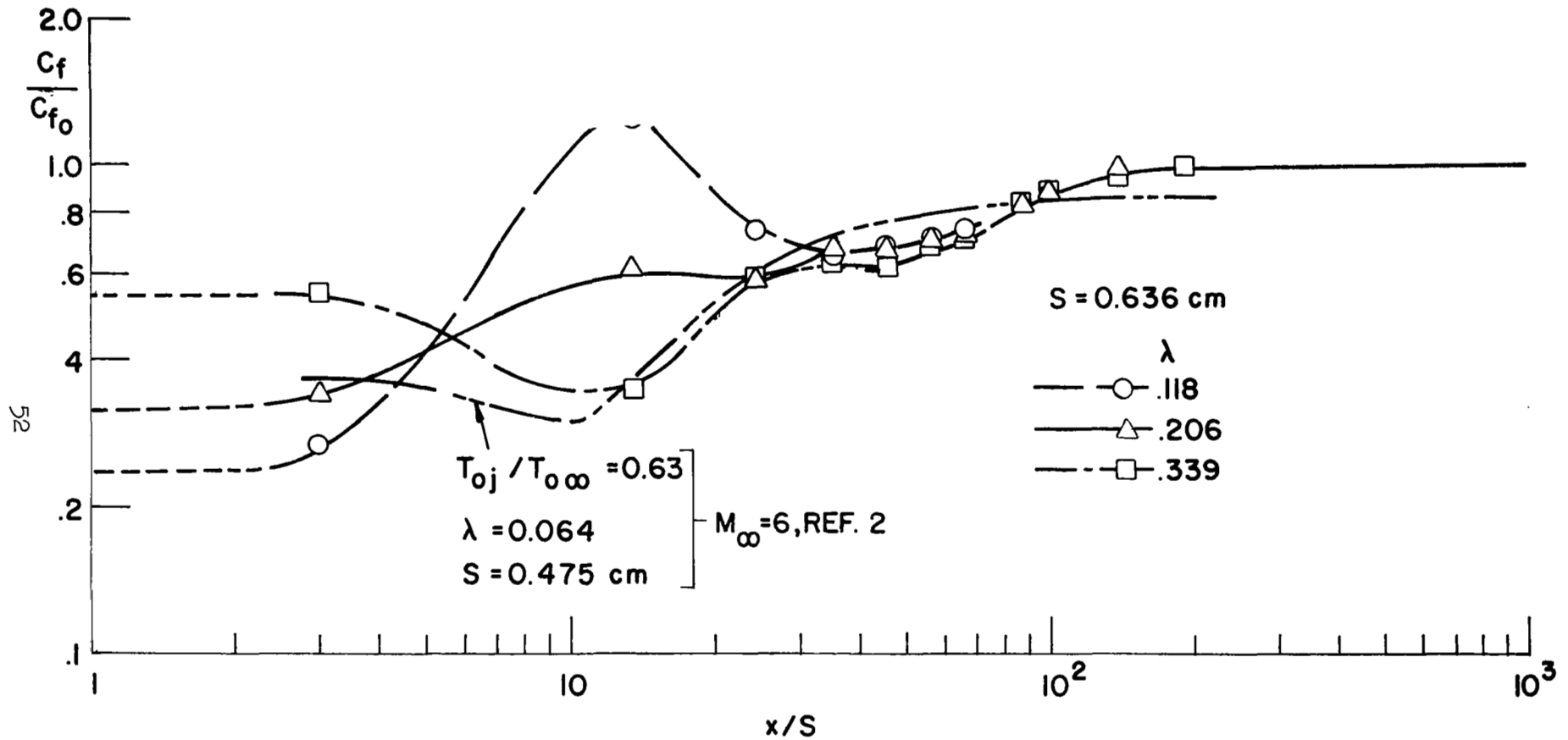

Fig. 29 Effect of single slot injection to the surface skin friction, s = 0.636 cm

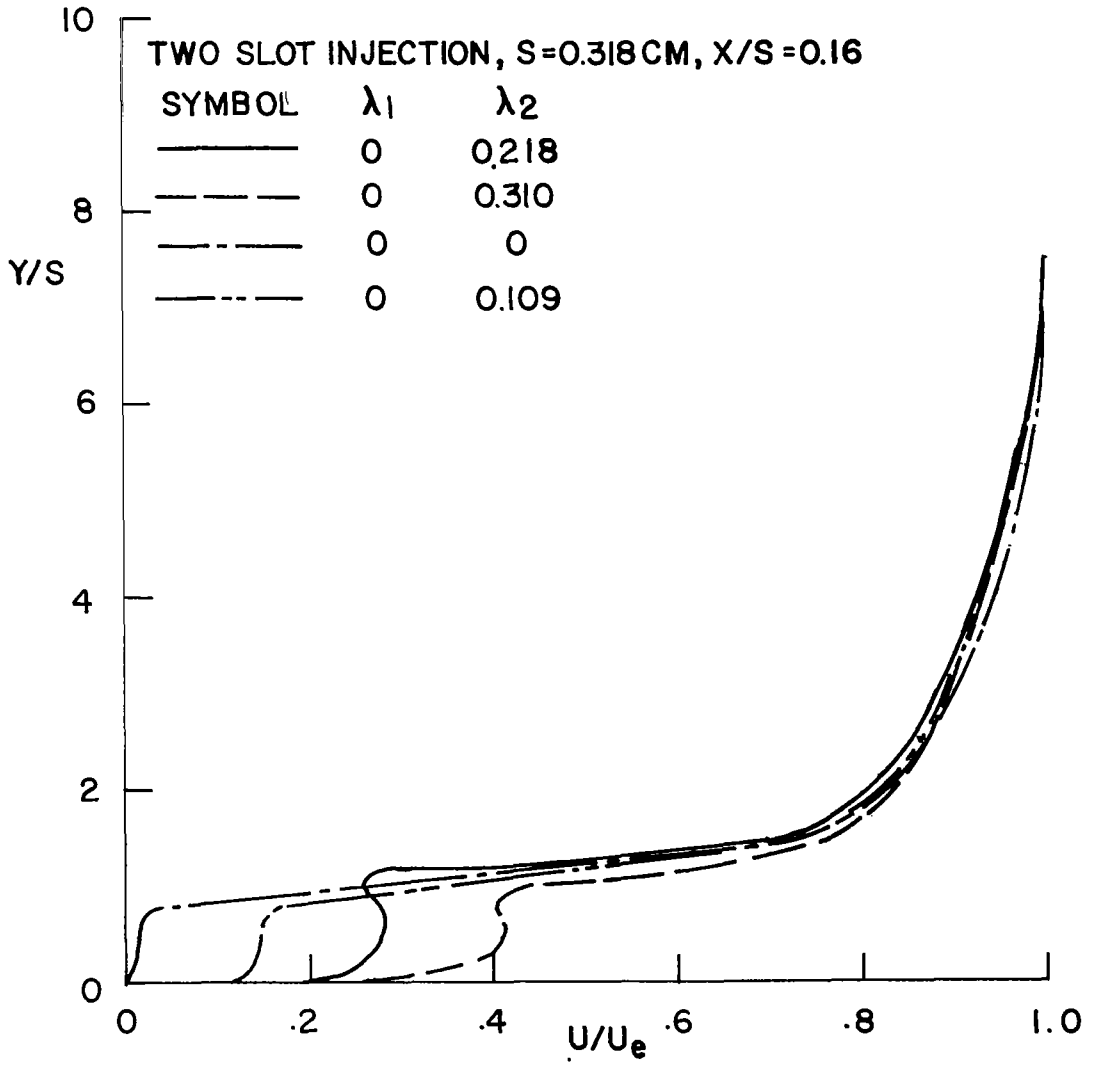

Fig. 30 Boundary layer profiles of velocity due to two slot injection

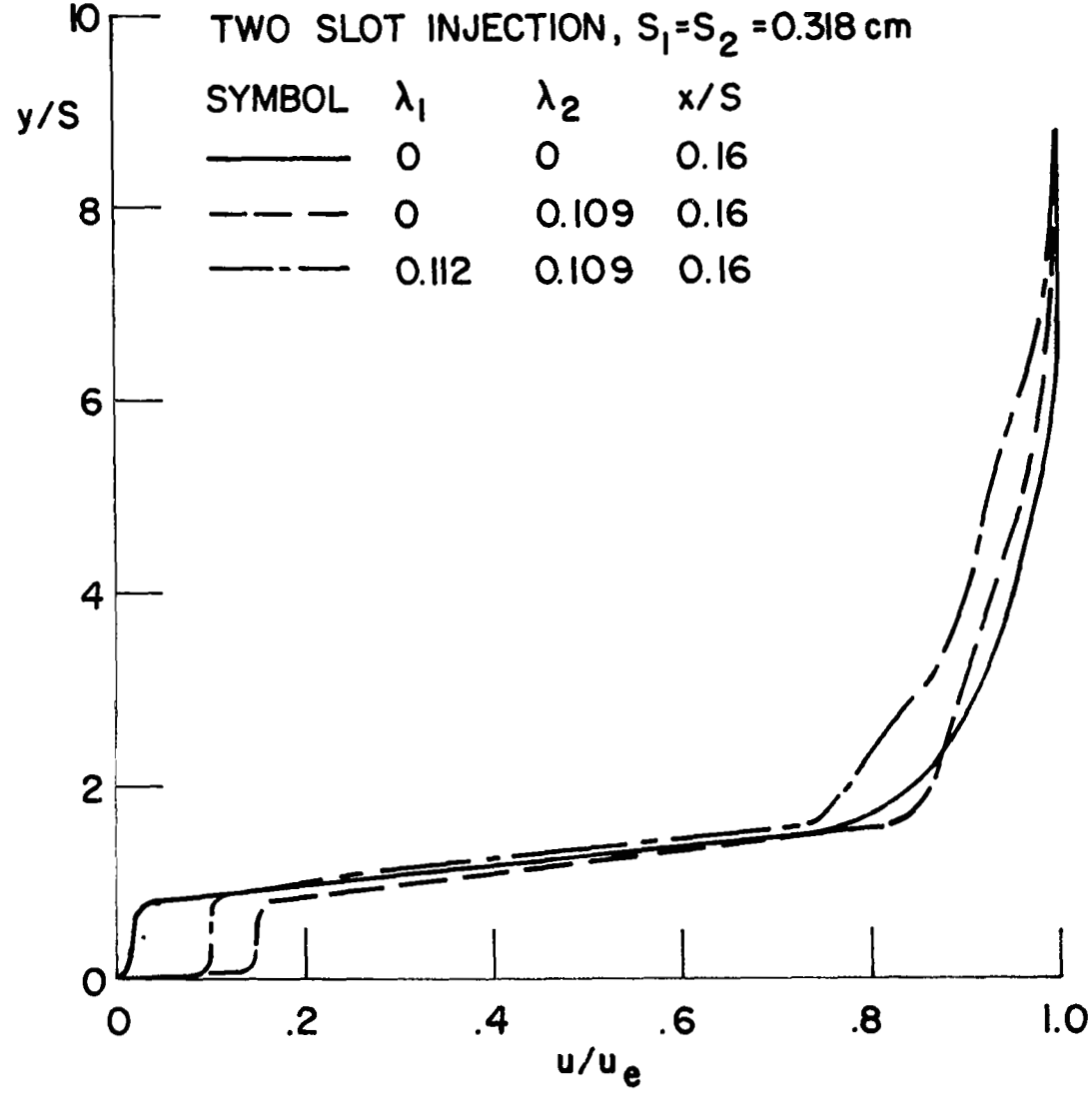

Fig. 31 Boundary layer profiles of velocity due to two slot injection

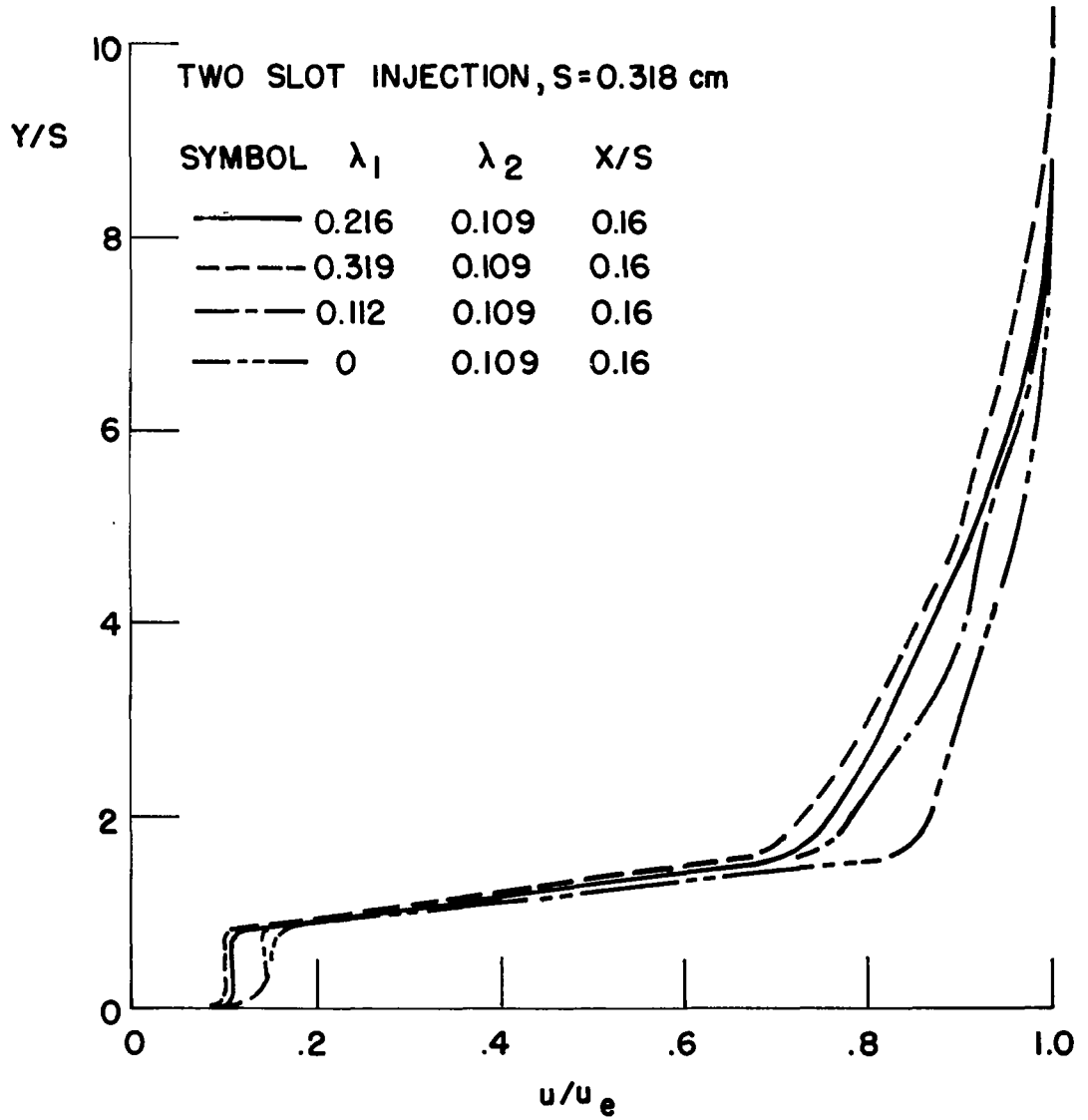

Fig. 32 Boundary layer profiles of velocity due to two slot injection

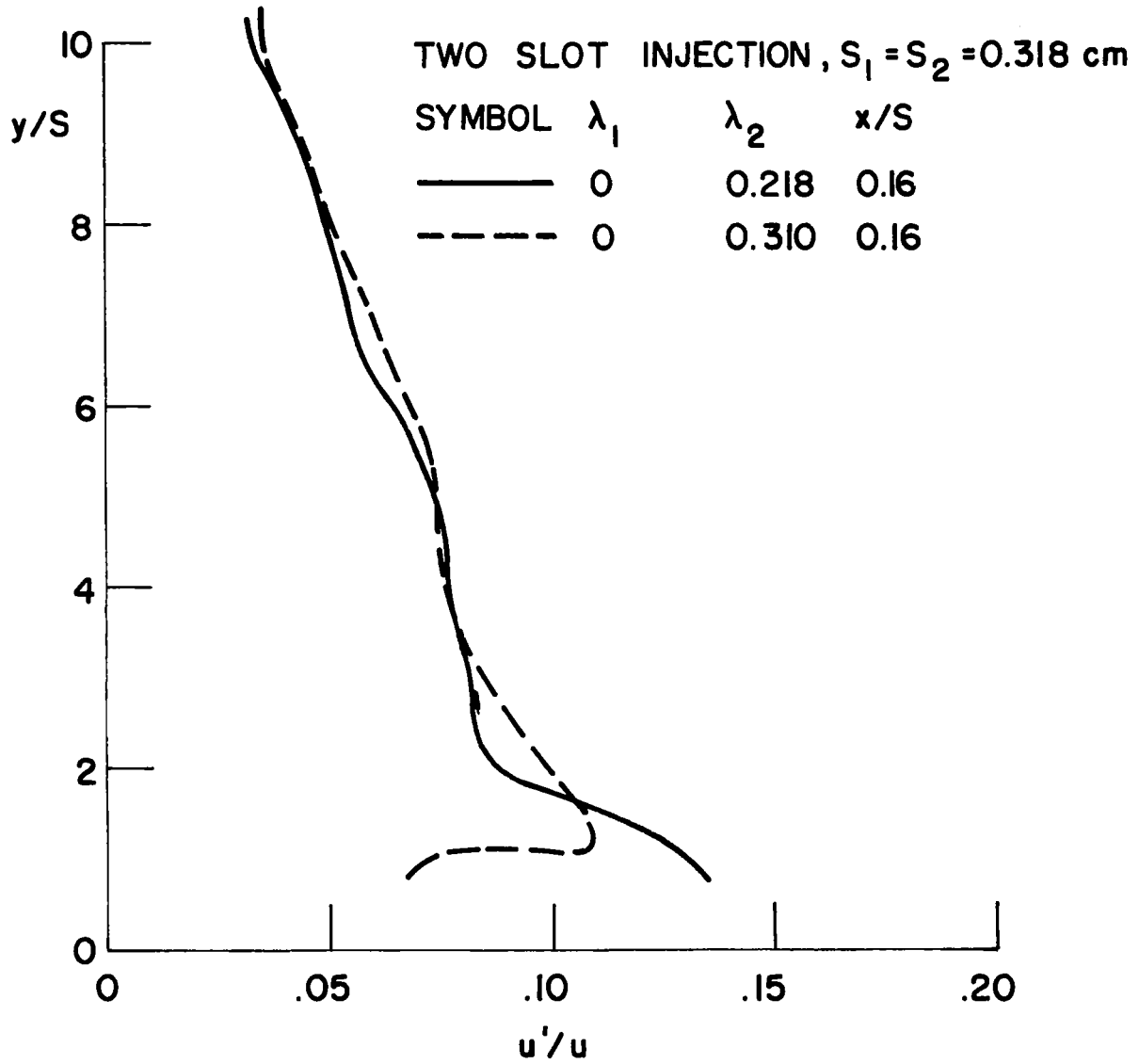

Fig. 33 Boundary layer turbulence intensity profiles due to two slot injection

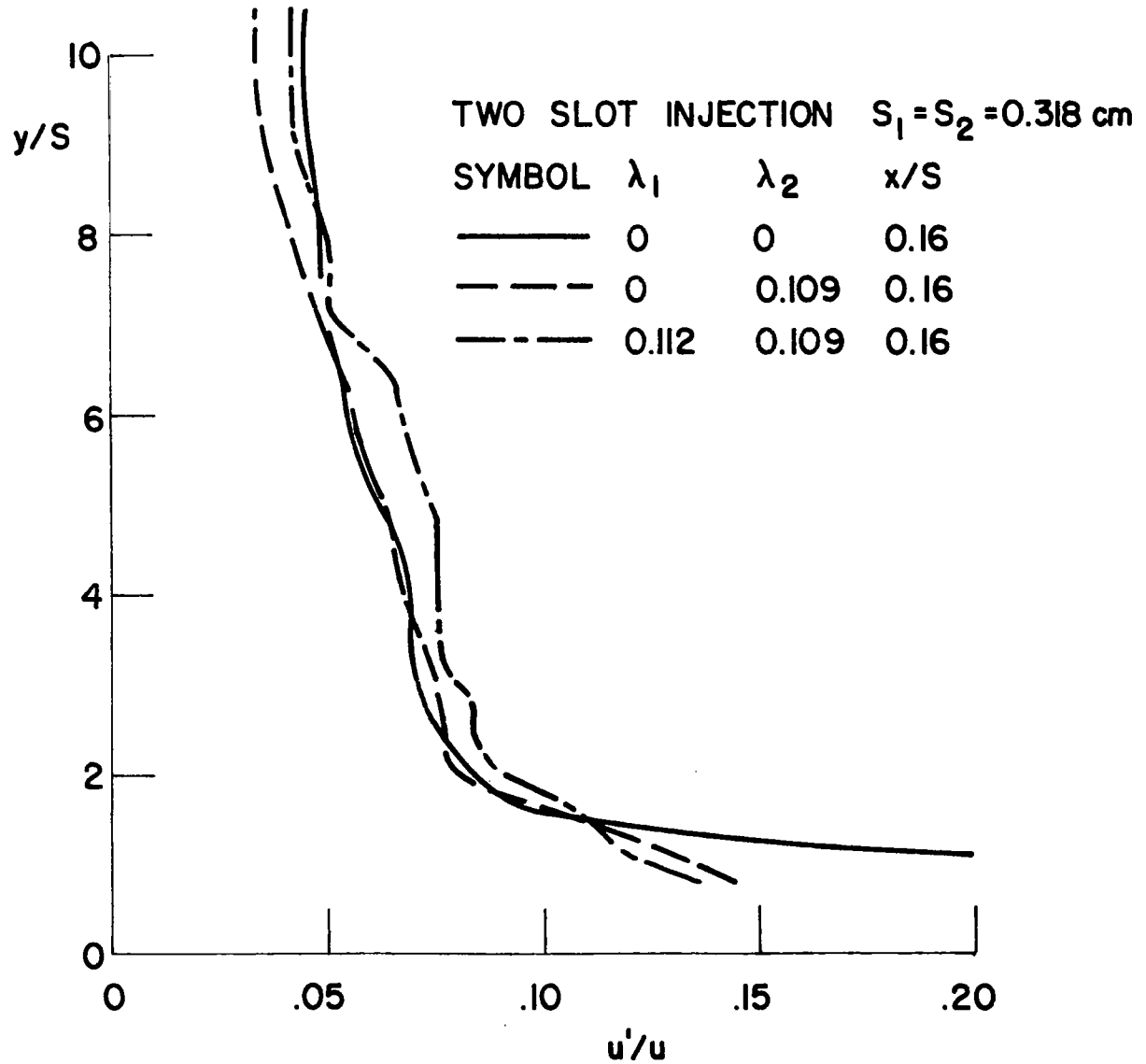

Fig. 34 Boundary layer turbulence intensity profiles due to two slot injection

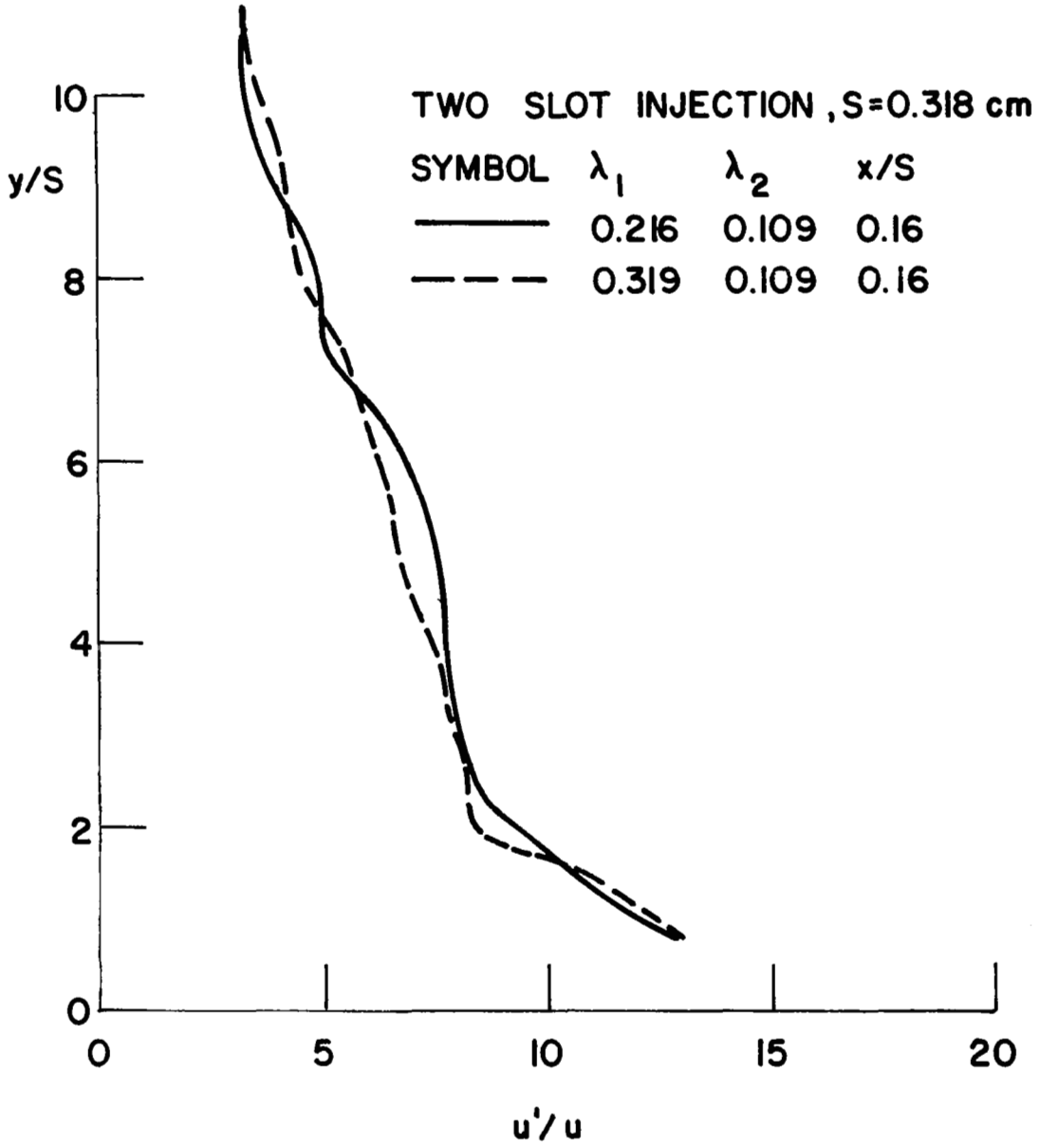

Fig. 35 Boundary layer turbulence intensity profiles due to two slot injection

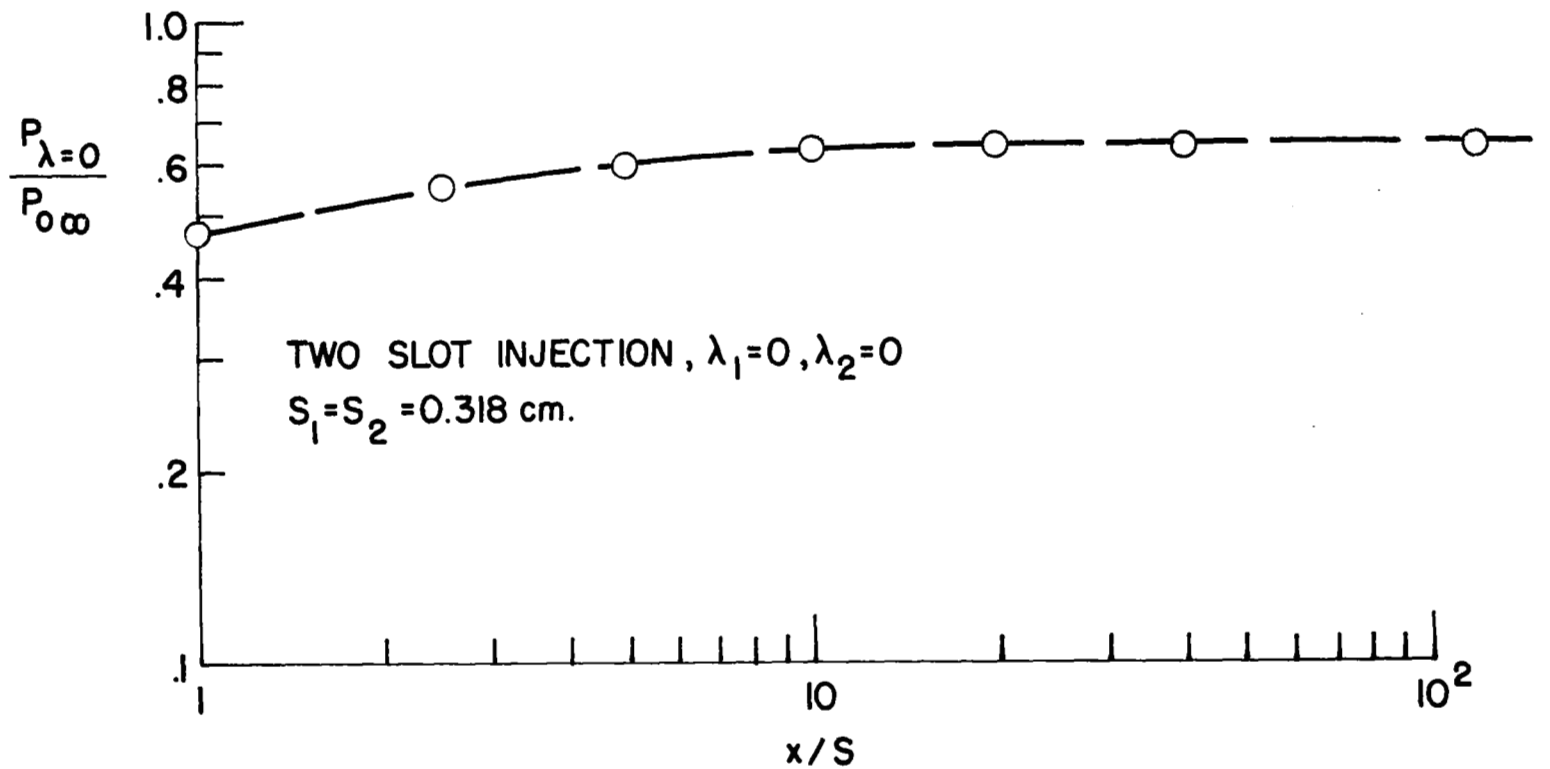

Fig. 36 Surface pressure distribution with $\lambda_1 = 0$ and $\lambda_2 = 0$

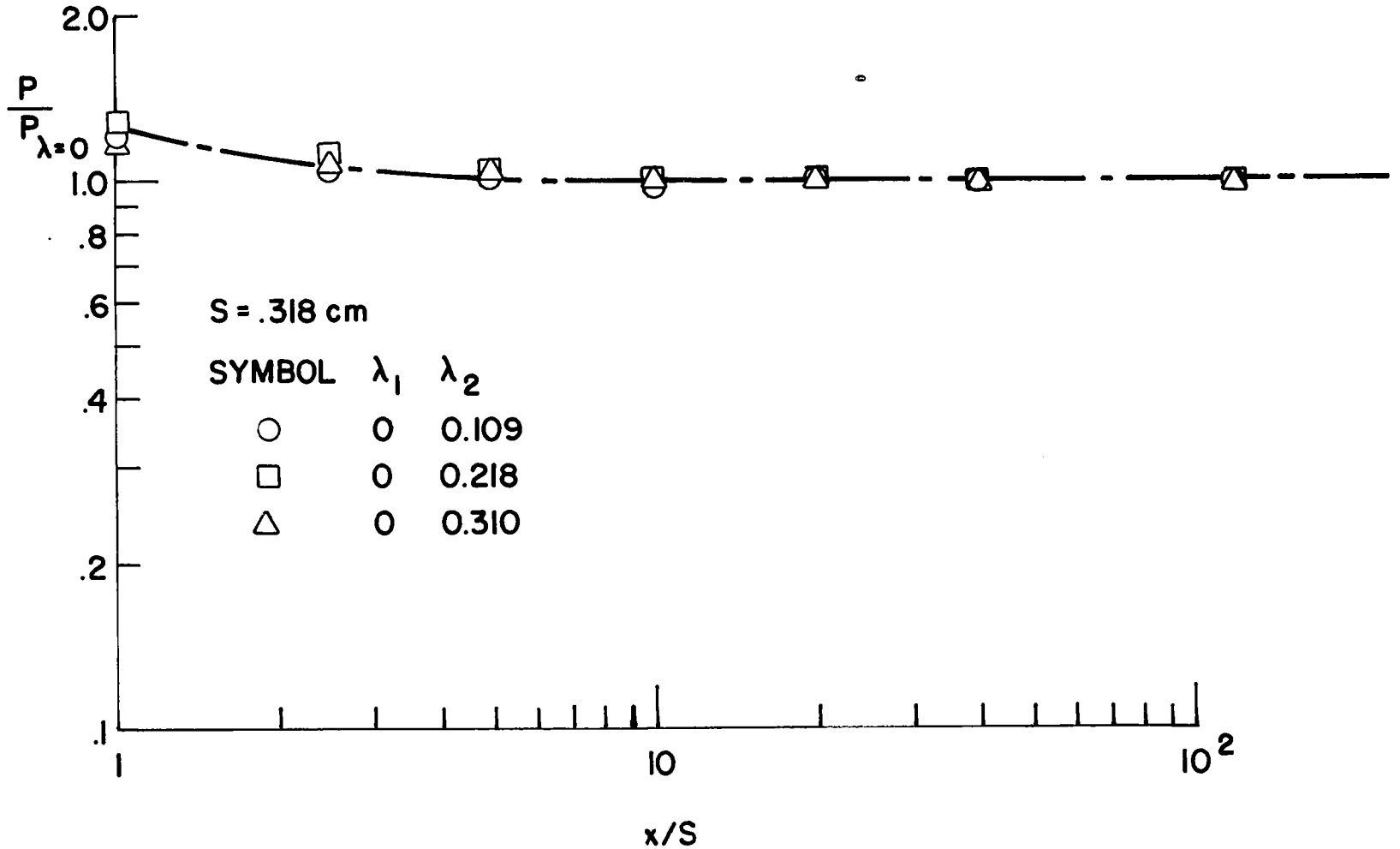

Fig. 37 Surface pressure distribution due to two slot injection

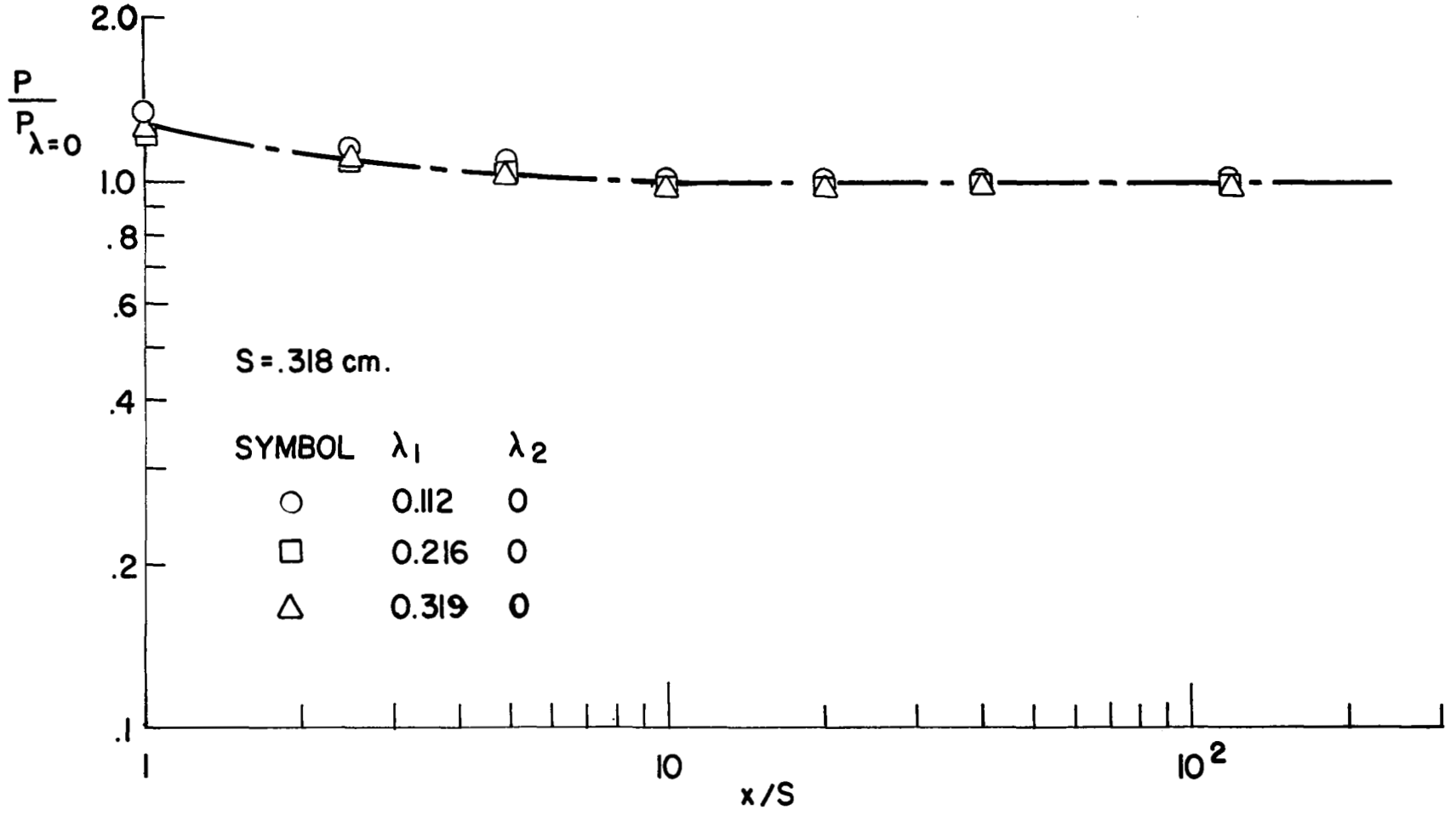

Fig. 38 Surface pressure distribution due to two slot injection

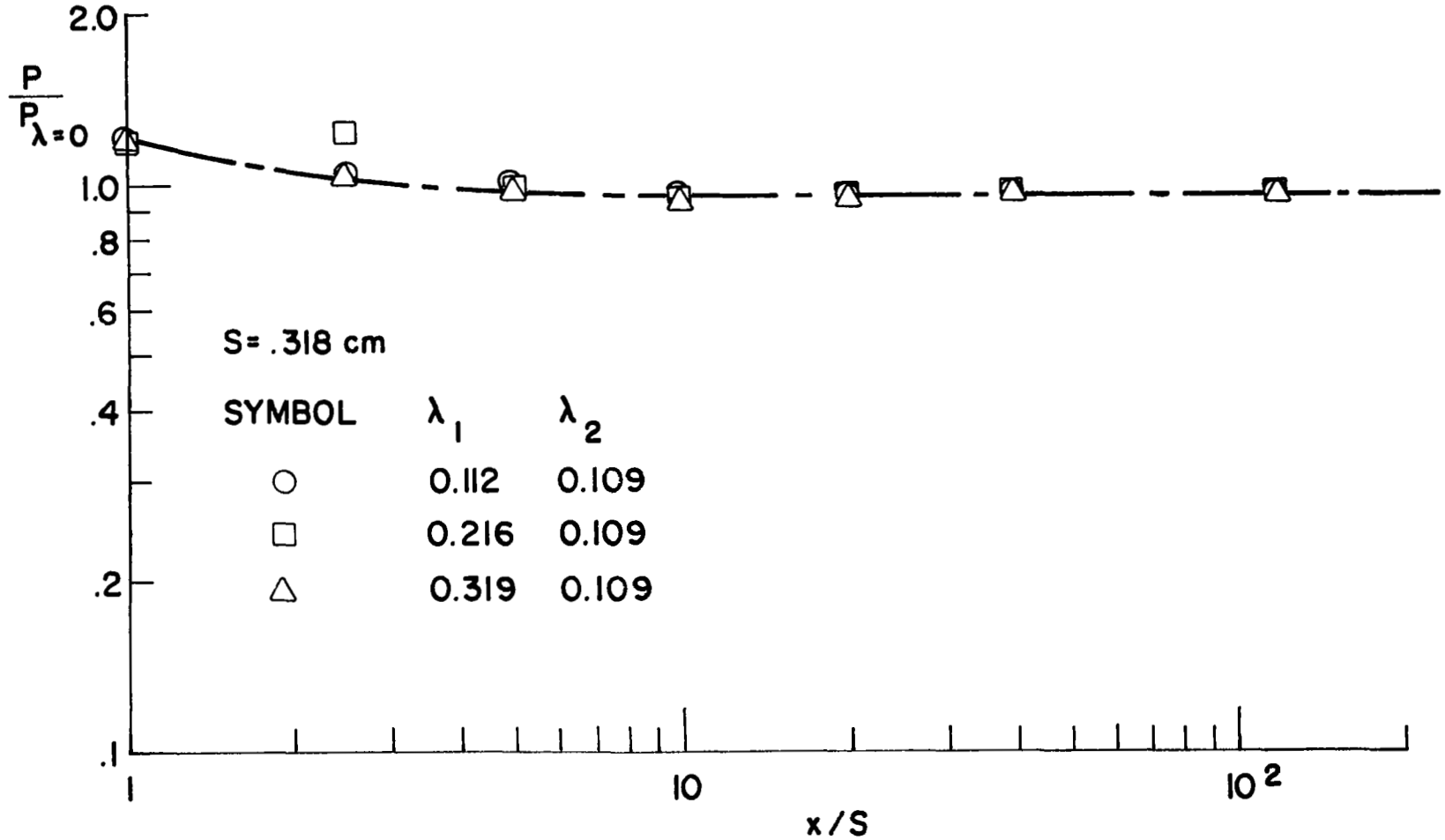

Fig. 39 Surface pressure distribution due to two slot injection

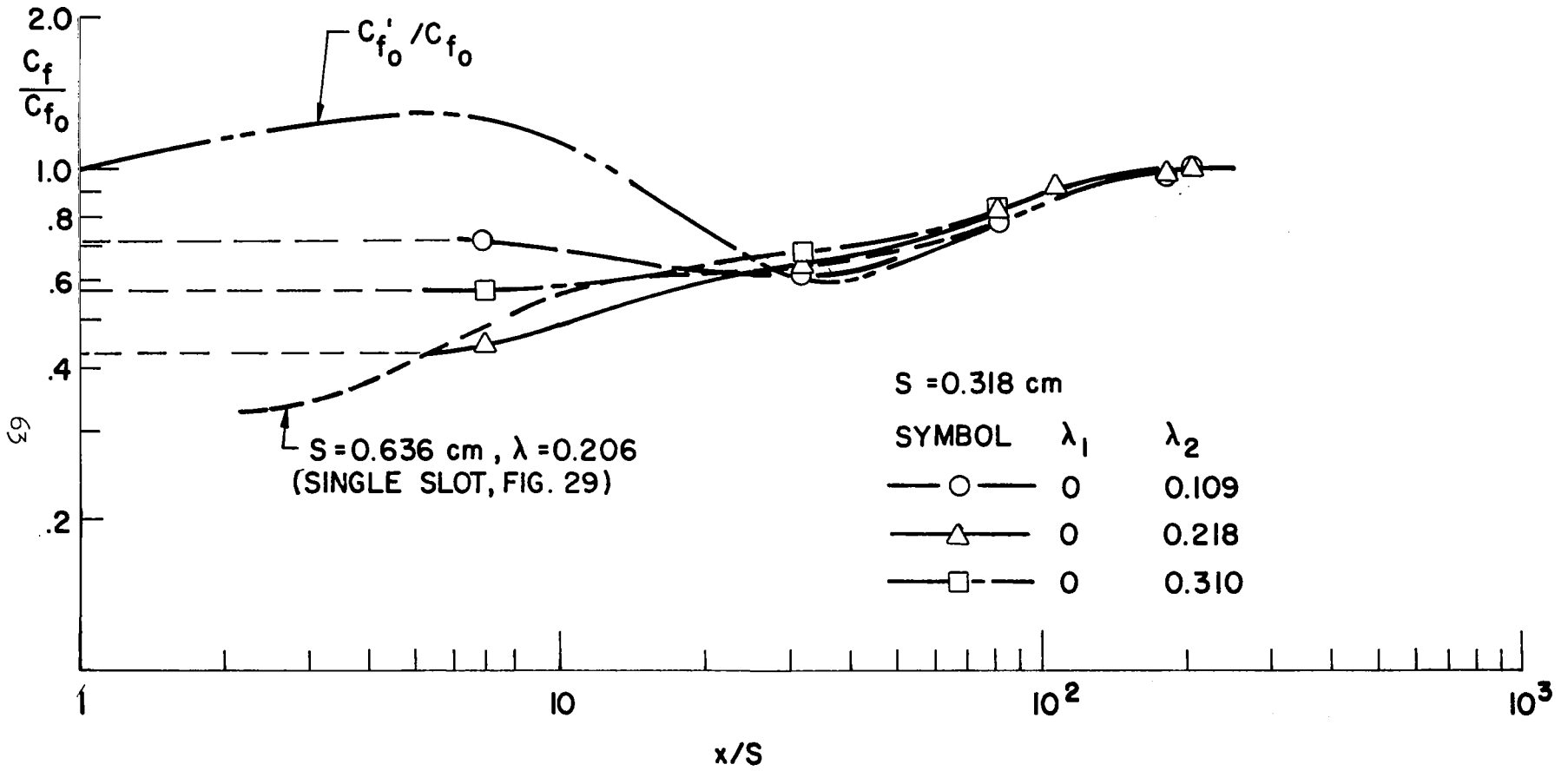

Fig. 40 Measurements of skin friction due to two slot injection, $\lambda_1 = 0$, $\lambda_\lambda \neq 0$

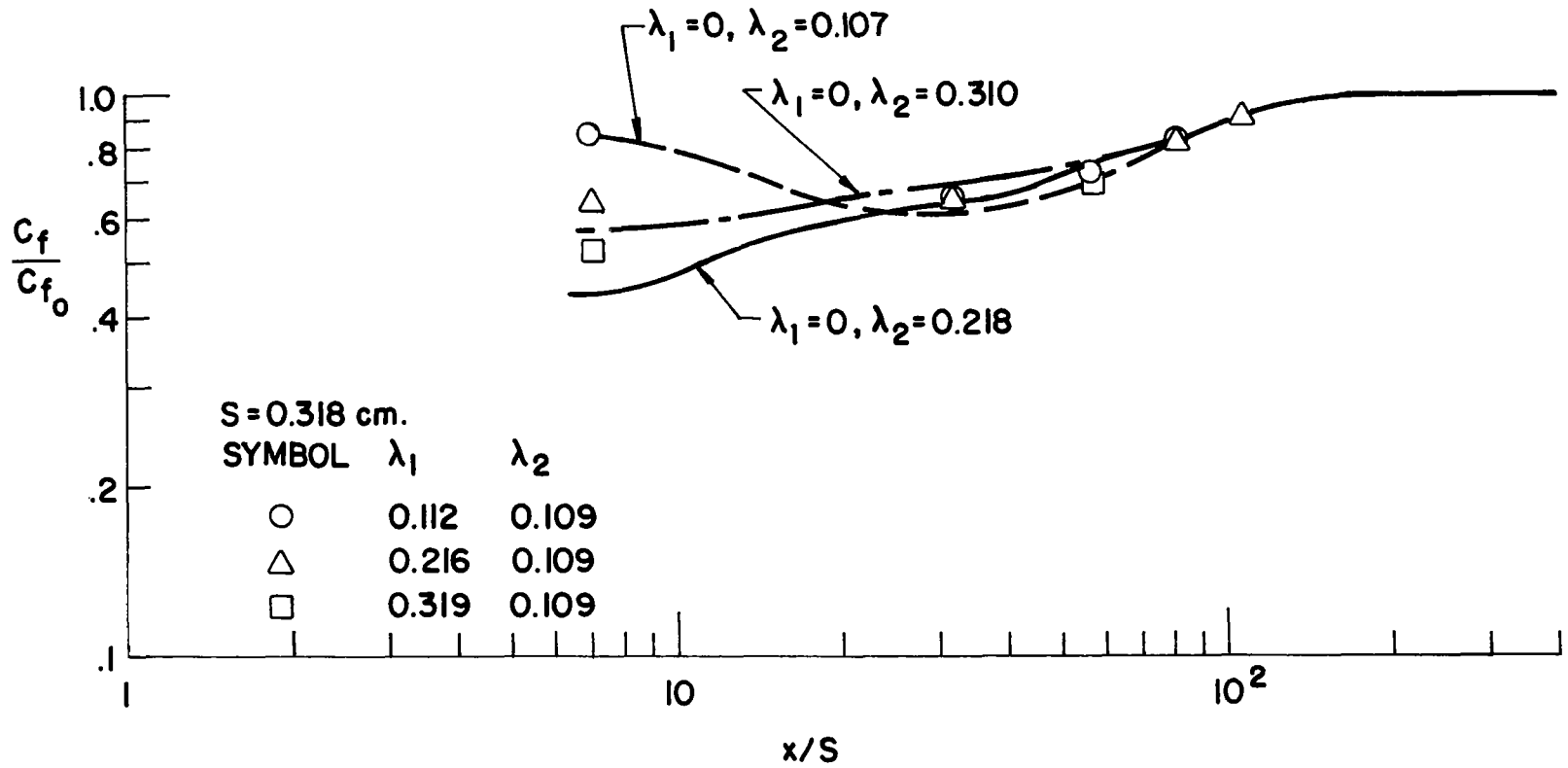

Fig. 41 Measurements of skin friction due to two slot injection with constant second slot injection

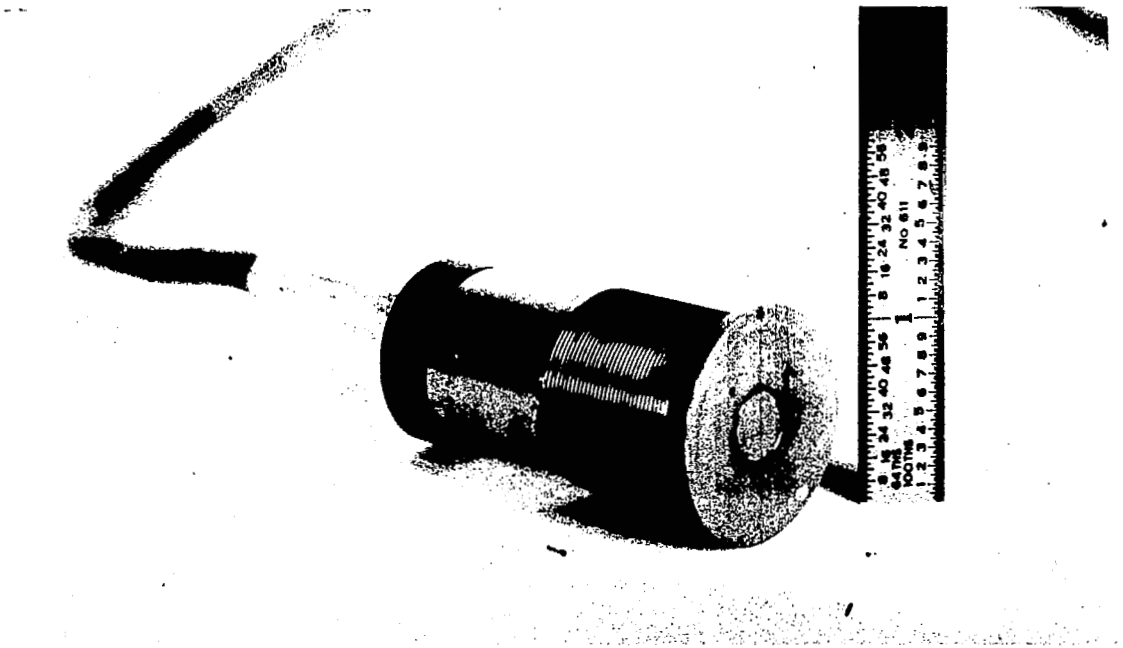

Fig. I-1 Floating skin friction balance

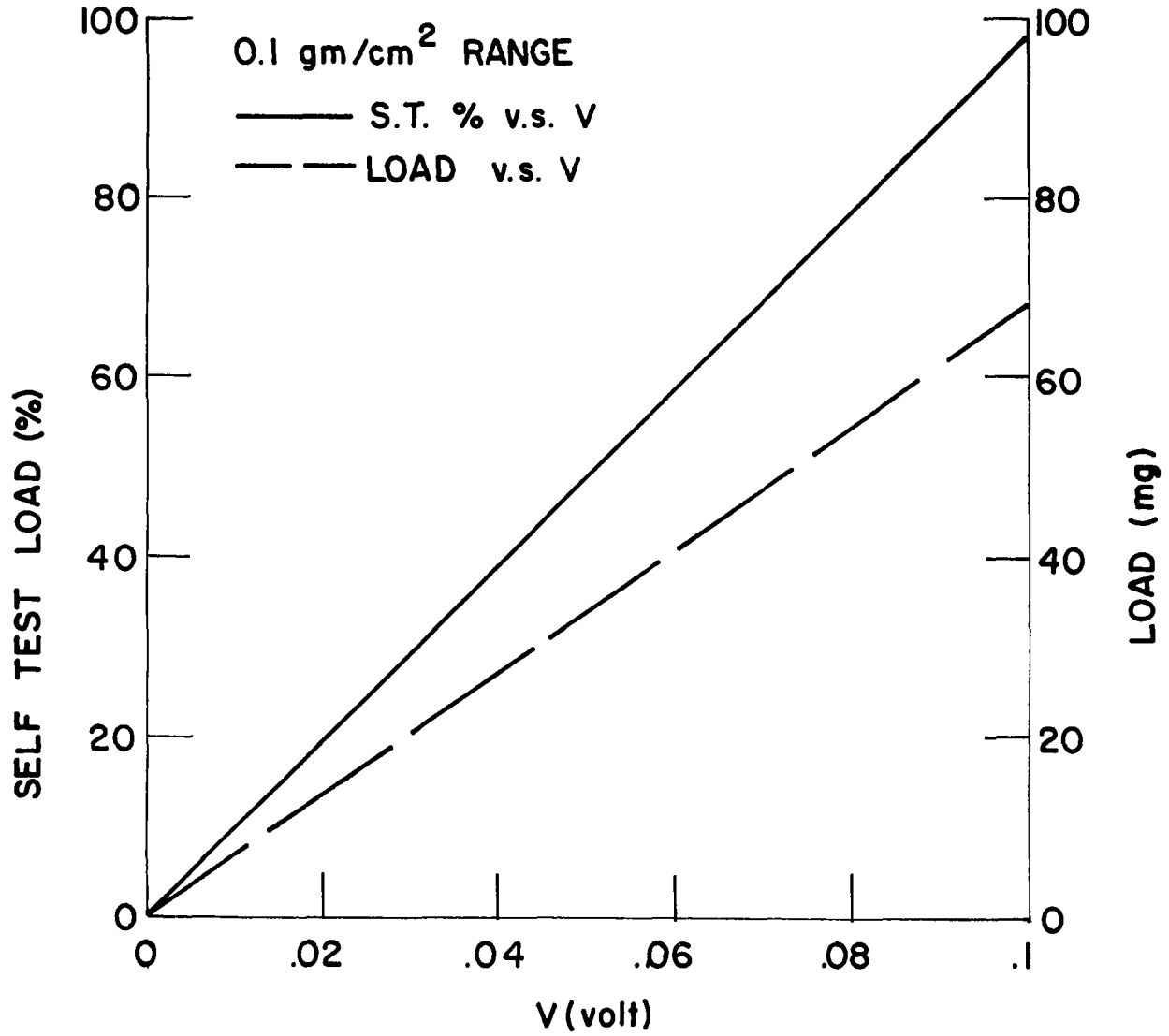

Fig. I-2 Calibration of the floating skin friction balance

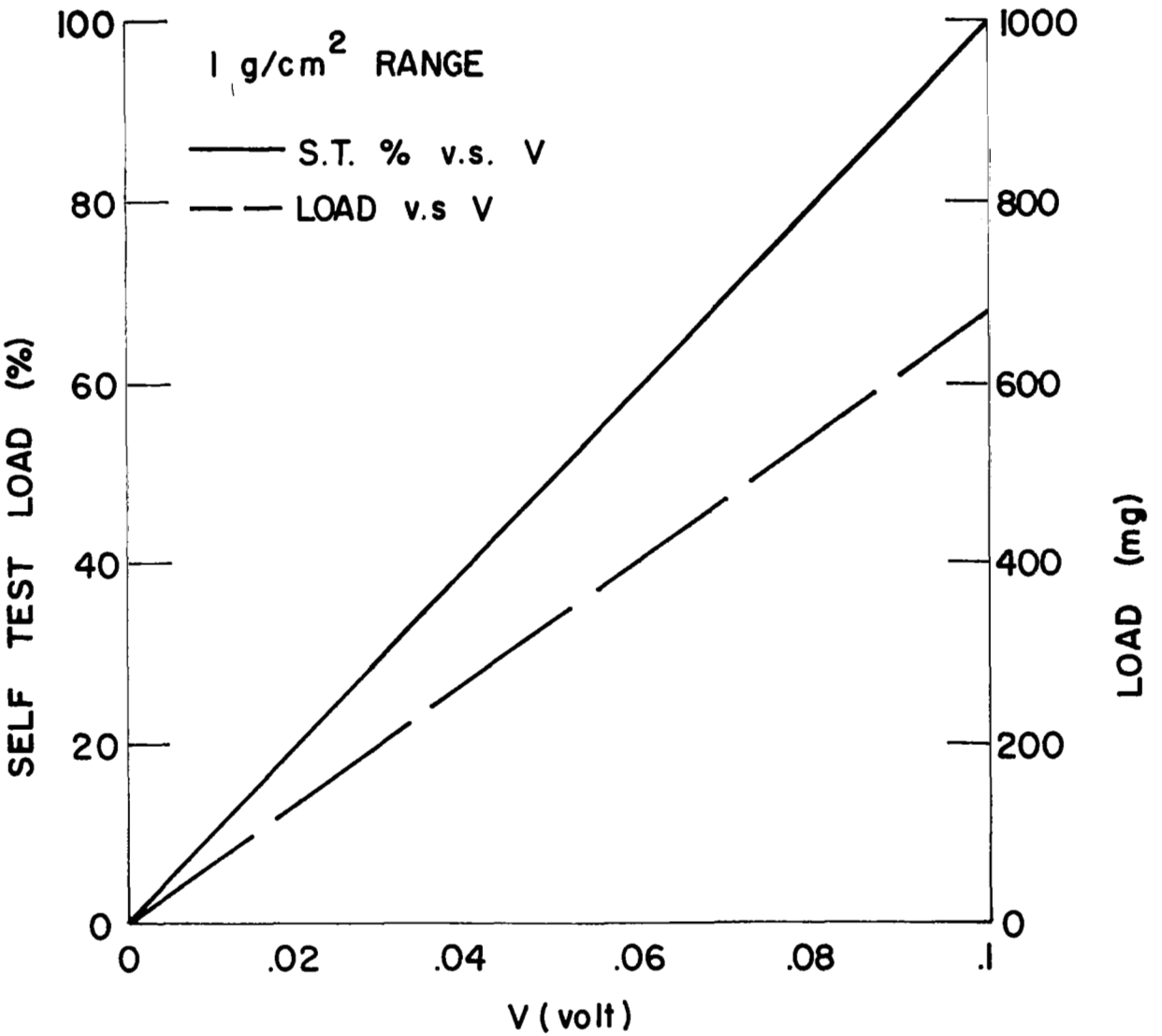

Fig. I-3 Calibration of the floating skin friction balance

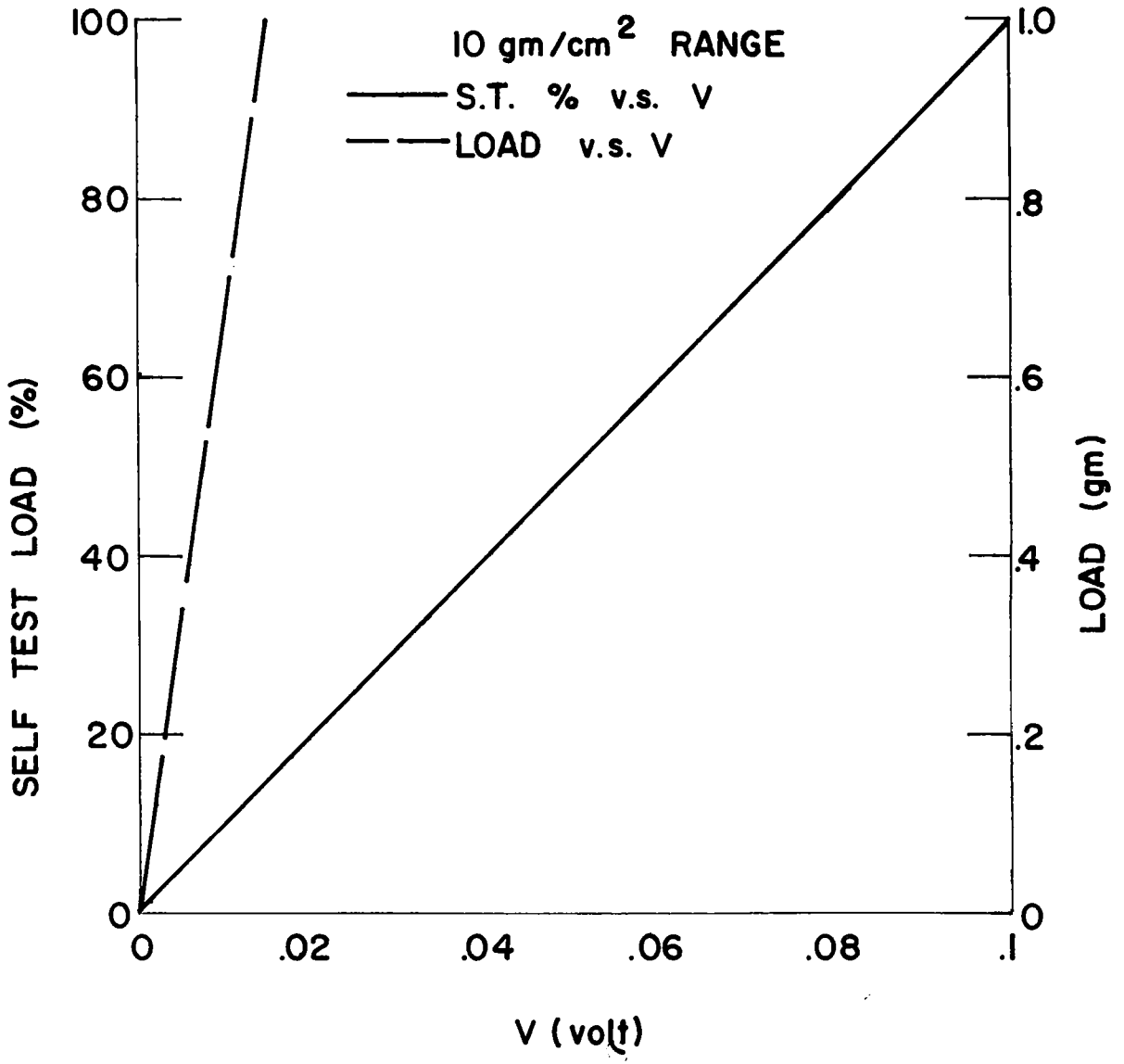

Fig. I-4 Calibration of the floating skin friction balance

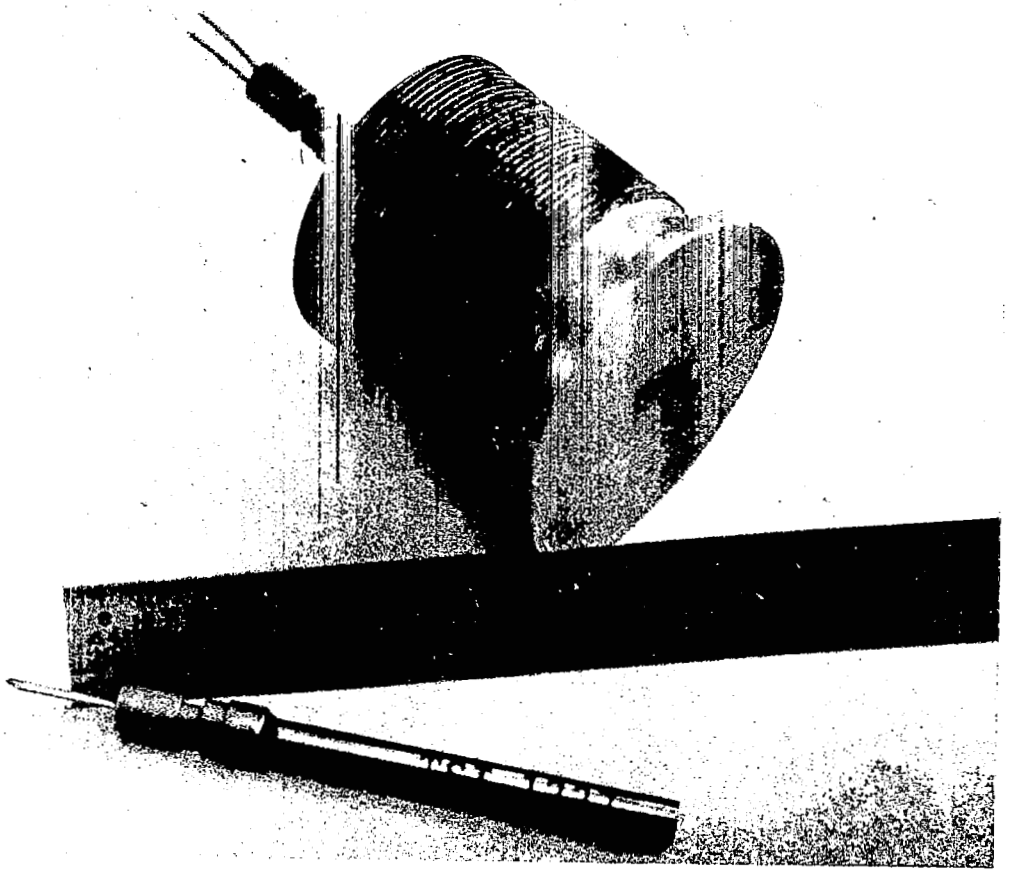

Fig. I-5 The flush mounted hot film probe

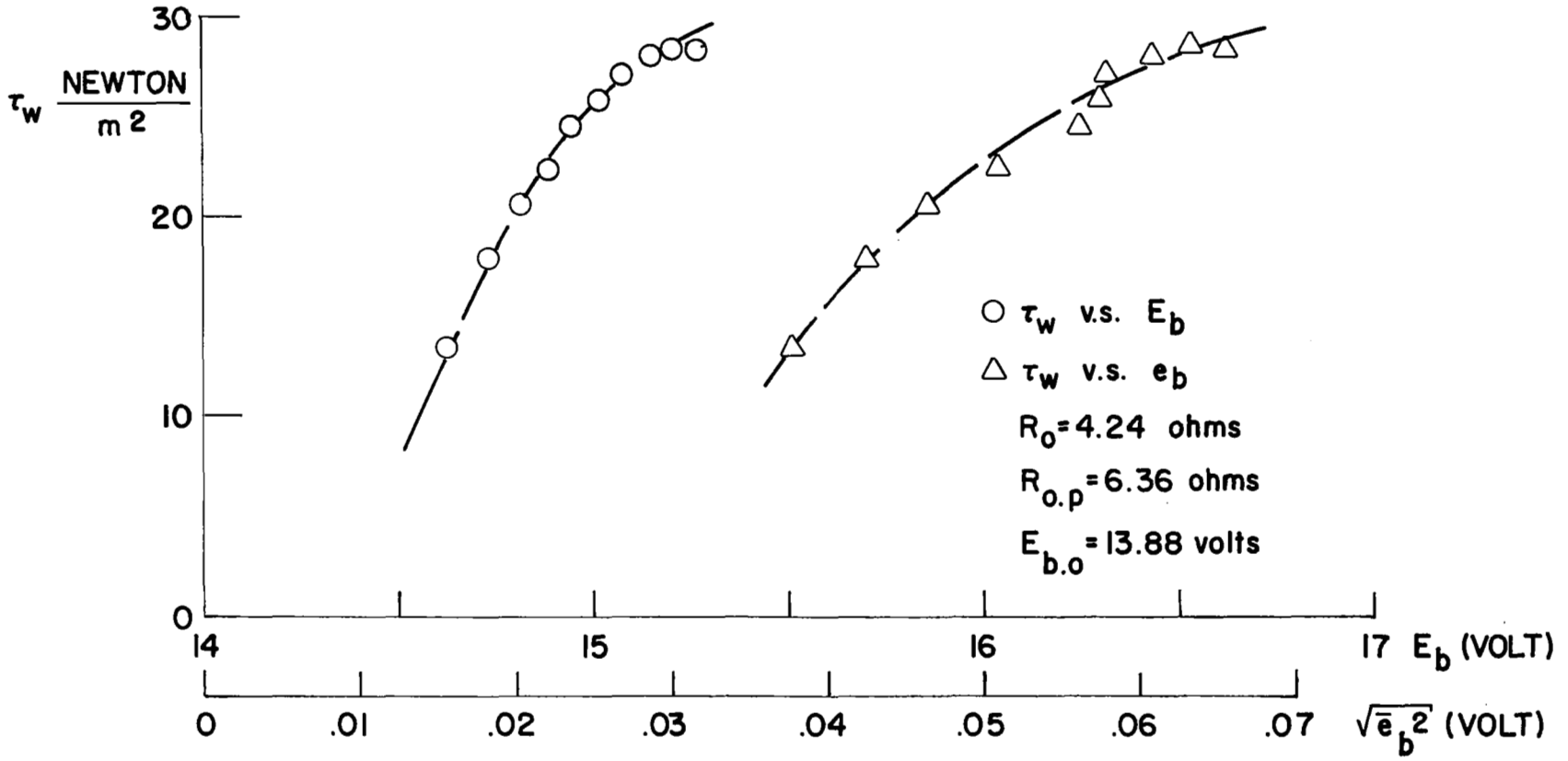

Fig. I-6 Calibration of the flush mounted hot film probe

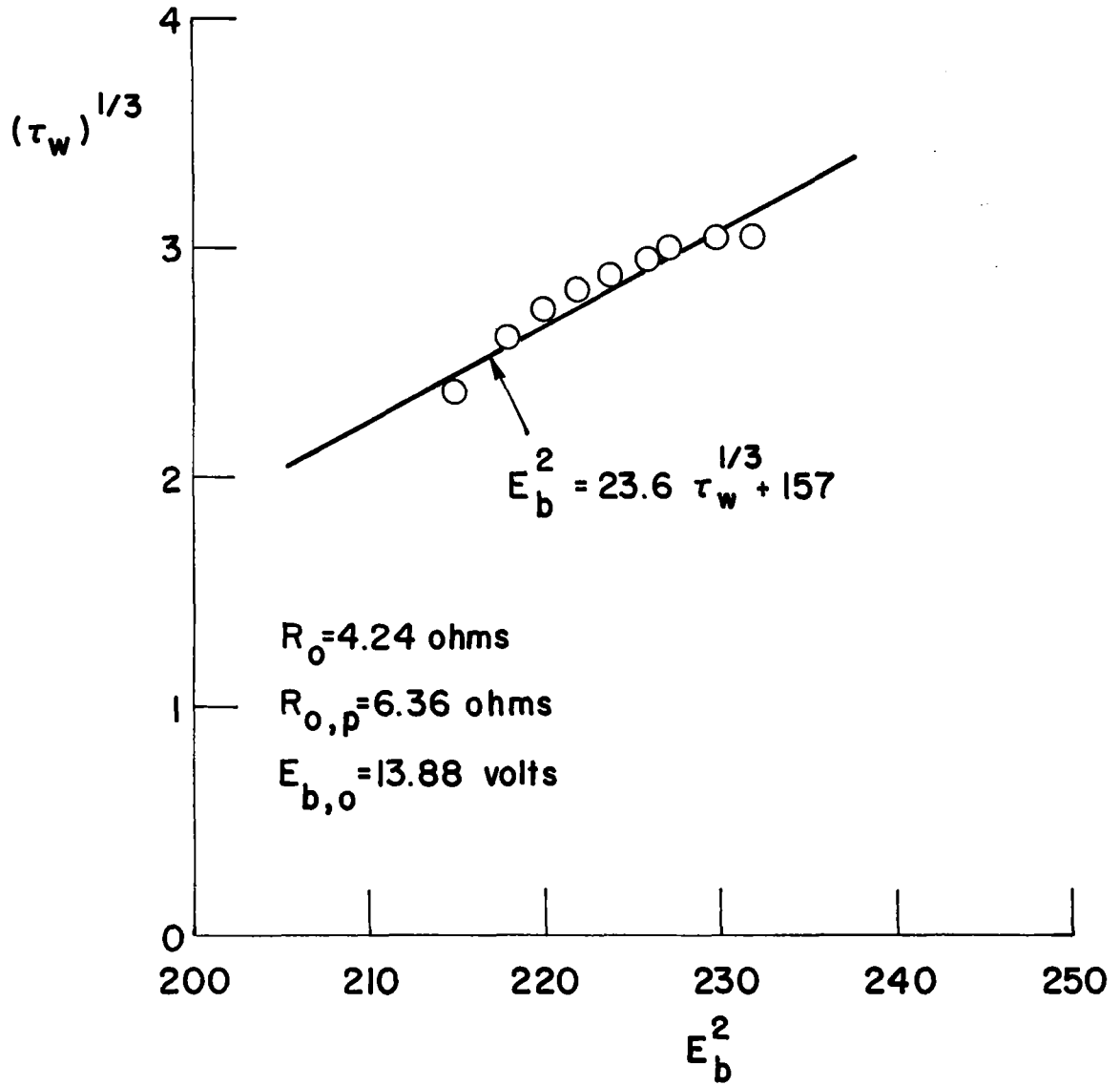

Fig. I-7 Correlation of the characteristic of the hot film probe, τ_w vs. E_b

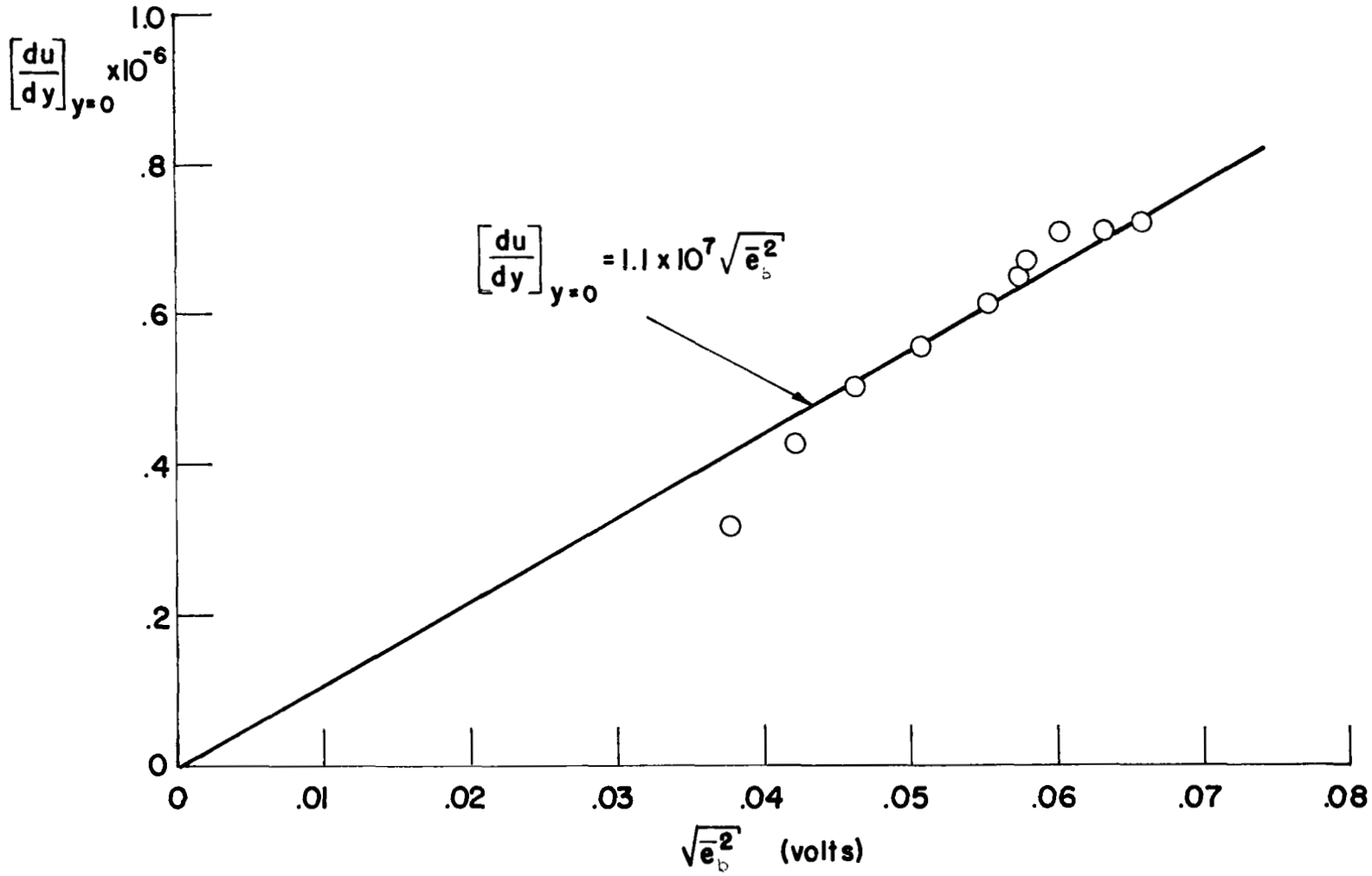

Fig. I-8 Correlation of the characteristic of the hot film probe, $du/dy\big|_{y=0}$ vs e_b

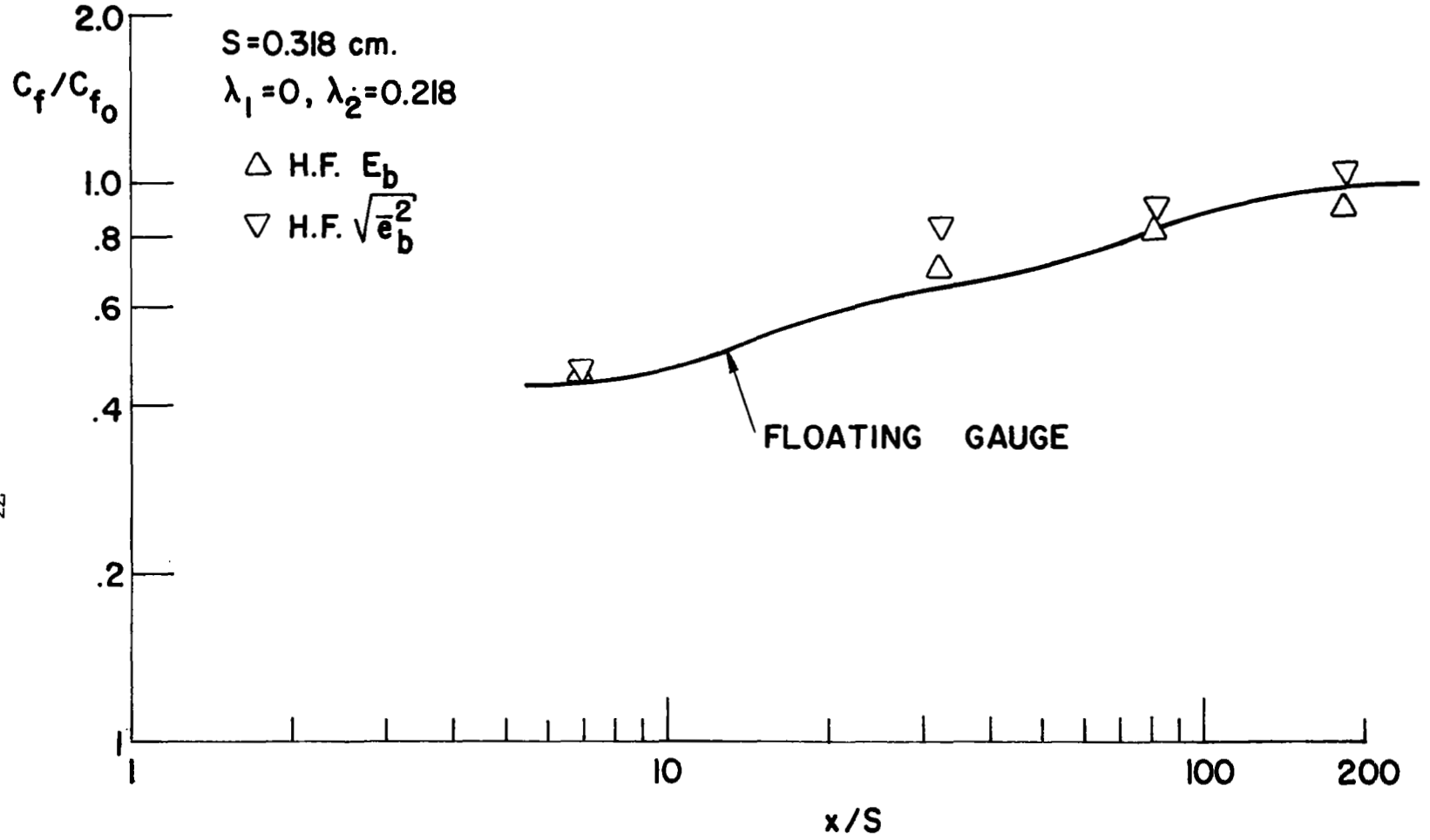

Fig. I-9 Comparison of the skin friction measurements between hot film probe and floating balance

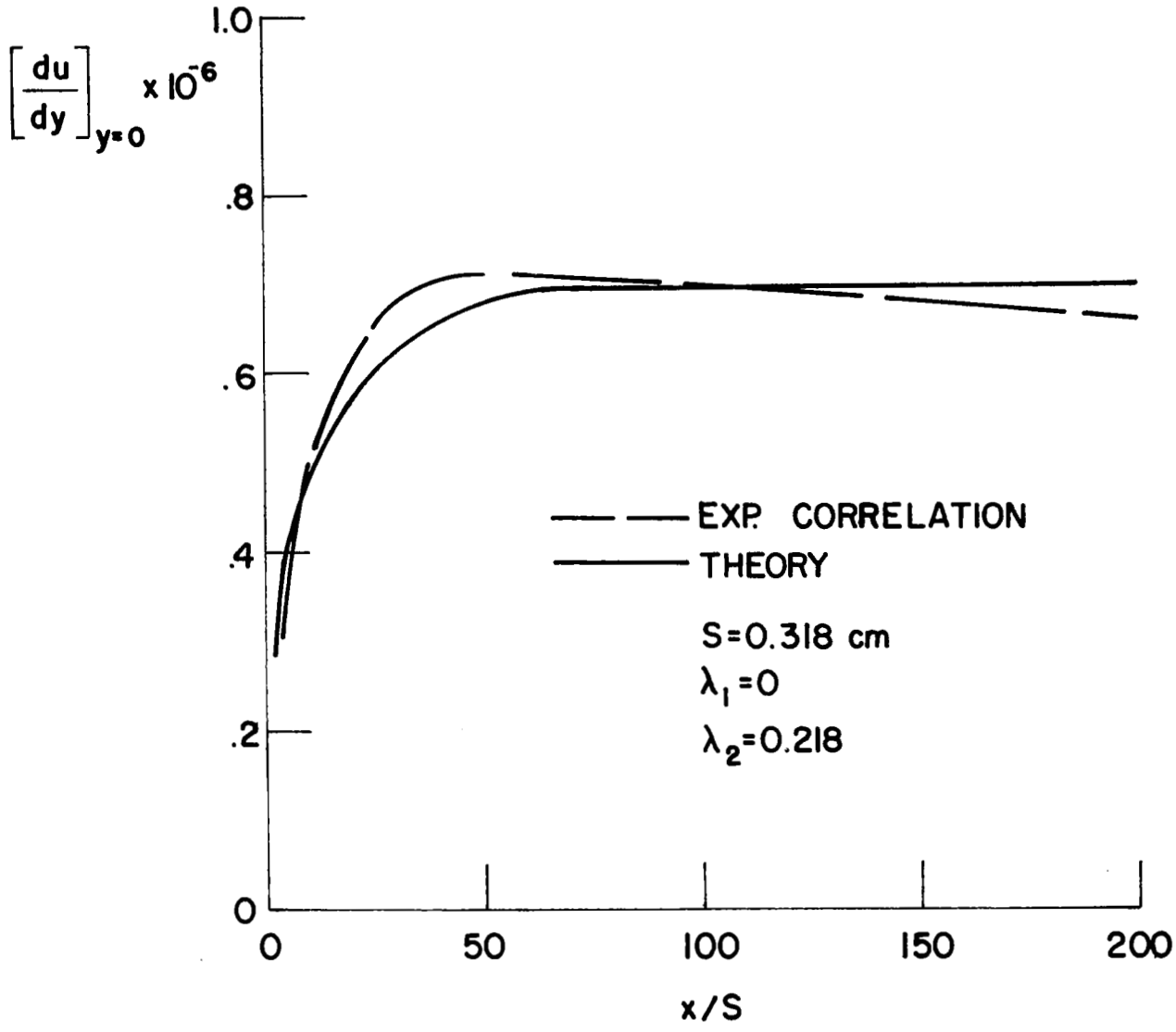

Fig. I-10 Comparison of the surface velocity gradient, s = 0.318 cm, λ_1= 0, λ_2 = 0.218

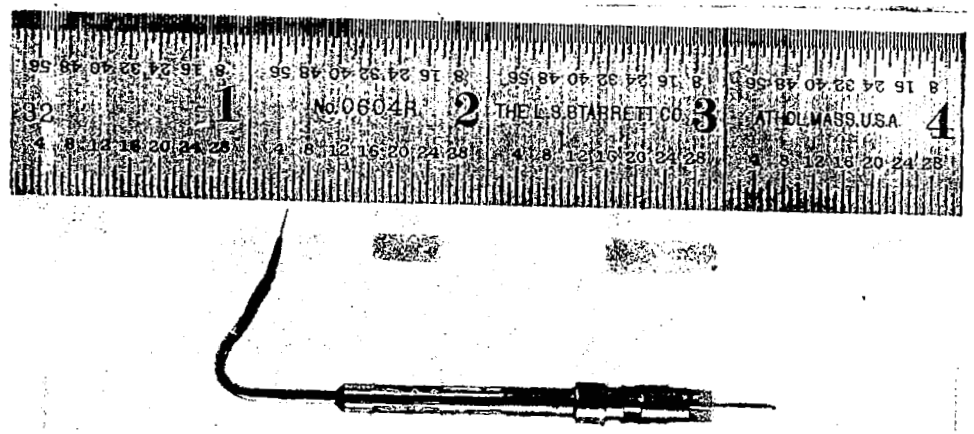

Fig. II-1 The boundary layer hot film velocity probe

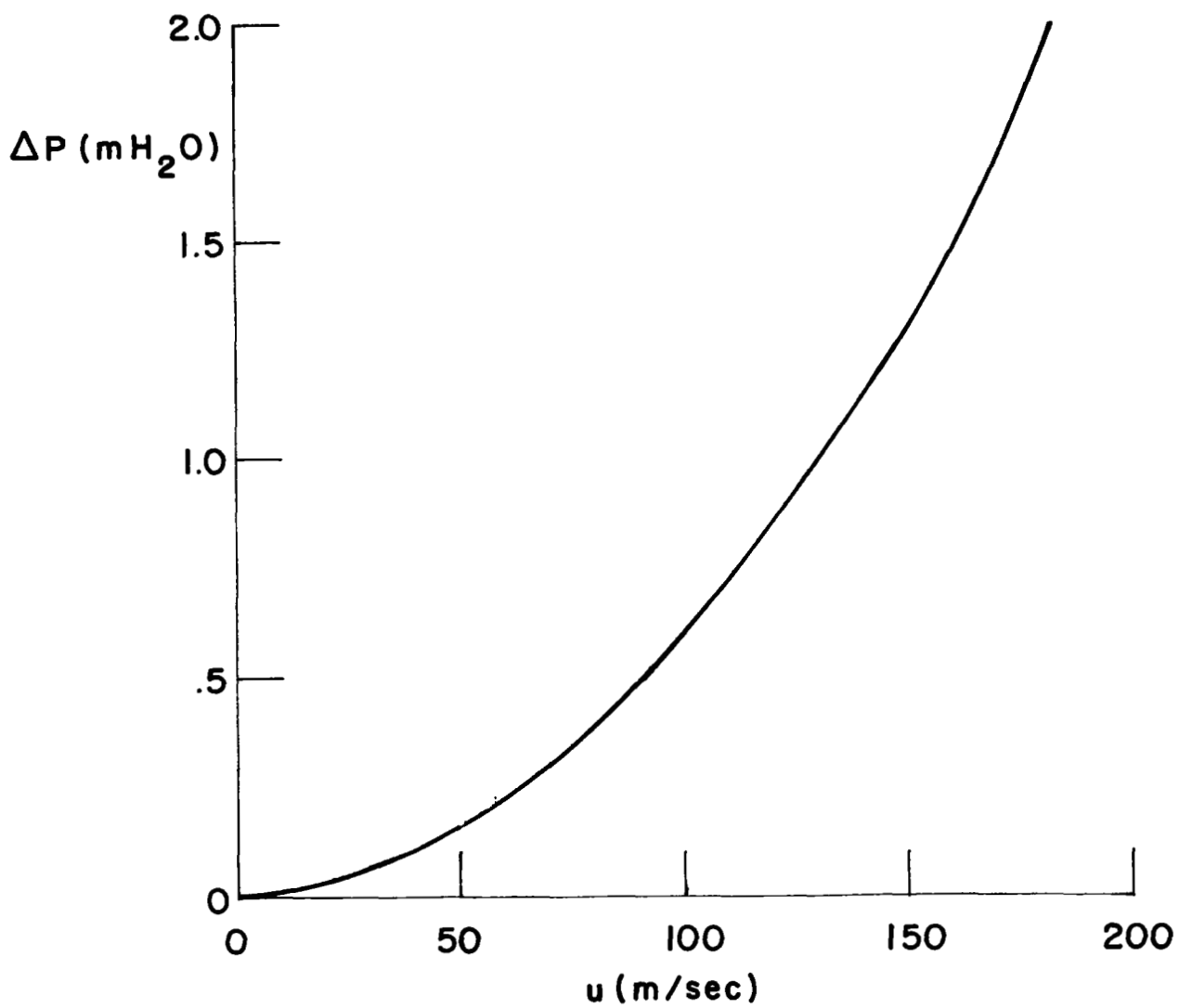

Fig. II-2 The characteristic of the DISA calibration wind tunnel

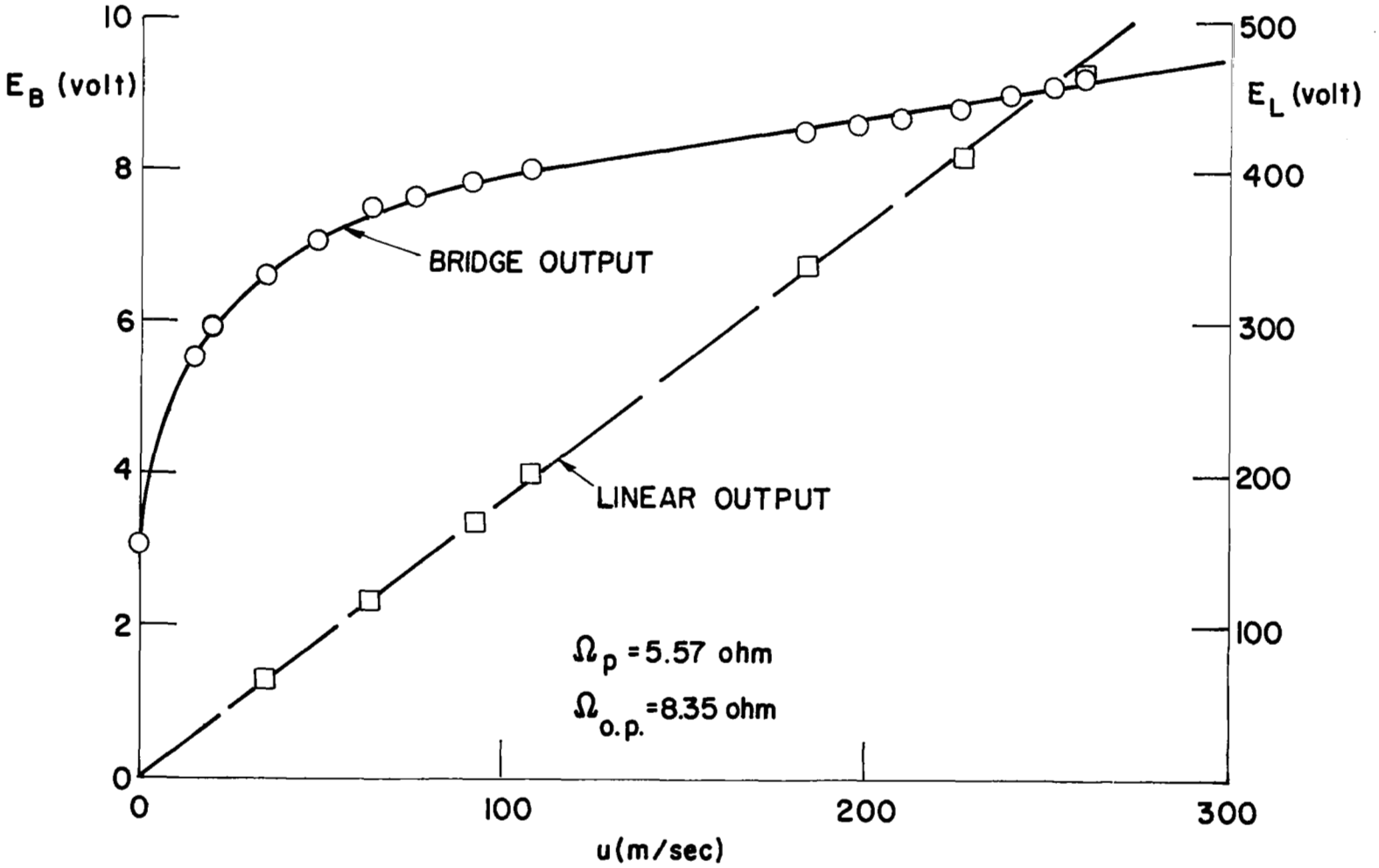

Fig. II-3 Calibrations of the hot film boundary layer velocity probe